# SYNTHESIS OF MOLYBDENUM DISILICIDE COMPOSITES USING *IN-SITU* REACTIONS

By

ANDRÉ LUIZ V. DA COSTA E SILVA

A DISSERTATION PRESENTED TO THE GRADUATE SCHOOL OF THE UNIVERSITY OF FLORIDA IN PARTIAL FULFILLMENT OF THE REQUIREMENTS FOR THE DEGREE OF DOCTOR OF PHILOSOPHY

UNIVERSITY OF FLORIDA

1994

## ACKNOWLEDGMENTS

The pursuit of a doctoral degree is no easy task. When this is done after a somewhat long interruption in one's student career, this endeavor can become quite a challenge. Fortunately, life has blessed me with a large enough number of people willing to support me facing this challenge. My family has been a constant source of support and encouragement, and I am sure the outcome of this exercise would not have been the same without their unconditional support; I have to especially thank my wife for the sacrifices she endured to make my aspiration come true. Prof. M.J. Kaufman has provided me not only with unequaled technical advice, but has also been a paradigm in his constant striving for betterment, sincere openness for discussion and honesty of purpose; I cannot thank him enough for his effect on my education. I was especially fortunate in following his advice in selecting members for my supervisory committee, who always found time in their busy schedules to give me advice, encouragement and guidance. An extremely gratifying surprise was the help I have received from unexpected sources: Prof. O.J. Kleppa, Prof. B. Sundman, Prof. Y.A. Chang, Prof. I. Ansara and Dr. Suzana Fries were some of the "people in high places" who were nice enough to endure my questions and give me suggestions. Other graduate students provided interesting suggestions and invigorating discussions, while others such as Mikael Lindholm became close friends and helped much more than I could hope. The Office of Naval Research has sponsored a significant part of this research and I am very grateful for the support and guidance of Dr. S. Fishman.

The Brazilian People through CAPES-Ministry of Education trusted me and invested in my education more than the average Brazilian worker will earn in his lifetime.

I hope I will be able to show it was a sound investment. Several individuals in Brazil gave me the encouragement to make the decision to come back to school: Profs. W.P. Longo, F.C. Rizzo and J.C. D'Abreu were among the biggest encouragers. José Dinis de Souza, at the time President of Eletrometal Metais Especiais Ltda., was a constant source of support, encouragement and inspiration; his vision of the importance of education for our country made a deep impression on me. Finally, to all those who helped me prepare samples, fix equipment, perform analyses and accommodated the idiosyncrasies of an "out-of-season" student, I extend thanks and best wishes.

TABLE OF CONTENTS

ACKNOWLEDGMENTS ..... ii

ABSTRACT ..... vi

CHAPTER 1 INTRODUCTION ..... 1

CHAPTER 2 LITERATURE REVIEW ..... 5
2.1 The Mo-Si System ..... 5
2.2 Silica in $MoSi_2$ ..... 9
2.2.1 Eliminating Silica ..... 13
2.3 Reinforcing Second Phases ..... 17
2.3.1 Nonmetallic Reinforcements ..... 17
2.3.2 Mechanisms and Kinetics of *In-situ* Reactions ..... 18
2.3.3 Refractory Metal Reinforcements ..... 24
2.4 Phase Diagram and Thermodynamic Data ..... 25
2.4.1 Estimation of Phase Diagrams and Thermodynamic Data ..... 26
2.4.2 Silica Modification with Aluminum ..... 32
2.4.3 Boride Formation through *In-situ* Displacement Reactions ..... 39
2.4.4 The Third Phase in $MoSi_2$-SiC Composites ..... 44

CHAPTER 3 EXPERIMENTAL PROCEDURE ..... 52
3.1 Raw Materials ..... 55
3.2 Sample Production ..... 55
3.2.1 Silica Modification ..... 55
3.2.2 Development of Second-Phase Reinforcements ..... 56
3.2.3 Equilibrium in the Mo-Si-Al System ..... 56
3.2.4 *In-situ* Production of Second Phases from Glass-Fiber Precursors ..... 57
3.2.5 Production of *In-situ* Coatings in Nb fibers ..... 57
3.3 Analytical Techniques ..... 58
3.3.1 Metallographic Preparation (SEM and EDS) ..... 58
3.3.2 Sample Preparation (XRD) ..... 59
3.3.3 Sample Preparation (TEM) ..... 59
3.4 Room Temperature Hardness and Indentation Crack Fracture Toughness ..... 60

CHAPTER 4 RESULTS AND DISCUSSION ..... 61
4.1 The Third Phase in $MoSi_2$-SiC Composites ..... 61
4.1.1 Thermodynamic Calculations ..... 61
4.1.2 Equilibration Experiments ..... 67
4.2 Silica Modification with Aluminum ..... 74
4.3 Silica Precursors for Alumina Reinforcement Formation ..... 78
4.4 *In-situ* Formation of Coatings in Niobium ..... 81
4.5 An Estimation of the Ternary Mo-Si-Al System ..... 86
4.5.1 Criteria for Preliminary Estimation of Mo-Si-Al Phase Equilibria ..... 86

4.5.2 An Estimation of the Binary Mo-Si ..... 87
4.5.3 An Estimation of the Binary Mo-Al ..... 89
4.5.4 Experimental Measurements in the Mo-Si-Al System ..... 93
4.5.5 Description of the Ternary Phases ..... 95
4.5.6 Results of the Estimations ..... 96
4.5.7 Application to *In-situ* Reactions ..... 101
4.6 Production of *In-situ* $MoSi_2$-Boride Composites ..... 102
4.6.1 Mo-Si-B System ..... 102
4.6.2 Mo-Si-B-Ti System ..... 110
4.7 Silica Modification in a MoB-$MoSi_2$ Composite ..... 131

CHAPTER 5 GENERAL DISCUSSION ..... 133

CHAPTER 6 CONCLUSIONS ..... 135

REFERENCES ..... 137

BIOGRAPHICAL SKETCH ..... 149

Abstract of Dissertation Presented to the Graduate School of the University of Florida in Partial Fulfillment of the Requirements for the Degree of Doctor of Philosophy

SYNTHESIS OF MOLYBDENUM DISILICIDE COMPOSITES USING *IN-SITU* REACTIONS

By

André Luiz V. da Costa e Silva

December, 1994

Chairman: Prof. Michael J. Kaufman
Major Department: Materials Science and Engineering

Two main avenues of application of *in-situ* processing of $MoSi_2$ were selected to demonstrate the feasibility of using available or estimated thermodynamic data to design *in-situ* processing schemes for intermetallic compounds, namely (a) the modification of silica through the addition of elements that should form more stable oxides and (b) the development of second-phase reinforcements through displacement reactions.

Techniques for modifying the silica present in $MoSi_2$ and its composites were explored through the addition of aluminum or zirconium prior to hot pressing. In particular, the use of aluminum additions to generate alumina was evaluated through the addition of different levels of aluminum. In order to better describe the processes occurring when this technique is used, different estimation techniques were used to appraise the thermodynamic functions of the species taking part in the process.

To demonstrate the possibilities in the *in-situ* development of second-phase reinforcements, borides were selected in view of their interesting high-temperature properties, as well as the potential for displacement reactions in the Mo-Si-B and other higher order systems. The possibility of generation and control of different molybdenum

borides through the use of different displacement reactions was evaluated using boron and lower molybdenum silicides as precursors. To make evident the generality of the approach, it was extended to a quaternary system, where the microstructural evolution was compared with that of elemental powders mixed to obtain the same stoichiometry.

Finally, the two approaches were combined in the production of silica-free, boride reinforced $MoSi_2$.

# CHAPTER 1

# INTRODUCTION

As the application temperature of superalloys approached their solidus temperatures in the last decade, the interest in intermetallics for structural applications has been renewed. This class of materials is broadly characterized by a mixed bonding character, more covalent than typical metals but less than covalent ceramics. Among the several families of intermetallics, probably the most interesting from the structural point of view are silicides and aluminides. These compounds, involving elements at the Zintl border in the periodic table and metals, have potential good oxidation resistance, due to the possibility of formation of protective silica or alumina films on their surfaces, as well as considerably high melting points, an evidence of their high stability. While in the case of aluminides it is frequent that the intermetallic phases have higher melting points than the constituent metals, this is not the rule in silicides which, although have high melting points, seldom exceed the melting point of the metal forming the silicide. An additional advantage of these compounds is their density, which is considerably smaller than that of superalloys.

It is speculated that the directionality of the covalent component of the bonding, together with their ordered structures, are the main reasons why intermetallics have low ductility at low to moderate temperatures; this is also frequently expressed as brittle behavior. At high temperatures, when these compounds deform, their strength is frequently too low for the desired applications.

Albeit the causes of the limited ductility as well as of the occurrence of the brittle to ductile transition are still the subject of controversy in several of those intermetallics

considered to be most promising for structural applications, it seems that the main approaches to control and improve these properties will be those classically employed in metals and ceramics such as the control of microstructural features like grain size and morphology, the introduction and control of second phases as well as alloying to influence these features and the deformation mechanisms.

Several processing techniques are available for the implementation of these approaches. Due to the high melting point and need for close control of stoichiometry of these compounds, however, the processing of silicides poses many challenging aspects. The family of processes grouped under the "*in-situ*" label offer very interesting possibilities for cost-effective microstructural control as well as introduction of second-phase reinforcements. In contrast to processes in which reinforcements are introduced in the material as a previously formed component (e.g., "engineered composites"), these processes are based on the occurrence of reactions in its original place, i.e., in the material, during processing, thus justifying the "*in-situ*" classification. In order for these processing routes to be effective, however, understanding of the thermodynamics of the systems under considerations as well as of the kinetics of the envisaged processes is essential.

One particularly interesting intermetallic is molybdenum disilicide, the silicide with the best oxidation resistance and with the longest history of commercial use. The specific challenges in this silicide encompass the need for room temperature toughening as well as high temperature strengthening. Most efforts to mitigate these problems have concentrated on the introduction of second-phase reinforcements. Evidently, the most basic requirements for a reinforcement would be high melting point, reasonable density (if aerospace applications are being considered) and mechanical properties commensurate with the properties which are to be improved. Thus, attempts to produce "engineered composites" through the introduction of refractory metals for toughening $MoSi_2$ at room temperature date back to the early 1970s while reports of high temperature strengthening

with SiC can be found in the first attempts to develop $MoSi_2$ as a high temperature structural material, in the 1950s. Evidently, some of these efforts were marred by lack of high temperature stability so the relevance of high temperature compatibility to the design of this type of materials has been highlighted.

Among the possible high temperature reinforcement candidates, work has been performed on the introduction of oxides, carbides, and, to some extent, nitrides and borides in $MoSi_2$. Most metal borides are characterized by extremely high bond strengths which is evidenced by high melting points and hardnesses. Besides, several of the borides have good electrical and thermal conductivities, favorable properties both from the manufacture and the high-temperature application points of view in $MoSi_2$-based composites. There are several metal borides that appear to be compatible with $MoSi_2$ at high temperature and it is possible to devise "*in-situ*" reaction schemes for the generation of boride reinforcements in molybdenum disilicide. Thus, it appears that borides, in particular molybdenum and titanium borides, would be particularly suitable candidates for the demonstration of the possibilities of generating reinforcements through "*in-situ*" reactions highlighting the advantages of the support of a thermodynamic analysis methodology.

Furthermore, silica or silicon-rich oxides are ubiquitous in $MoSi_2$-based materials and it is now established that their control is necessary for the effective potential utilization of this material's desirable properties in structural applications. Based on the accumulated experience with the processing of other classes of materials such as metals for instance, different routes can be conceived for the elimination of silica that would be broadly classified, in the metals processing industry, as deoxidation or inclusion morphology control, depending on whether the oxygen present in silica is removed from the system or just combined in a less detrimental compound. While some of these techniques have been successfully transplanted into the field of intermetallics processing,

most have not yet been attempted and are worth being considered, following the analytical framework developed for this class of reactions in metals.

# CHAPTER 2

# LITERATURE REVIEW

## 2.1 The Mo-Si System

Molybdenum and silicon form three stable silicides. Table 2.1 presents the relevant structural information on these compounds. Phase relations in the Mo-Si system have been well established for some time [1- 3] as shown in Figure 2.1. However, although it has been accepted until recently that $MoSi_2$ had a polymorphic transformation at 1850°C ($C11_b$ to C40) [2, 3], Boettinger and coworkers [4] demonstrated that $MoSi_2$ retains the $C11_b$ structure up to its melting point and that the C40 phase reported in other studies was caused by contamination. $MoSi_2$ has a narrow stability range (2.5% Si max. at 1500°C [5]) while it is speculated that the stability range of the other molybdenum silicides is even narrower [6].

Table 2.1 Structural Information of Phases in the Mo-Si System

| Phase | Strukturbericht Designation | Space Group | a nm | c nm | Reference |
|---|---|---|---|---|---|
| $MoSi_2$ | $C11_b$ | I4/mmm | 0.3202 | 0.7843 | [3] |
| $Mo_5Si_3$ | $D8_m$ | I4/mcm | 0.9648 | 0.4910 | [3] |
| $Mo_3Si$ | A15 | Pm3n | 0.4890 | | [3] |
| Mo | A2 | Im3m | 0.31470 | | [3] |
| Si | B3 | F43m | 0.54306 | | [3] |

2.1.1 $MoSi_2$ Characteristics

$MoSi_2$ seems to be the most promising disilicide for high temperature applications due to its excellent oxidation and corrosion resistance, reasonably low density (6.31 $g/cm^3$) and high melting point (2020°C). By virtue of these properties together with its electrical characteristics, $MoSi_2$ has found extensive use as a high temperature heating element [7].

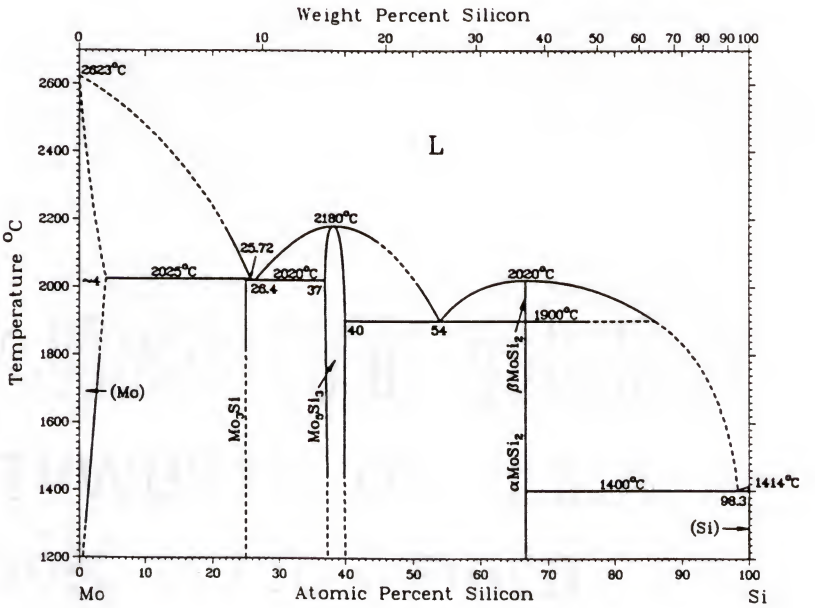


Figure 2.1 The Mo-Si Phase Diagram [3].

Plastic deformation is limited in the ordered $C11_b$ structure of $MoSi_2$, and only becomes significant at high temperatures, above the brittle-to-ductile transition temperature (BDTT) [8]. Figure 2.2 presents the unit cell of $MoSi_2$. Perhaps not surprisingly, since many different definitions are still used for metals, there is no unique definition for the BDTT in intermetallics.

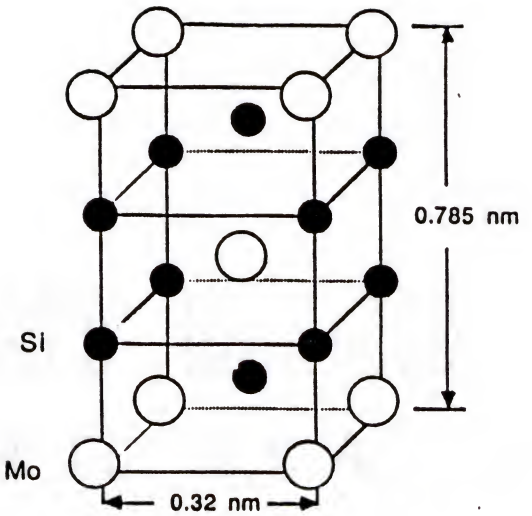


Figure 2.2 $MoSi_2$ unit cell.

The temperature-dependent mechanical behavior of $MoSi_2$ comprises three ranges: (1) strong and brittle up to approximately 1000°C (BDTT ), (2) strong and "ductile" (1000-1250°C) and (3) weak and ductile above 1250°C [9]. Evidently, there are several possible routes for the improvement of the mechanical properties of $MoSi_2$. First, understanding the fundamental causes of this behavior, as well as the effect of chemical composition (both stoichiometry and residuals) is essential if a systematic control of product properties is to be achieved. The fundamental importance of this type of work has been demonstrated before in other classes of materials [10], and all the improvements that may be achieved using other techniques are, without doubt, conditioned to the progress in this basic area. Besides efforts in single crystal mechanical behavior [8, 11-14], studies in this area have been lacking, especially insofar as the effect of residual elements.

A second tool is microstructural control, i.e., the manipulation of grain size and shape as well as their dispersion; this area has received some nonsystematic attention starting with the work of Fitzer and collaborators (e.g., [15]). Finally, in the absence of viable phase transformations (e.g., martensite formation), the introduction and control of second phases is the remaining family of processes available to control mechanical properties. Evidently, this encompasses a vast scope of processes and possibilities ranging from undesirable second phases originating in processing (such as nonmetallic inclusions in steels and alloys or silica in the case of $MoSi_2$) to fine dispersoids designed for dispersion hardening and artificially introduced reinforcements to produce engineered composites. A critical issue in the introduction and control of second phases is the compatibility or stability of these phases in the matrix. While most classical processes for introducing second phases are based on precipitation reactions and thus have modest to no deviation from thermodynamic equilibrium (stable or metastable) with the matrix, the introduction of artificial second-phase "reinforcements" can result in large deviations from equilibrium. In order to better identify the generation of phases through reactions occurring during the processing of materials, the term "*in-situ* processing" was conceived. *In-situ* processing can be a valuable tool in the production of reinforcements in structural materials, especially those for high-temperature applications, when reinforcement-matrix interaction becomes more important. Several excellent reviews [7, 9, 16] on $MoSi_2$ and its applications are available and in a recent symposium (see [16]), the properties of $MoSi_2$ and its composites have been reviewed extensively. Presently, there is still controversy on the relative importance of the different mechanisms such as dislocation movement, microcracking and plastic flow due to second phases, in the "plasticity" of $MoSi_2$ above the "apparent" BDTT. In this section, some aspects that were not the main focus of these reviews are highlighted, with an emphasis on those efforts aimed at controlling silica and introducing reinforcing second phases, both via *in-situ* reactions.

## 2.2 Silica in $MoSi_2$

Most silicides have high melting points and are not amenable to melt processing, making powder processing (sintering [17, 18], hot pressing and hot isostatic pressing (HIP) [19]) the techniques of choice. Some effort has also been dedicated to less conventional techniques such as reactive sintering ("self-propagating synthesis") [20, 21], plasma spraying [22, 23] and CVD [24].

Due to surface oxidation and/or oxygen absorption, silica is almost always found in $MoSi_2$ bodies produced via powder processing. As a consequence of its narrow stability range, silica formation in stoichiometric $MoSi_2$ is usually accompanied by the formation of $Mo_5Si_3$. There has been no specific study on the mechanical properties of this silicide although Basu and Ghosh [25] have investigated the properties of $MoSi_2$-$Mo_5Si_3$ composites. It is known that it has lower oxidation resistance that $MoSi_2$ [26] and its presence has been associated with the occurrence of the phenomenon of disintegrating oxidation termed "pest" (e.g., [27, 28]).

The occurrence of silica in powder-processed $MoSi_2$ has been observed since it was first considered for structural applications (e.g., [29, 30]). Both Maxwell [29, 30] and Fitzer and coworkers (e.g., [17, 31]) observed the relationship between oxygen content, powder particle size and processing conditions on the amount of silica and $Mo_5Si_3$ present in the final product (Figure 2.3).

With the renewed interest on silicides for structural applications, the occurrence of silica was again brought to attention when Cotton and coworkers [32] reported the presence of 5-10 % vol. of silica in samples produced from powders obtained by grinding arc-melted $MoSi_2$. Since then, several investigators reported the observation of silica in $MoSi_2$-based materials.

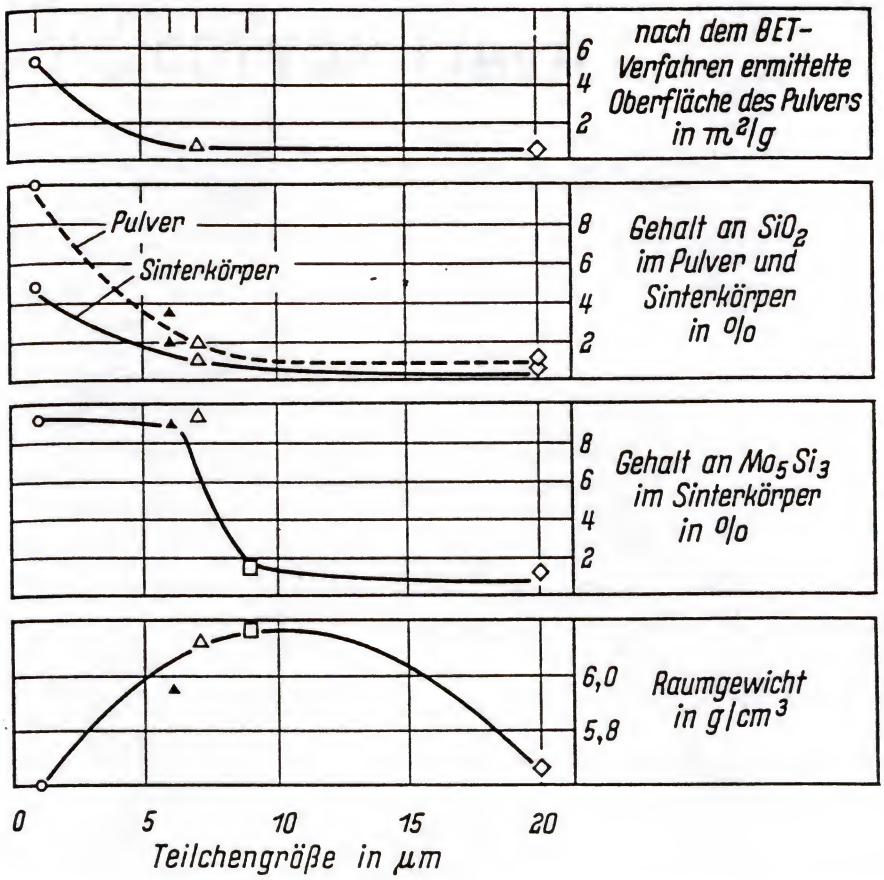


Figure 2.3 Effect of $MoSi_2$ particle size on sintered product characteristics. Adapted from ref. [17].

There is, however, no agreement on the morphology and distribution of silica in $MoSi_2$ nor on the effects of processing variables on these characteristics. A number of authors claim that silica "wets" the grain boundaries or that it concentrates in triple points (e.g., [32, 33]) while others [34- 37] observed globular silica particles both at grain boundaries and inside grains. The TEM analysis of [34] failed to reveal any evidence of an amorphous phase wetting the grain boundaries while others [33, 38] claimed that some glassy phase was present along grain boundaries.

Wade and Petrovic [37] analyzed the path followed by cracks emanating from hardness indentations in samples produced from commercial powders (18 µm grain size).

The silica particles present inside grains and at grain boundaries apparently did not interfere with crack propagation. Aikin [35] reported almost 100% intergranular failure at 1300°C in a 20 μm grain size material containing silica particles both inside grains and at grain boundaries. In a 10-20 μm grain size material containing silica both inside the grains and at grain boundaries [36], the room temperature fracture was almost 100% intergranular both in bending tests and in cracks emanating from hardness indentations. Auger analysis of specimens fractured *in-situ* did not indicate any oxygen enrichment of the grain boundary surfaces implying that silica does not wet grain boundaries.

Since silica is initially present on the powder particle surfaces, it is conceivable that at some stage during the processing it may be distributed along grain boundaries, although that does not seem to be the most frequently observed distribution in the consolidated products. While silica and silicates wet several ceramic systems, they do not wet most metals (silicate inclusions in steels being a classic example) and there is no *a priori* reason to assume that silica will wet $MoSi_2$ grain boundaries. At the high consolidation temperatures, silica seems to coalesce into the globular shapes shown in Figure 2.4; this indicates a relatively high surface energy between $MoSi_2$ and $SiO_2$. This should not be confused with the surface energy in systems where air is present; in these systems, it has been established that molten silica does not wet $MoSi_2$, this being the reason for the loss of oxidation resistance above approximately 1700°C [27].

Basu and Ghosh and also Gibala and coworkers [25, 38] tested Kanthal Super heating elements as material representative of $MoSi_2$ with a high volume fraction of silica (15% vol.) and observed a significant decrease in creep resistance in comparison to material containing a much lower volume fraction of silica. Although the effect is what would be expected, its magnitude may have been enhanced since the second phase in heating elements is not pure silica: clays and other oxides are frequently introduced as plasticizers and resistivity-controlling additions [27].

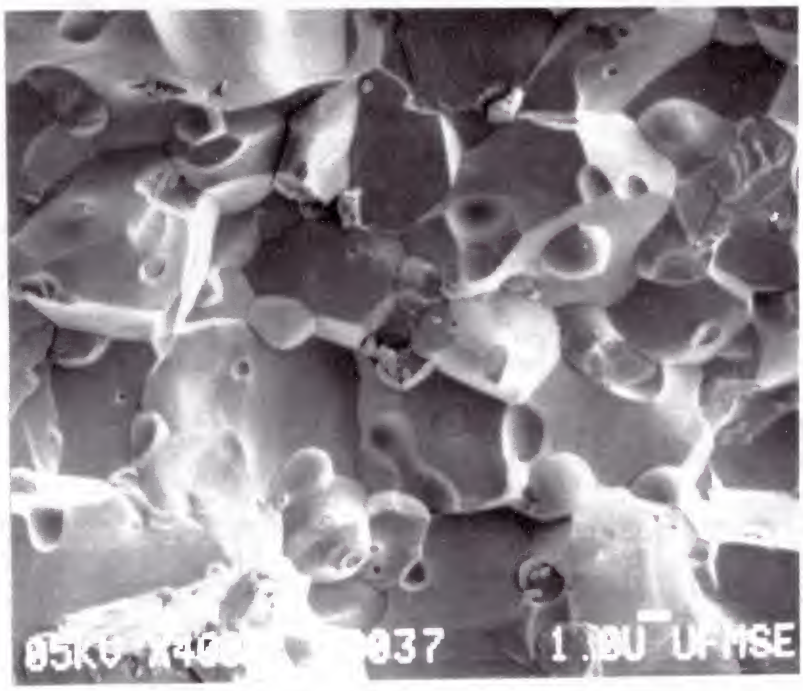

Figure 2.4 Scanning electron micrograph (SEM) of a fractured surface of hot pressed $MoSi_2$. Globular particles are silica.

Ramamurty and coworkers [39] studied the creep-fatigue of $MoSi_2$-based composites and concluded that the viscous flow of the glassy silica phase appears to have a more important effect on deformation than dislocation plasticity at their testing conditions and suggested that silica control, e.g. through carbon additions, is essential for the improvement of creep and creep-fatigue of silicide-based composites.

There is also considerable disagreement concerning the effect of silica on the BDTT of $MoSi_2$. While Aikin [35] observed no difference when 6% vol. fraction silica was present as scattered globules and when this phase was mostly absent (0.8% vol.), he claimed that the lower BDTT reported by other authors could be due to the presence of continuous silica films along grain boundaries. In another study [40], it was suggested

that the BDTT of $MoSi_2$ is decreased in the presence of $SiO_2$ and, hence, the observed values in polycrystalline $MoSi_2$ and its composites may be due to the presence of silica and not to the onset of plastic deformation by slip.

It is evident that there is no consensus concerning the morphology and distribution of silica in polycrystalline $MoSi_2$ and its effects on mechanical properties. There seems to be clear agreement, however, that $MoSi_2$-based materials should benefit from the elimination of silica in several aspects: (1) probable improvement in high-temperature mechanical properties and (2) closer control of matrix stoichiometry.

### 2.2.1 Eliminating Silica

Three approaches have been proposed to eliminate silica from $MoSi_2$ products: (1) reduction with carbon; (2) reaction synthesis of high purity powders followed by "clean" processing and consolidation, and (3) surface etching of the powders with, for instance hydrofluoric acid, followed by consolidation. Besides, sintering under a hydrogen atmosphere has also been shown to result in significant reduction of the silica content of the final product [17, 18].

Processes in which a low carbon monoxide pressure is established for carbon deoxidation are powerful processing techniques in both steel and superalloy making (e.g. AOD, VOD, VIM, VAR) [41]. Besides the evident thermodynamic advantage associated with lowering the activity of the reaction product, these processes benefit from the enhanced cleanliness associated with the formation of a gaseous oxide that can readily leave the liquid metal. The transfer of this technique to powder processing introduces interesting challenges. In Maxwell's [30] pioneering work with this technique, he observed increased porosity in his compacts although the total oxygen content was reduced from 1.4% wt. when no carbon was added, to a minimum of 0.15% wt. when carbon reduction was used. Jayashankar and Kaufman [42] developed a technique based

on the mechanical alloying of Mo, Si and C powders, followed by hot pressing, to produce silica-free $MoSi_2$ matrix composites. A sophisticated sequence of processing steps [43] was developed to achieve carbon monoxide elimination prior to final consolidation. Maloy and collaborators [33] reported extremely high weight losses after using a technique similar to Maxwell's, i.e., carbon additions to $MoSi_2$ powders. Although the magnitude of their losses somewhat defies explanations through plausible mass balances, enhanced losses of volatile species such as silicon and SiO could occur in conjunction with CO elimination at their consolidation temperatures (1830°C). In recent work, Jacobson and coworkers [44] analyzed Maloy's results and suggested that the losses could be due to inaccuracies in the control of the hot pressing temperature, leading to the formation of an eutectic liquid between SiC and $Mo_5Si_3C$ that exudes from the die. Indeed, Nowotny and coworkers in their measurements of the liquidus surface of the Mo-Si-C system [45] proposed the existence of a ternary eutectic in the $MoSi_2$-$Mo_5Si_3C$-SiC field at 1850°C. Henager, Brimhall and Hirth [46] reported results similar to those of Jayashankar and Kaufman. None of the latter have reported the oxygen contents of their products. The interesting feature of the approach is that not only can silica be eliminated but SiC can be produced as an *in-situ* second phase [42] as described below.

A processing route under which all steps starting with elemental powder manufacturing and ending at the HIP stage were performed under vacuum or protective atmospheres [47] resulted in a final oxygen content of 0.16% wt. or, when the cold pressed compacts were machined in air, 0.35% wt. Schwarz and coworkers [48] claimed to have achieved 310 ppm wt. oxygen in final compacts using similar techniques. Hardwick and collaborators [9] questioned the analytical technique of Schwarz in view of the order-of-magnitude difference between their measured oxygen concentrations. This does not appear to be justified since O'Hare [49] has recently reported the use of $MoSi_2$ containing 338 ppm wt. of oxygen produced in accordance with a Japanese patent [50] in

which oxygen elimination appears to be achieved by degassing and elimination of high vapor pressure oxides during heating of the elemental powders under vacuum.

The surface etching techniques described by Maxwell [30] did not find many followers thus far. One limitation seems to be the fact that, once the powder surface is "cleaned" of silica, a fairly sophisticated handling system similar to that used by Hardwick and coworkers [47] has to be followed.

Gibala and coworkers [38] added erbium when arc melting Mo and $MoSi_2$ to produce $Mo_5Si_3$-$MoSi_2$ composites. The Er addition was intended as a "microstructural refiner" and as an "additional means of removing oxygen from the melt." The formation of a mixed silicide was reported but neither oxygen concentration nor oxide type/content were given.

Fitzer and coworkers at Karlsruhe perfected sintering techniques for $MoSi_2$ [15, 17, 18, 31, 51] employing hydrogen atmospheres, which resulted in significant reductions of the silica content in the final product; this was particularly evident when finer powder was used as starting material. The only barrier to silica reduction in this case is kinetic since even "commercial" grade hydrogen gas has a sufficiently low $H_2O$ content to viabilize the reduction reaction at the sintering temperatures [52]. To prevent volatilization losses of silicon, the gas was saturated with silicon vapor prior to introduction in the sintering furnace. Somewhat surprisingly, in view of its relative simplicity, only recently have sintering techniques received renewed attention with the work of Petrovic and Idasetima [53] who attempted to study the sintering behavior of $MoSi_2$.

It is rather surprising that the logical concept of using other elements to form oxides less detrimental than silica has not been attempted earlier since there are several elements (e.g. Al, Zr, Mg and Ca) that will form more stable oxides than silica, apart from the rare earths and carbon under low CO pressures.

2.2.1.1 Silica modifiers

Evidently, the selection of an addition to modify silica through a displacement reaction cannot be based only on the stability of the product oxide. Among other factors, (a) the behavior of the resulting oxide as a second phase in $MoSi_2$, (b) the possibility of forming low-melting silicides or other undesirable phases and/or silicates and (c) the ease of handling and adding the reactant must be considered. Besides, the displacement reaction must be analyzed using the available thermodynamic data. Among the elements that do not pose excessive difficulty in handling, aluminum, zirconium, calcium, magnesium and the rare earths are potential candidates to take part in displacement reactions to eliminate silica from $MoSi_2$. Not surprisingly these are the elements the steel industry has been resorting to since it decided to eliminate silicate inclusions and achieve lower contents of dissolved oxygen in the metal.

The main displacement reaction to be considered is:

$$\underline{D}(a_D) + SiO_2 = D_xO_y\,(a_{DxOy}) + \underline{Si}\ (a_{Si} \text{ in } MoSi_2 \text{ or in } Mo_\xi D_\psi Si_\zeta) \qquad (2.1)$$

The displacing element activity ($a_D$) will be fixed by its behavior in the D-Si-Mo system (assuming that oxygen solubility in the phases involved has negligible effects), whereas the $D_xO_y$ activity will be determined by the potential reactions in the D-O-Si (or $D_xO_y$-$SiO_2$ system). The silicon activity will be defined by the silicide(s) present; care should be exercised to adjust the additions in order to prevent the occurrence of pure Si or pure D in the final product since these could be low-melting phases.

$Al_2O_3$ and $ZrO_2$ have been demonstrated to be satisfactory reinforcements in previous $MoSi_2$ composite studies (e.g., [15, 16, 54]) but there is little data for the behavior of CaO as a reinforcement [38], and no study is known that considered MgO or rare-earth oxides as reinforcements in silicides. The latter, being high density oxides, would furthermore limit the possible advantages of decreasing the overall density through

the addition of a second phase. In order to understand the behavior of reaction (2.1), data on the Mo-Si-D and D-O-Si systems are needed. Also, in this respect, Al and Zr offer advantages since more data are available in the systems involving these elements as described below in Section 2.4.

## 2.3 Reinforcing Second Phases

The criteria for selecting reinforcements for composites have been extensively reviewed elsewhere (e.g., [55- 57]). These include but are not limited to mechanical properties, CTE compatibility, physical properties (such as density) as well as microstructural stability, especially for high temperature applications.

### 2.3.1 Nonmetallic Reinforcements

The introduction of reinforcements to improve the mechanical properties in $MoSi_2$-based composites has been reviewed by Vasudevan and Petrovic [16]. They have shown that, of all composites explored thus far, $MoSi_2$-SiC composites exhibit the best high temperature properties, albeit the improvements in toughness are still mediocre. Besides the artificial compositing efforts in this system described in [16], the *in-situ* work of Jayashankar and Kaufman [42, 43, 58] as well as that of Henager, Brimhall and Hirth [46, 59] should be mentioned. Henager and coworkers [46, 59] explored the *in-situ* production of $MoSi_2$/SiC through solid-state displacement reactions between molybdenum carbide and silicon. A drawback of this approach is the fixed volume of the reinforcing phase that can be generated, based on the stoichiometry of the displacement reaction. Jayashankar and Kaufman developed an *in-situ* technique for the production of $MoSi_2$/SiC composites combining the elimination of silica, as described previously, with the generation of SiC reinforcements. While Jayashankar and Kaufman observed that compositions which deviate from the precise $MoSi_2$-SiC stoichiometry towards the

silicon-lean direction consistently retained $Mo_5Si_3C$ to room temperature, Henager and coworkers [59] failed to define conclusively whether the "third phase" observed in their alloys was $Mo_5Si_3C$ or $Mo_5Si_3$. The phase equilibria in these composites needs clarification, since there are two conflicting isotherms proposed for this system, as will be discussed in section 2.4. Jayashankar and Kaufman reported homogeneous distributions of the reinforcing phase up to 20% vol. and their technique places no limit on the maximum volume of the reinforcing phase that can be generated. Since then, samples with as much as 60% vol. SiC have been produced [60]. An additional aspect that may have to be taken into consideration is the effect of the "third phase" (either $Mo_5Si_3$ or $Mo_5Si_3C$) on the composite behavior since $Mo_5Si_3$ and $Mo_5Si_3C$ have different crystal structures and, more importantly, considerably different ranges of compositional stability, i.e., whereas $Mo_5Si_3$ is a line compound, $Mo_5Si_3C$ can exist over a significant range of compositions and is able to dissolve other interstitials such as nitrogen and oxygen.

*In-situ* techniques have also been used to introduce boride reinforcements into $MoSi_2$-based composites. Borides have, in general, high hardness and relatively good corrosion resistance [61, 62] as well as other desirable physical properties such as good thermal and electrical conductivity and relatively high CTE [61, 62] making them interesting candidates for reinforcing $MoSi_2$. Table 2.2 summarizes the physical properties of some borides that can be considered as potential reinforcements for $MoSi_2$. Borides have been introduced into $MoSi_2$ via the patented XD™ [63] process which involves an *in-situ* precipitation reaction in the liquid phase followed by grinding and hot consolidation.

### 2.3.2 Mechanisms and Kinetics of *In-situ* Reactions

The mechanisms and kinetics of *in-situ* displacement reactions have been described by several authors, often by adapting Wagner's models for transport-controlled

Table 2.2 Physical Properties of the Relevant Phases in $MoSi_2$ - Boride Composites.

| .Compound | Space Group | Melting Point (K) [a] | Lattice Parameters a (nm) | Lattice Parameters c(nm) | Density ($g/cm^3$) | CTE $10^{-6}/K$ | Hardness (GPa) |
|---|---|---|---|---|---|---|---|
| $MoSi_2$ | I4/mmm | 2293 | 0.32 | 0.785 | 6.31 | 6.8 [b] | |
| αMoB | $I4_1/amd$ | t2073<br>2873 | 0.311 | 1.697 | 8.77 | - | 23.0-24.5 |
| $Mo_2B_5$ | R3m | 2413 | 0.301 | 2.094 | 7.45 | 8.6-9.9 | 23.0 |
| $MoB_2$ | P6/mmm | 2648 | 0.304 | 0.307 | 7.99 | 7.7 | 11.8 |
| $TiB_2$ | P6/mmm | 3498[c] | 0.3030 | 0.3230 | 4.52 | 8-11.2 | 25.5-33.0 |

All data from [64], except where otherwise indicated.
[a] From [2].
[b] From [27].
[c] From [65].

oxidation (e.g., [66]). For example, Rapp and coworkers [67, 68] formulated a model aimed at predicting the morphology of the products of displacement reactions based on the transport characteristics of the different species and on the postulate that the balanced fluxes are maximized at steady state. Although Rapp and collaborators were able to predict morphologies and layer growth kinetics in some oxide systems, Backhaus-Ricoult and coworkers later demonstrated [69, 70] that the flux maximization may not be a universal postulate. In fact, she was able to show the stability of non-planar growth leading to "interwoven" microstructures under conditions where the Rapp model indicated that a planar interface should be stable.

The application of these models to complex multi-component systems such as intermetallic-matrix composites is limited by the scant knowledge of diffusion data as well as the plethora of intermediate phases frequently present. Although Henager and coworkers [46, 59] attempted to rationalize their results in the Mo-Si-C and Ni-Al-O

systems based on the Rapp model, most of their conclusions are only qualitative in nature. Without attempting to model the kinetics of the reactions in question, Jayashankar and Kaufman [43] followed the phase evolution of mechanical-alloyed (MA) Mo-Si and Mo-Si-C mixtures using a combination of DTA, TEM and XRD analyses of mixtures heated under flowing argon to several intermediate temperatures. When analyzing the Mo-Si mixtures, they observed that some $MoSi_2$ (both $C11_b$ and C40) was already formed during mechanical alloying, if the attrition time was sufficiently long. Furthermore, the volume fraction of $C11_b$ $MoSi_2$ increased when samples were heated to above 580°C and the conversion to this phase was almost complete when samples were heated to 1070°C. Even though there are several variables involved in the process, it appears that the rate of formation of $MoSi_2$ from MA elemental molybdenum and silicon is significant in the range of 600 to 1100°C, since these experiments were conducted at a heating rate of 10°C/min with no holding time at the final temperature.

*In-situ* processes have also been applied to the production of boride bodies and powders and there has been a significant effort aimed at explaining the mechanism and the kinetics of these reactions, especially in the case of the diborides, in view of the armor applications of some of these compounds (e.g., [64, 71]). Most of the effort devoted to describing the mechanisms and kinetics of the formation of high-melting borides is concentrated on the family of processes classified as occurring by "self-propagating high-temperature synthesis" (SHS). In these processes, an exothermic reaction is started through some ignition technique and ideally proceeds in a stable fashion until complete consumption of the reactants. The application of these processes to borides is especially interesting in view of their high thermodynamic stabilities [64] associated with their high enthalpies of formation, and the considerable difficulty in sintering these materials [72, 73]. For a given initial temperature of the system ($T_0$), one can define the adiabatic temperature ($T_{ad,\,T_0}$) of a SHS process as the temperature the products should reach if the reaction occurs adiabatically. In the SHS literature it is usual to compare values of

$T_{ad,298K}$ , which is normally refered to as the adiabatic temperature of the system [74]. For instance, $TiB_2$ produced from titanium and boron has an adiabatic temperature of 3190K [72, 75] while that of $MoSi_2$ can be calculated as 1900K [75]. While different criteria have been established to screen for the possibility of self-propagating synthesis ($\Delta H^0_{298}/C_{p\,298} > 2000K$, [76] or $T_{ad,\,T_0} > 1800K$, for instance), there remains considerable controversy as to the conditions for the initiation and the occurrence of these reactions, as well as the mechanism(s) involved. It is common to refer to an "ignition temperature" above which the SHS reaction proceeds rapidly. One must consider, however, that any of these reactions involves a series of thermally-activated processes and thus has a rate that varies with temperature, as opposed to having a transition from no reaction to explosive formation at a single, well-defined temperature. Evidently, when one of the reactants melts and wets the other causing a sudden change in the reaction mechanism as well as the contact area, the reaction rate data may convey the impression of the existence of a critical "ignition temperature". This issue is discussed in detail elsewhere [75].

From the point of view of understanding the reactions occurring during the *in-situ* formation of borides in $MoSi_2$, however, useful information can be derived from the combustion synthesis literature if these limitations are kept in mind. Thus, it has been shown in several systems that lower heating rates can lead to a low rate of dissipation of the reaction heat without combustion. Specifically in the case of $TiB_2$, the use of diluents (pre-reacted $TiB_2$ or inert material) has also been shown to delay and, above certain volume fractions, suppress combustion [77, 78]. Furthermore, the particle sizes of the boron and titanium have been shown to effect the kinetics of the combustion synthesis of $TiB_2$ [73, 77, 78].

Evidently, the rapid kinetics of the SHS reactions pose extreme experimental challenges. Holt and coworkers [77] suggested a solid-state mechanism rather than the participation of a liquid phase in the formation of $TiB_2$ based on the high activation energies they measured. This was also the conclusion of Popov and coworkers [78] who

observed in very careful experiments that thermal explosions only occurred when heating the Ti + 2B mixture to 1500 K, which is substantially below the melting point of titanium. They suggest that, in the formation of $TiB_2$, at least the first stages are controlled by diffusion in the solid state. An Arrhenius plot of the heat evolution rate versus temperature did not indicate any change in the range 1700-2200 K; thus, there does not appear to be any change in the reaction mechanism caused by the melting of titanium. This offers an interesting contrast with other examples where the "ignition temperature" can be correlated to melting of one of the phases. For example, in the SHS of $Ni_3Al$ some solid state reaction is observed at low temperature and the "ignition" is associated with the melting of the Al-rich eutectic [79]. Also, in the reaction of Ni-Al "foil sandwiches," the ignition appears to occur only when both metals are in the liquid state [80]. Anselmi-Tamburini and coworkers [80] speculated that the different behavior observed in comparison with the reaction of Ni-Al powders may be due to the different heat conduction conditions due to the foil morphology, as well as to the significant differences in surface-to-volume ratios.

When producing $TiB_2$ using various combinations of precursors, Itoh and coworkers [73] monitored the relative X-ray intensity of the different phases formed after holding the reactants at increasing temperatures for varying times. In the case of $TiB_2$ a holding time of 60 minutes at 1100 to 1200°C, depending on the reactants used, was required to achieve a relative intensity of 20% of that of the completely reacted powders. Sigmoidal curves were observed, as expected, for the extent of reaction, as measured by the relative intensity versus temperature or time.

In an attempt to elucidate the reaction of Ti and B, Neronov and coworkers [81] performed *in-situ* TEM analysis of particles of one of the reactants placed on top of films of the other. In their experiments the heat generated by the electron beam was used to initiate the reaction. When a titanium particle was placed on top of a boron film, they observed that the interaction only started after the metal was partially melted. They

identified the formation of a reaction layer between the particle and the film but also noticed appreciable transport of titanium through the gas phase, since liquid drops were observed away from this interface. Based on their inability to identify $TiB_2$ in this interaction zone, they proposed that the reaction proceeds through the formation of other borides, such as TiB and $Ti_3B_4$ and that the diboride is only formed in the final stages of the process. When a boron particle was placed on a titanium film, transport through the gas phase was also observed. However, diffraction patterns obtained from the interaction layer could not be indexed to any known phase in the Ti-B-O system. Based on these data, they postulated that the reaction only starts when either liquid Ti or the Ti-rich eutectic (around 1540°C) is formed. This is followed by the formation of a two-zone product layer that separates the reactants; they proposed that the portion of the layer adjacent to the boron side is composed of $Ti_3B_4$ and liquid while the other zone consists of TiB, although this is not supported by their second set of experiments (boron particles vs. titanium films). In their conjecture, the reaction would proceed by the dissolution of titanium through the product layer and its further reaction with boron. They assumed that $TiB_2$ is formed only at later stages, when liquid titanium in the product zone becomes saturated with boron. Neronov and coworkers suggest that this mechanism is consistent with experimental observations of a plateau in the SHS of Ti-B mixtures, reportedly observed at 1650°C. There are several unexplained points in their argument, such as the influence of the enhanced vapor phase transfer observed in the high vacuum environment of the TEM as well as the inconsistency between the processes observed in the two types of experiments. Therefore, their proposed mechanism may not represent reality.

Lastly, in a technological study of the production of $TiB_2$ from titanium oxide, carbon and boron carbide, Levinskii and Petrov observed that 1h at 1600°C was the shortest practical thermal cycle to achieve total conversion [82].

Evidently, the understanding of the kinetics and mechanisms of the reaction between boron and titanium is not very clear, but some facts seem to be well established:

a) the activation energy for the reaction is probably high, and considerable reaction rates are only observed at temperatures above 1000°C; b) SHS occurs in undiluted Ti-B mixtures above 1500 K and apparently is controlled, over a large range of temperatures, by solid-state mechanisms, i.e., melting of one of the components is not critical for the reaction to proceed; c) the SHS can be prevented by dilution with inert material, as is the case in any SHS process; and d) powder size and morphology probably play a significant role in the overall kinetics.

### 2.3.3 Refractory Metal Reinforcements

Refractory metals have been identified as potential reinforcements for $MoSi_2$ since the work of Kehr [83] who studied the reinforcement of $MoSi_2$ with niobium. However, $MoSi_2$ and refractory metals interact resulting in the growth of intermediate layers of lower silicides at the interfaces; this has been well characterized by Fitzer and coworkers (e.g., [6]) who showed that interphase growth in refractory metal/$MoSi_2$ diffusion couples is controlled by silicon diffusion up to 1700°C. At that time, Kehr suggested that the Nb-$MoSi_2$ interaction could have a positive influence on properties by increasing the adhesion between the fiber and matrix phases and could explain the significant improvements observed in bending strength up to 1250°C and in room temperature toughness. However, a later study [84] demonstrated how significant toughening is obtained in these composites when debonding is promoted by the use of $MoGe_2$ as an additive to the matrix, the same compound Kehr used as a sintering aid.

More recently, several authors confirmed the interactions characterized by Fitzer (e.g., [85- 87]) and, in order to prevent these interactions, investigated the coating of the metal with an oxide diffusion barrier [87- 89]. Thus, $Al_2O_3$, $ZrO_2$ and $Y_2O_3$ coatings were applied to the refractory metals by different processes and it was observed that, when the coating was continuous and of sufficient thickness, such interactions could be

effectively prevented. Additionally, some oxide coatings promoted debonding causing a significant enhancement in toughness [87]. Both Xiao and Abbaschian [87] and Lu and coworkers [88] observed some localized coating degradation and proposed that this could be due to the effect of $SiO_2$ in the matrix. In any case, it seems that the main limitation to their approach of pre-coating the reinforcement is the unavoidable damage suffered by this coating during handling and consolidation. An interesting alternative to prevent this damage would be the production of interfacial barriers by *in-situ* reactions.

It is evident from the above discussion that, besides the reasons already mentioned in the previous section, $MoSi_2$ composites would also benefit from the elimination of silica due to the exclusion of interactions with reinforcements or protective coatings (e.g. $Al_2O_3$). It is also clear that second phases formed during *in-situ* processing may be closer to equilibrium with the matrix than artificially-introduced phases. This should result in significant advantages from the microstructural stability point of view.

In this work, the development and control of second phases in various $MoSi_2$-based model systems via *in-situ* displacement reactions is demonstrated. A basic condition for the design and control of *in-situ* processes is the understanding of the thermodynamics and kinetics aspects. Since reliable phase diagram and thermodynamic data are scarce for most systems of higher order and also for some binaries, techniques for the estimation of thermodynamic functions and thus of phase diagrams are important accessories in this design process, as described in the next section.

## 2.4 Phase Diagram and Thermodynamic Data

Thermodynamic and phase diagram data are crucial for the evaluation of *in-situ* reactions, as discussed above. In this section, the data available for the systems relevant to the present study are summarized, emphasizing their deficiencies; techniques for the estimation of these data are also presented.

2.4.1 Estimation of Phase Diagrams and Thermodynamic Data

The ability to know which phases will be in equilibrium in a given system at a certain set of conditions is essential to the design of *in-situ* processes, as well as to the evaluation of microstructural stability of materials. This information is available in the form of phase diagrams, which are fairly well established for most binary systems [90]. However, that is not the case in ternary and higher order systems, where the percentage of systems that is reasonably well characterized decreases dramatically with the increase in order [90]. Phase diagrams are unique representations of the thermodynamic functions of the phases involved and thus can be, in principle, constructed based on this knowledge. The converse, however, is not true and, as pointed out by Brewer [2] for instance, there is an infinite set of combinations of thermodynamic functions that will result in a given phase diagram. While several techniques are available to exclude impossible phase diagram constructions based on the behavior of the lower order systems (e.g., [91, 92]), presently there are only two ways to construct high order phase diagrams, namely, (a) the performance of the required equilibration experiments in conjunction with the methods mentioned above or (b) the calculation of the phase diagram based on the knowledge of the thermodynamic functions of the various phases. From a practical standpoint, a combination of methods (a) and (b) above is normally most effective. It is important to realize that the calculation of phase diagrams can reduce dramatically the number of equilibration experiments needed in most cases. As the order of the system increases and entropy plays an increasing role, the formation of quaternary or higher intermediate ordered phases is depressed to lower (and thus less important) temperatures [93] and the ability to calculate phase diagrams based on thermodynamic data acquired for lower order systems improves. One has to be aware, however, that, with the present state of knowledge, the ability to predict or calculate thermodynamic functions from first

principles is limited and a precondition for a reasonable prediction of higher order system are well established binary systems.

Methods of different complexity can be employed for the estimation of the thermodynamic functions of phases. In the case of intermetallics, for instance, when the phase diagram is known and the free energy of formation of only one of the phases is unknown, limits can be established for the unknown free energy of formation, based on the known values. In this technique, which is totally equivalent to the analysis of several viable and impossible reactions between compounds [94], one defines an upper and a lower limit for the unknown free energy of formation based on which equilibria are present and absent in the phase diagram. In the case of line compounds, the molal free energy of mixing can be derived directly from the free energy of formation of the compound. The knowledge of the free energies of formation of compounds can thus lead to the construction of a phase diagram via the concept of minimization of free energy or the "taut string" method [95]. While the knowledge of the phase diagram at a given temperature does not allow the derivation of the exact value of the free energy of mixing (or formation) of compounds for which it is not known, it may allow the establishment of ranges of possible values if data is available for other compounds. Figure 2.5a presents a simple example of a binary system A-B in which negligible solubility in the terminal phases and the existence of two line compounds ($A_2B$ and $AB_2$, for instance) is assumed.

Obviously, only compounds with negative free energies of formation can be stable; it is the relative magnitude of their free energies of formation that defines which phases will be present at equilibrium. Thus, if a third line compound AB is stable at a given temperature, the minimum magnitude of its free energy of formation can be estimated based on the values for $A_2B$ and $AB_2$ (Figure 2.5b). Alternatively, if AB is unstable (Figure 2.5c), the magnitude of its free energy of formation is limited by a maximum value established by the common tangent between the other two line compounds (Figure 2.5d).

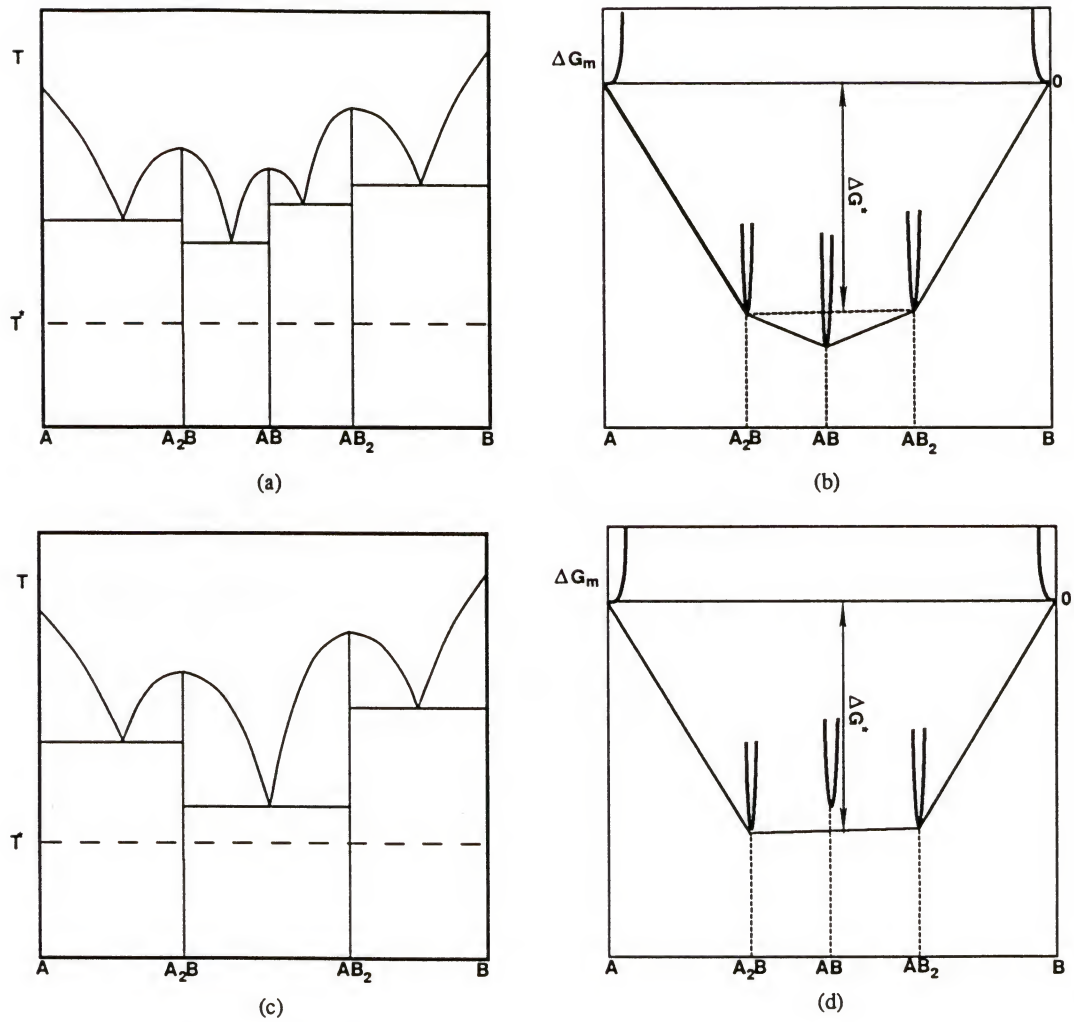


Figure 2.5 Hypothetical phase diagrams and corresponding free-energy vs. composition diagram for the AB system: (a) If AB is stable at $T^*$, the magnitude of its molal free energy of formation cannot be less than $\Delta G^*$ in (b). Conversely, if AB is not stable at $T^*$, as shown in (c), the magnitude of its molal free energy of formation cannot be greater than $\Delta G^*$, indicated in (d).

This approach is equivalent to the analysis of the thermodynamic viability of the following reaction:

$$^1/_3\ A_2B + {}^1/_3\ AB_2 = AB \qquad (2.2)$$

A shortcoming of this method is that its application to compounds with a variable composition becomes very complex.

Several interesting correlations have been established to predict enthalpies, entropies and free energies of formation of compounds. These are, unfortunately, quite imprecise and, in most cases, give only a first approximation. Kubaschewski and collaborators have summarized many of these correlations in [96]. The most powerful of the semi-empirical correlations presently appears to be "Miedema's model" [97] where heats of formation for transition-metal alloys are predicted based on two semi-empirical coordinates, the electron density at the boundary of the Wigner-Seitz atomic cell and the chemical potential for electronic charge. Their results show reasonable agreement with experimental values measured in several systems, but are not accurate enough to be used exclusively for phase diagram calculations.

Klingbeil and Schmidt-Fetzer developed an interesting approach in which they combined the values calculated in accordance with Miedema's model with the simple method of computing stable equilibria between line compounds using the free-energy change of displacement reactions to generate simplified ternary and quaternary phase diagrams [98].

The most complete and successful approach, presently, is the so-called computer assessment of phase diagrams. In this approach, a series description is adopted for the free energies of the different phases. Using experimental thermodynamic and phase diagram data, this series is adjusted to the data, through a least squares technique. This approach of the "computer calculation of phase diagrams" was first described in detail by Kaufman and Bernstein [99]. Presently, several approaches are available to confront

the two basic problems in this area, namely (a) the adjustment of series to the free energies of the different phases in order to minimize the error with respect to the selected experimental data, and (b) given the description of the free energy of all phases in a system, finding the equilibrium phases for a given set of conditions. As far as the first problem, the most efficient approach seems to be the one adopted by Lukas and collaborators [100]. This program, however, has limitations in the description of ternary and higher order phases [101]. The Thermocalc program, albeit less efficient in its least-squares fit routine, is the most complete as far as describing high-order systems as well as one of the most "user-friendly" and well documented, thus better suited for more pragmatic use.

When there is no composition dependence, series approaches such as that suggested by Kubaschewski for $C_p$ [96] or more complete ones such as the extension adopted by the SGTE (Scientific Group Thermodata Europe) [102] (when the available data justifies) can be used. To incorporate composition dependencies beyond ideal mixing, the excess free energy of mixing has to be described. The description first proposed by Hildebrand and also by Guggenheim [103] and presently known as the Redlich-Kister [104] model is the most widely accepted. In the case of a binary system, this series is given by a common factor $x_1x_2$ that multiply a power series of terms with the argument $(x_1-x_2)$ or $(1-2x_1)$, where the coefficients may be functions of temperature and pressure. The common factor guarantees that the excess term vanishes for the pure components, while the use of $(x_1-x_2)$ as an argument simplifies the presentation of the free energy as a function of either composition variable, and guarantees that the maxima for the different terms do not occur at the same composition value, minimizing the correlation of coefficients [105]. Other series are also available and can be directly transformed into each other in a binary system and, while a series of Legendre polynomials offers mathematical advantages (e.g., [100, 105]), the widespread adoption

of the Redlich-Kister polynomial is due to its ease in handling, according to Lukas and collaborators [100].

In order to describe ternary and higher order solutions based on data for the binary solutions, some criterion has to be established for predicting and representing the properties of the higher order phases as a function of those of the lower order systems. Various empirical methods are available as reviewed by Hillert [106] and Ansara [107]. All involve the selection of a certain composition in each of the binaries from which the binary excess properties are calculated; a weighing factor applied to these values is then used to estimate the free energies of the ternary phases. Figure 2.6 summarizes the three most common methods (Kohler, Colinet and Muggianu) as applied to a ternary system. Since the models are empirical, there is ample room for discussion as to which is the more adequate to fit real systems (e.g., [108]). Lukas proposes two principles for the evaluation of these models, namely (a) that the three components (in a ternary) should be treated in the same way and (b) that if in an A-B-C system, B and C become equal, the model should reproduce the A-B binary over the whole ternary. These principles are conflicting and only asymmetrical models [106, 109] can satisfy condition (b) by treating one component differently from the others, and thus fail to satisfy condition (a). Evidently, all models are built in a way that when the concentration of one of the components vanishes, the remaining binary is reproduced. Following a suggestion by Hillert [106], the Muggianu method is selected in Thermocalc [110] and in this work.

Albeit different formalisms can be used to describe ordered phases [111], the resulting mathematical expressions describing their thermodynamic functions are quite similar and, in some cases, equivalent. These mathematical similarities extend even to some of the models known as "associated solution models" [112]. From the simple mathematical point of view, the most complete model is the "sublattice" model, as described by Hillert [112- 114].

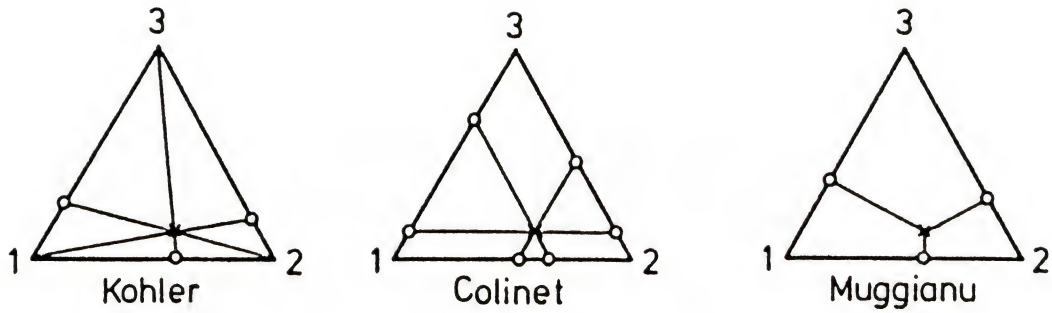


Figure 2.6 Illustration of some methods of predicting ternary properties based on binary ones. The properties of the binary compositions indicated on the triangle sides are weighted to obtain the corresponding property of the ternary composition. Adapted from ref. [107].

2.4.2 Silica Modification with Aluminum

The relevant systems in this case are the Mo-Si-Al and the $SiO_2$-$Al_2O_3$ systems.

2.4.2.1 The Mo-Si-Al system

Binary phase diagrams. The Mo-Si phase diagram (Figure 2.1), as discussed previously, is reasonably well established if the absence of the $MoSi_2$ $C11_b$ to C40 transformation is accepted, while the Al-Si diagram may be considered well established with a simple eutectic and no stable intermediate compounds. There are significant discrepancies in the currently accepted diagrams for the Mo-Al system as shown in Figure 2.7. Not only are different phases reported in the two versions of the diagram, but also there is no agreement in some of the invariant transformations. Table 2.3 presents the data for the invariant temperatures in this system.

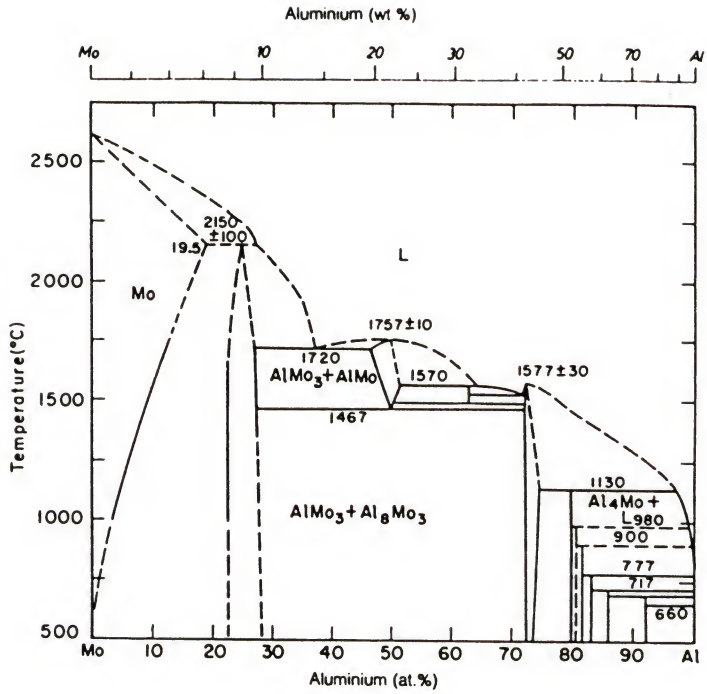


(a)

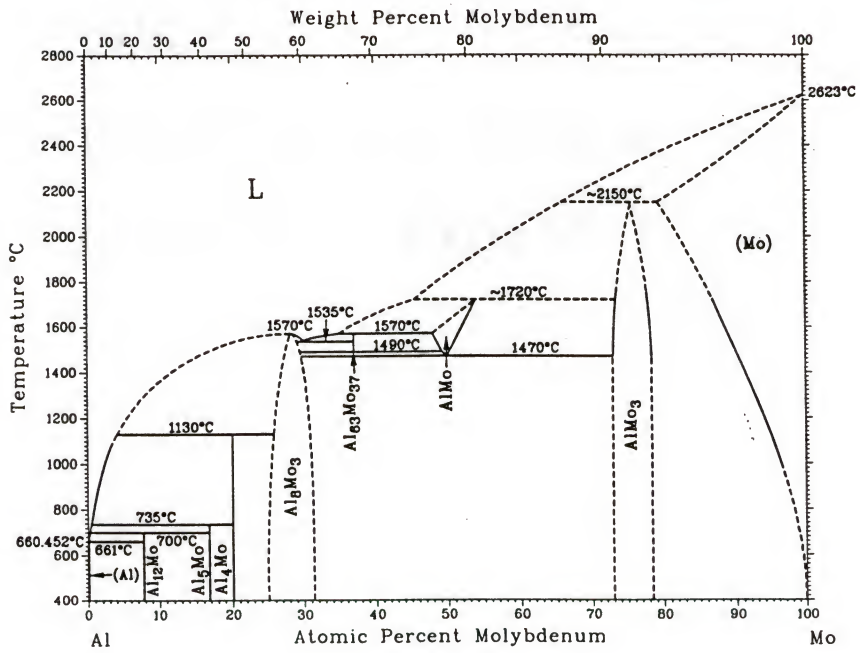


(b)

Figure 2.7 The Mo-Al Phase Diagram. (a) From Brewer [2]. (b) From Saunders [115].

Table 2.3 Special Points in the High-Molybdenum Range of the Al-Mo System.

| Reaction | Temperature (°C) | Reaction Type | Reference |
|---|---|---|---|
| L+Mo = $Mo_3Al$ | 2150±100 | Peritectic | [2, 115] |
| L+$Mo_3Al$ = MoAl | 1720 | Peritectic | [115] |
| L = MoAl + $Mo_3Al$ | 1720 | Eutectic | [2] |
| L = MoAl | 1757±10 | Congruent | [2] |
| L + MoAl = $Mo_{37}Al_{63}$ | 1570 | Peritectic | [2, 115] |
| L = $Mo_3Al_8$ | 1577±30 | Congruent | [2] |
| L = $Mo_3Al_8$ + $Mo_{37}Al_{63}$ | 1535 | Eutectic | [2, 115] |
| $Mo_{37}Al_{63}$ =$Mo_3Al_8$ + MoAl | 1490 | Eutectoid | [2, 115] |
| MoAl =$Mo_3Al_8$ + $Mo_3Al$ | 1470 | Eutectoid | [2, 115] |
| MoAl =$Mo_3Al_8$ + $Mo_3Al$ | 1467 | Eutectoid | [2] |

Ternary isotherms. Two isotherms are currently available for the Mo-Si-Al system (Figure 2.8): the 1600°C isotherm proposed by Brukl and collaborators [116] and its modification at 1550°C proposed by Yanigihara and coworkers [117]. The recent review of this system by Guzei [118] does not add any relevant information. Yanigihara and collaborators attempted to correct the use of "$MoAl_2$" as a stable phase by Brukl by sketching an equilibrium between C40 and $Mo_3Al_8$. However, this equilibrium led to the elimination of the C54-$Mo(Si,Al)_2$ phase observed by Brukl and which, based on the evaluation of several other silicide systems [119-122] is likely to be present in this ternary. Besides, they omit the $Mo_{37}Al_{63}$ phase that should be present at 1550°C in accordance with the accepted Mo-Al binary diagram proposed by Brewer [2]. The most interesting contribution in the Yanigihara isotherm is the proposal of a new set of tie-lines between the C40 and $Mo_5Si_3$ (T1) phases; these are more plausible than the ones proposed by Brukl and coworkers.

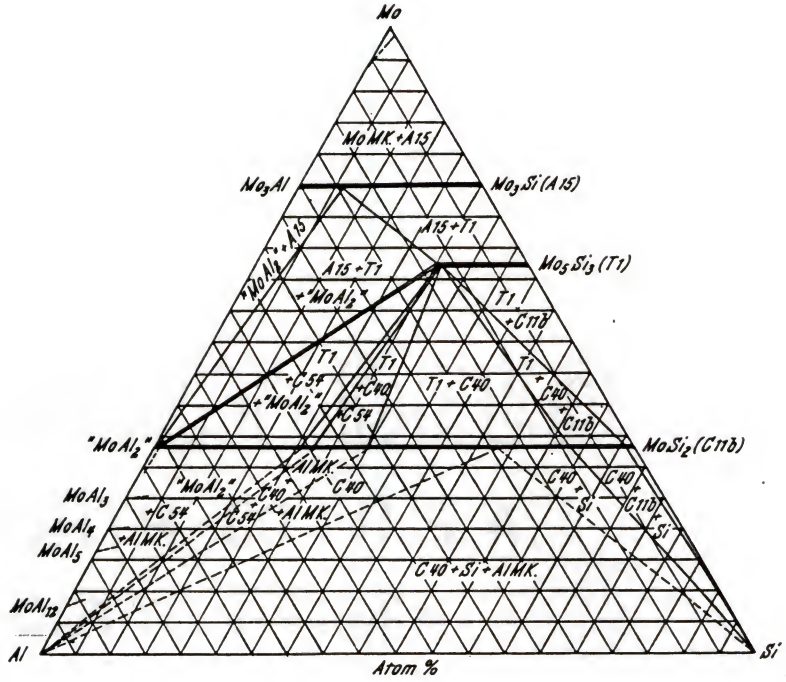


(a)

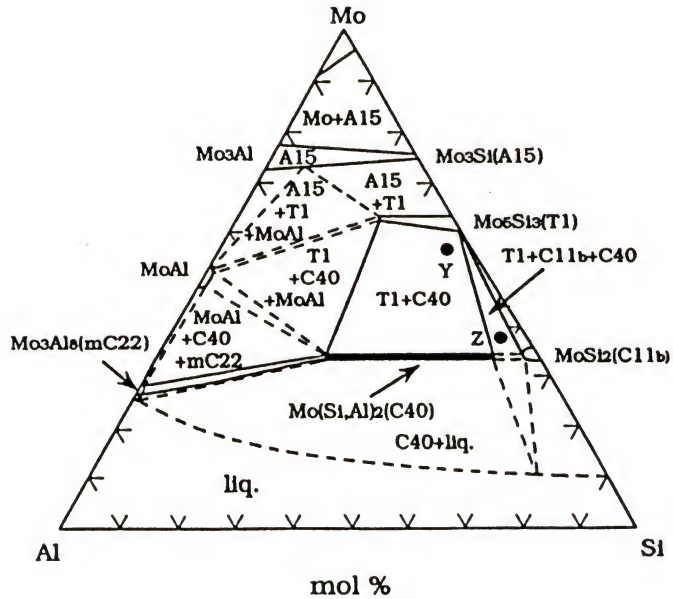


(b)

Figure 2.8 (a)The 1600°C Mo-Si-Al isotherm proposed by Brukl and collaborators [116] and, (b) its modification at 1550°C proposed by Yanigihara and coworkers [117].

It is apparent from the shape of the phase fields for $C11_b$-$MoSi_2$, C40-$Mo(Si,Al)_2$, C54- $Mo(Si,Al)_2$ and T1-$Mo_5Si_3$ that aluminum substitutes for silicon in its sub-lattice in each of these structures. This is also supported, at least in the case of C40-$Mo(Si,Al)_2$ where measurements are available as a function of composition, by the lattice parameter data of Brukl and collaborators [116].

The Mo-Si-Al system highlights the interesting possibilities created by the solution of an element used to displace oxygen from silica in $MoSi_2$ and the corresponding effects on its properties as well as the production of a matrix composed of more than a single silicide, e.g., the production of mixtures of the C40 ($P6_222$) $Mo(Si,Al)_2$ and the $C11_b$ $MoSi_2$ (with dissolved aluminum) phases, as well as the production of a single-phase silicide with variable stoichiometry depending on the amount of aluminum added. The C40 phase may have interesting mechanical properties [123] and has been shown to have excellent oxidation resistance [117, 124] despite early conflicting reports [7]. Furthermore, a silicide of variable stoichiometry makes possible the consideration of other *in-situ* displacement processes such as the generation of coatings in reinforcements, as discussed in the next section.

Thermodynamic properties: Mo-Si. Chandrasekharaiah and coworkers [125] have recently surveyed and assessed the thermodynamic properties of several disilicides, including $MoSi_2$. Schlesinger [126] has reviewed the thermodynamic data of a large number of transition metal-silicon systems, presenting recommended data for each of the compounds; although he analyzed a large number of references, in most cases the justification for his recommendations is unclear. Previously, Brewer [2] had summarized the properties of molybdenum compounds, including those with silicon, and Chart had assessed the thermochemical data for several metal silicides in the early seventies [127, 128]. Table 2.4 presents a summary of the experimental data available for the different silicides of molybdenum, including the most recent values of O'Hare [49] for $MoSi_2$.

Table 2.4 Summary of Thermodynamic Data for Mo-Si Compounds.

| Compound | $-\Delta H^0_{298}$ (KJ/g-at) | $\Delta S^0_{298}$ (J/g-at K) | Method | Reference |
|---|---|---|---|---|
| $MoSi_2$ | 43.7 ±3.3 | | Calorimetric | [129] |
| $MoSi_2$ | 45.7±1.3 | -(1.0±0.1) [a)] | Calorimetric | [49] |
| $MoSi_2$ | 47.3±1 | | Calorimetric | [130] |
| $MoSi_2$ | 44±3 | | Assessment | [127, 128] |
| $MoSi_2$ | 43.9 | -0.42 | Knudsen cell/ assessment | [131] |
| $Mo_5Si_3$ | 38.7 | 1.0 | Knudsen cell/ assessment | [131] |
| $Mo_3Si$ | 29.1 | 0.4 | Knudsen cell/ assessment | [131] |

Notes:
a) Assumed to be the same as for $WSi_2$.

Arpaci and Froberg [132] measured the enthalpies of mixing of Mo-Si liquids containing up to 0.4 mole-fraction of silicon using levitation calorimetry around 3000 K, while Sudavtosva and coworkers [133] reported enthalpies of mixing for dilute solutions of molybdenum in silicon without giving details of their experimental calorimetric method or the errors they expected.

Thermodynamic properties: Mo-Al. Brewer [2] reviewed the data available on the Mo-Al system in 1980 and estimated the enthalpies of formation of the molybdenum aluminides based on the emf measurements of Belyaeva and collaborators [134] and the calorimetric data of Dubrovin [135]. Although Brewer did not consider these data sufficiently accurate, he considered them useful in "fixing the strength of bonding in the Al-Mo phases". Shilo and Franzen [136] assessed the enthalpies of formation of $Mo_3Al_8$, MoAl and $Mo_3Al$, as well as the enthalpy of solution of aluminum in BCC molybdenum based on their Knudsen cell measurements. Recently, Meschel and Kleppa [137] measured the enthalpy of formation of $Mo_3Al_8$ and $Mo_3Al$ using a drop calorimeter. These results, as well as those estimated by Brewer for the molybdenum-rich aluminides are given in Table 2.5. As can be seen in Figure 2.9, the values are quite conflicting. In this study, the aluminum-rich aluminides (richer than $Mo_3Al_8$) are not considered

important since they occur out of the composition range of interest. Besides, in view of the conflicting data on these compounds, little can be gained by including them in the present analysis.

Table 2.5 Summary of Thermodynamic Data for High-Molybdenum Mo-Al Compounds.

| Compound | $-\Delta H^0_{298}$ (KJ/g-at) | $\Delta(G^0-H^0_{298})/RT$ (J/g-at K) | Method | Reference |
|---|---|---|---|---|
| $Mo_3Al_8$ | 48.9 | 0.6 | Assessment | [2] |
| $Mo_3Al$ | 50.4 | 0.2 | Assessment | [2] |
| $Mo_{37}Al_{63}$ | 48.8 | 0.5 | Assessment | [2] |
| MoAl | 49.4 | 0.4 | Assessment | [2] |
| MoAl | 31.3 | | Knudsen cell/ assessment | [136] |
| $Mo_3Al_8$ | 39.3 | | Knudsen cell/ assessment | [136] |
| $Mo_3Al$ | 21.4 | | Knudsen cell/ assessment | [136] |
| $Mo_3Al_8$ | 33.0 | | Calorimetric | [137] |
| $Mo_3Al$ | 22.3 | | Calorimetric | [137] |

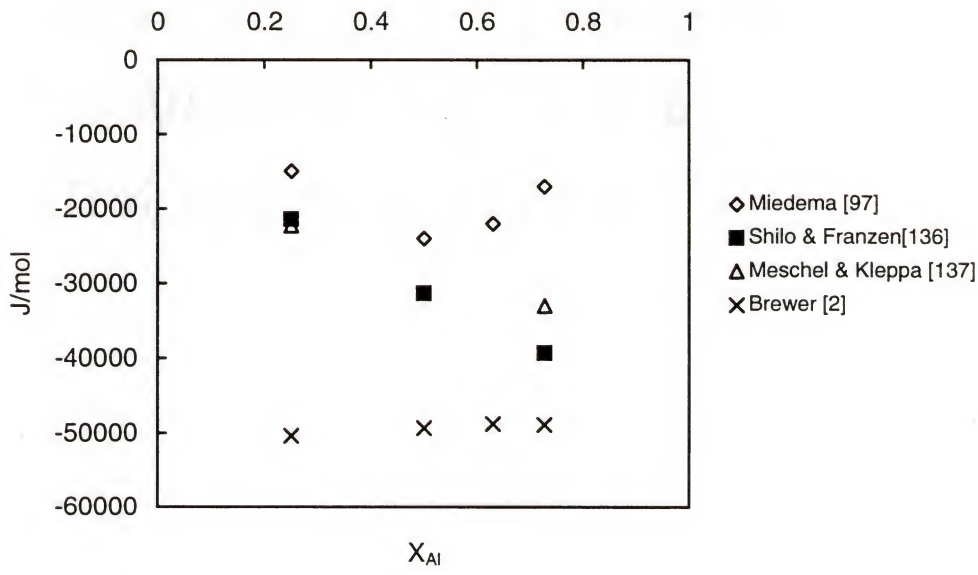


Figure 2.9 Reported molal heats of formation for high-molybdenum aluminides [2, 136, 137]compared with estimations based on Miedema's model [97].

Using emf measurements, Belyaeva and coworkers [134] reported in 1967 data for the molybdenum-aluminum system, including the aluminum-rich liquid, but Hultgren [138] and Brewer [2] considered their data so unsound as to be of little use. This may be due, in part, to their assumption of the exclusive presence of trivalent aluminum in the halide electrolytes used.

Thermodynamic properties: Si-Al. For the purposes of the present study the Si-Al system is considered well established and the description of Chakraborti and Lukas [139], based on that of Dörner and coworkers [140] is accepted. This is due to the fact that the data in this system is only used, in the present study, in the estimation of the Mo-Si-Al ternary.

### 2.4.2.2 The system $Al_2O_3$-$SiO_2$

Figure 2.10 shows the accepted silica-alumina phase diagram. An intermediate phase, mullite, is present at the composition $(Al_2O_3)_3\ (SiO_2)_2$. The Gibbs free energy of formation of mullite from the pure oxides is given by Kubaschewski [96]. Thus, the activity of silica can be shown to vary between unity and 0.26 in this system at 1400°C. This indicates that even in high alumina compositions, the activity of silica is rather high. This is further enhanced by the fact that in some cases mullite may not be formed, and metastable silica-alumina mixtures will be present for most of the solid compositions with a corresponding unit activity for silica.

### 2.4.3 Boride Formation through *In-situ* Displacement Reactions

In the case of generation of boride reinforcements through the use of *in-situ* displacement reactions, two systems are of importance in the present study, namely the Mo-Si-B and the Mo-Si-B-Ti, as described in the following sections.

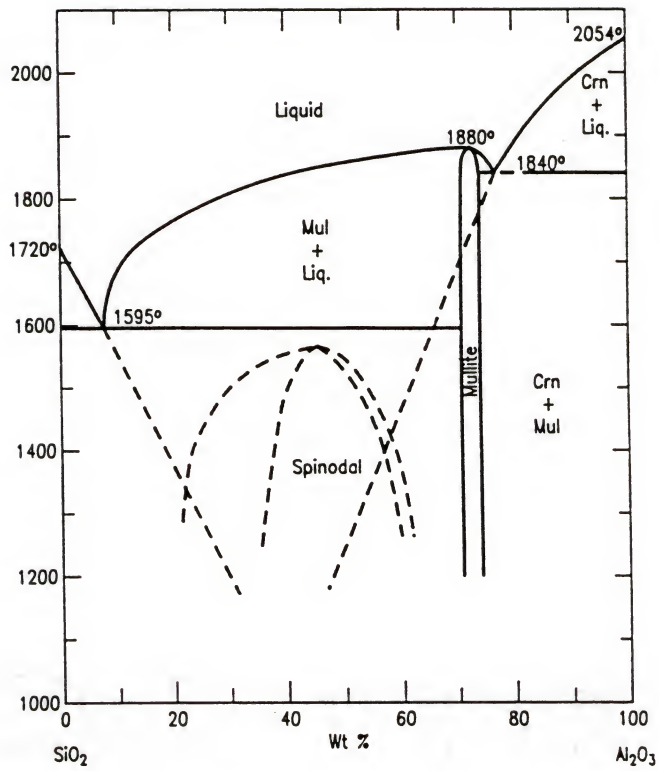


Figure 2.10 The silica-alumina ($SiO_2$-$Al_2O_3$) phase diagram [141].

2.4.3.1 The Mo-Si-B system

Binary phase diagrams

Two binary systems not previously discussed are relevant in this system, the Mo-B and the Si-B systems. Figure 2.11 presents the binary Mo-B as assessed by Brewer [2] as well as the calculated diagrams by Spear and Wang [142] and Kaufman [143]. There is good agreement in the main features of these diagrams. The most notable aspect is the very high melting point of the molybdenum borides. The Si-B system has been assessed by Olesinski and Abbaschian [144] and is presented in Figure 2.12 together with the

calculated diagram by Kaufman [143]. Most of the uncertainty in this diagram is in the boron-rich region, well out of the area of interest for the displacement reactions of this study.

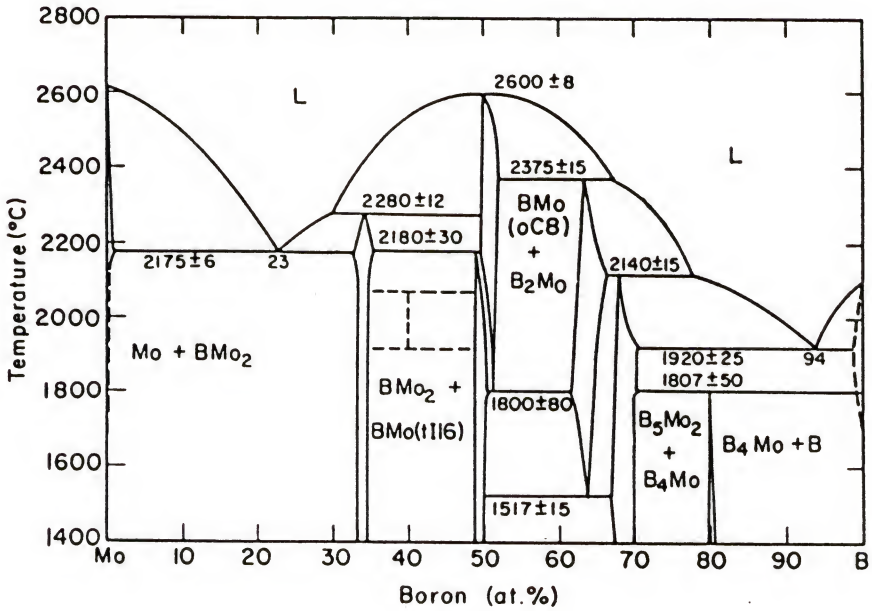


(a)

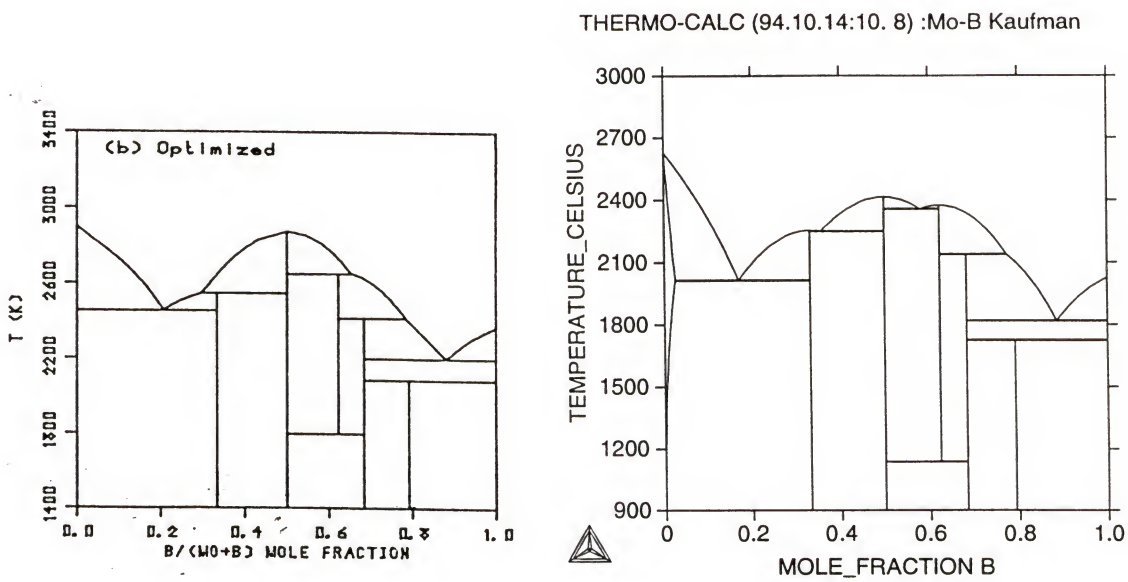


(b) (c)

Figure 2.11 The Mo-B Phase Diagram (a) assessed by Brewer [2], (b) calculated by Spear and Wang [142] and, (c) by Kaufman [143].

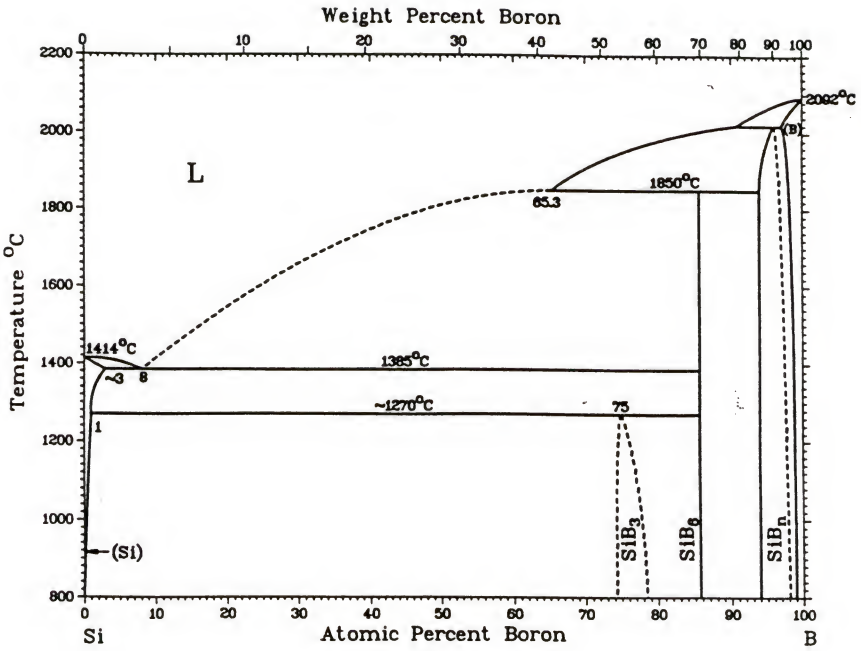


(a)

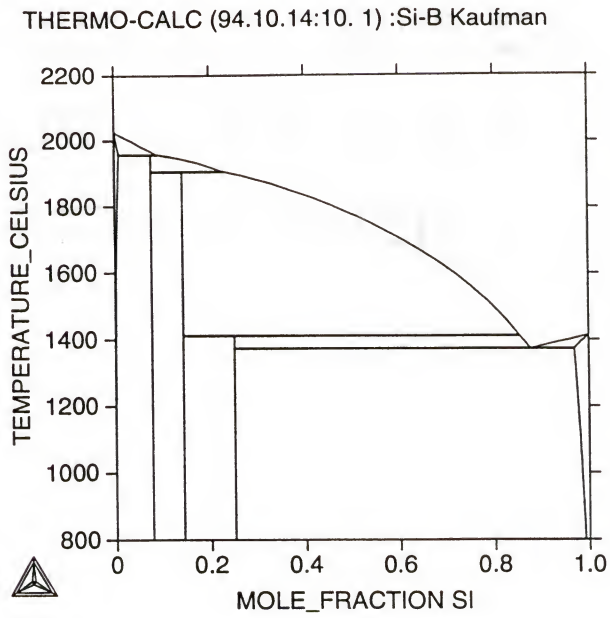


(b)

Figure 2.12 The Si-B Phase Diagram . (a) Assessed by Olesinski and Abbaschian [144] and, (b) Calculated by Kaufman [143].

Ternary isotherms. Nowotny and coworkers [145, 146] studied the behavior of several transition-metal-silicon-boron systems. Their proposed 1400°C isotherm for the Mo-Si-B system is given in Figure 2.13. Besides the known binary phases, they include a ternary phase $Mo_5SiB_2$ which was confirmed and characterized later by Aronsson [147]. The extent of the solubility of silicon in the molybdenum borides, as well as that of boron in the silicides was not clearly established in these studies by Nowotny and collaborators. The single phase fields sketched in the isotherm are, thus, inexact estimates.

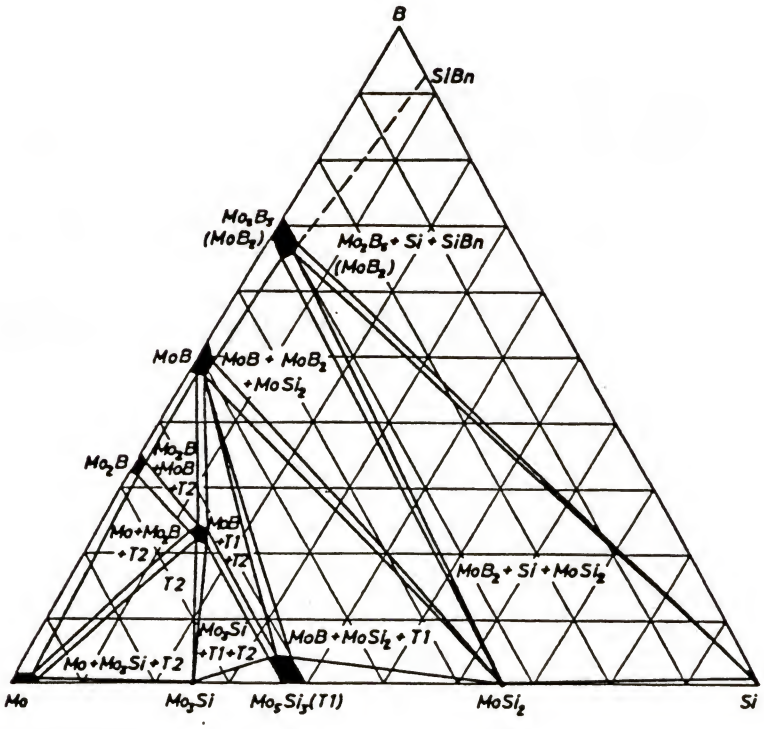


Figure 2.13 Proposed 1400°C isotherm for the Mo-Si-B system [145, 146]

Thermodynamic properties. For the extent of predicting the viability of displacement reactions between silicides and boron, the available phase diagram data are

sufficient, and, provided they are correct, no supplementary thermodynamic data are needed for this study.

#### 2.4.3.2 The Mo-Si-B-Ti system

In order evaluate the possibility of extending the displacement reaction approach to a quaternary system using thermodynamic knowledge, a large amount of information is required. Thus, additional binary and ternary systems must be known to some extent, at least, as well as the existence or absence of quaternary phases (somewhat unlikely, see section 2.4.4).

Binary phase diagrams. Murray has assessed the Mo-Ti [148] and the Ti-Si systems [151]. Kaufman [143] has used simple models to calculate their main features as shown in Figure 2.14. The Ti-B system has been assessed by Murray, Liao and Spear [65] and also calculated with the use of simple models by Kaufman [143]. These diagrams are compared in Figure 2.15. For the extent of the evaluations performed in the present study, these data were considered sufficient, as will be discussed in Chapter 4.

Ternary isotherms. Figure 2.16 presents the partial information in the Mo-Ti-Si system available from Svechnikov and Kocherzinsky [149] and Alisova and Budberg [150] who reported the presence of a ternary phase (with approximate compositions 45% at. Si, 20% at. Mo, close to the $Mo_5Si_3$ -$Ti_5Si_3$ two-phase field). This is the only data, besides that for the Mo-Si-B readily available in the literature.

### 2.4.4 The Third Phase in $MoSi_2$-SiC Composites

#### 2.4.4.1 The Mo-Si-C system

Binary phase diagrams. The three relevant binary systems Mo-Si, Si-C [152] and Mo-C [2, 153], are fairly well established. Table 2.6 presents a summary of the structures of the phases relevant to this study not previously described.

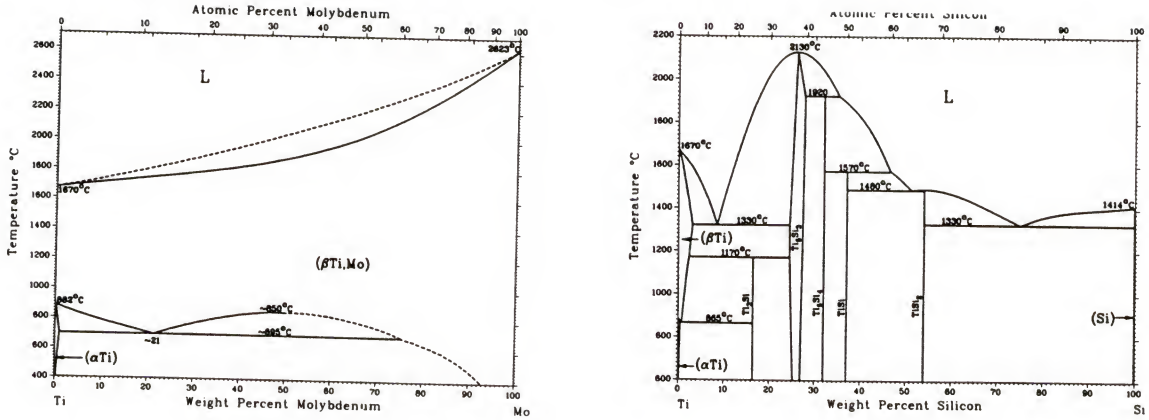


(a)

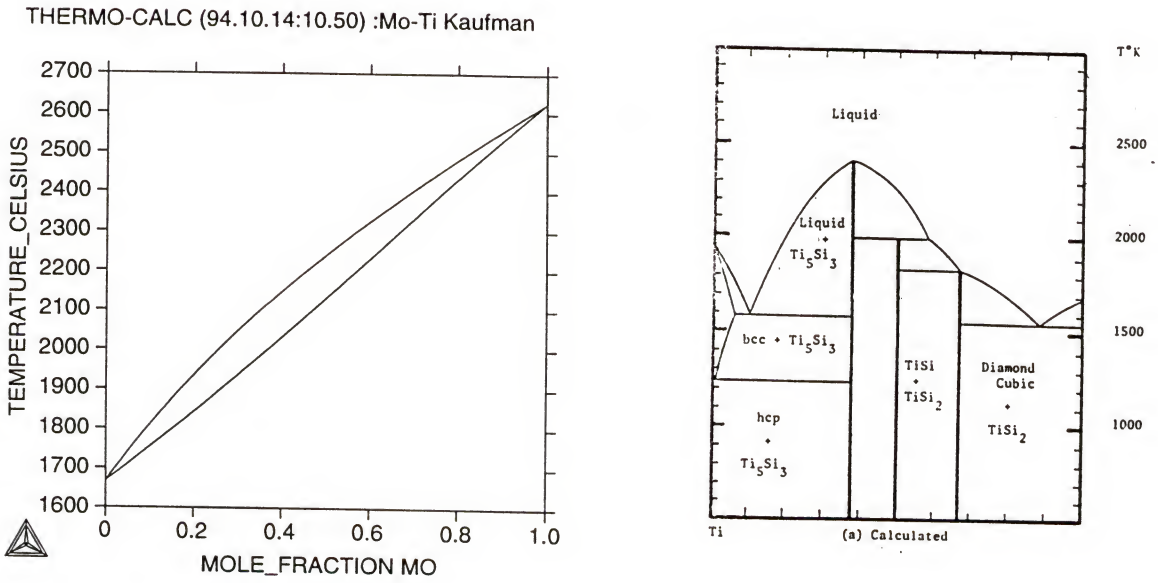


(b)

Figure 2.14 The Mo-Ti and Ti-Si Phase Diagrams. (a) Assessed by Murray [148, 151] and (b) calculated by Kaufman [143].

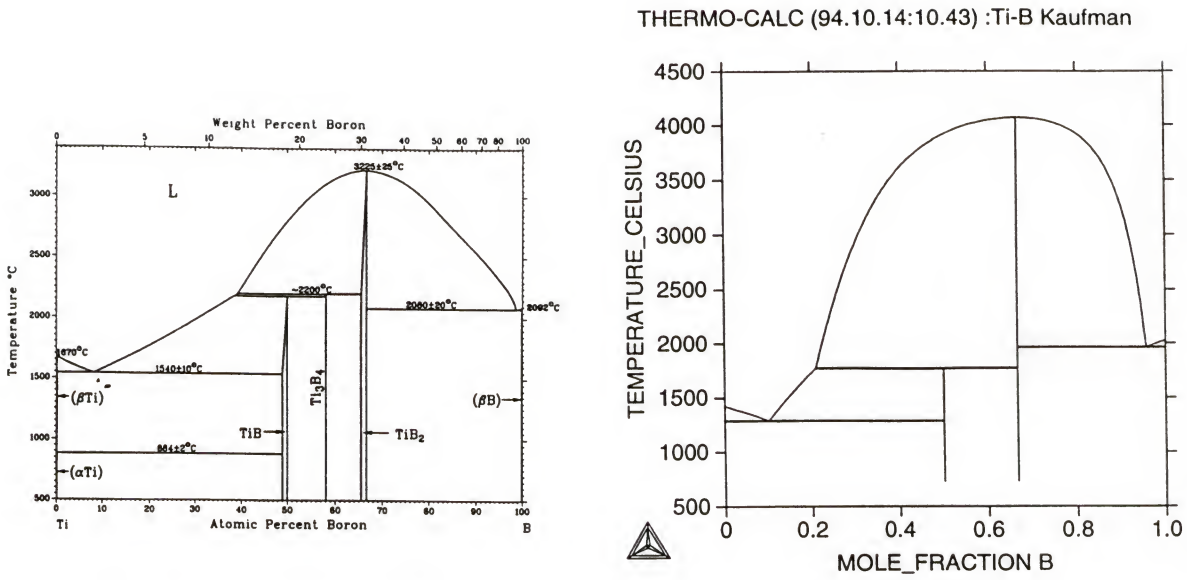


(a) (b)

Figure 2.15 The Ti-B Phase Diagram. (a) Assessed by Murray, Liao and Spear [65] and, (b) calculated by Kaufman [143].

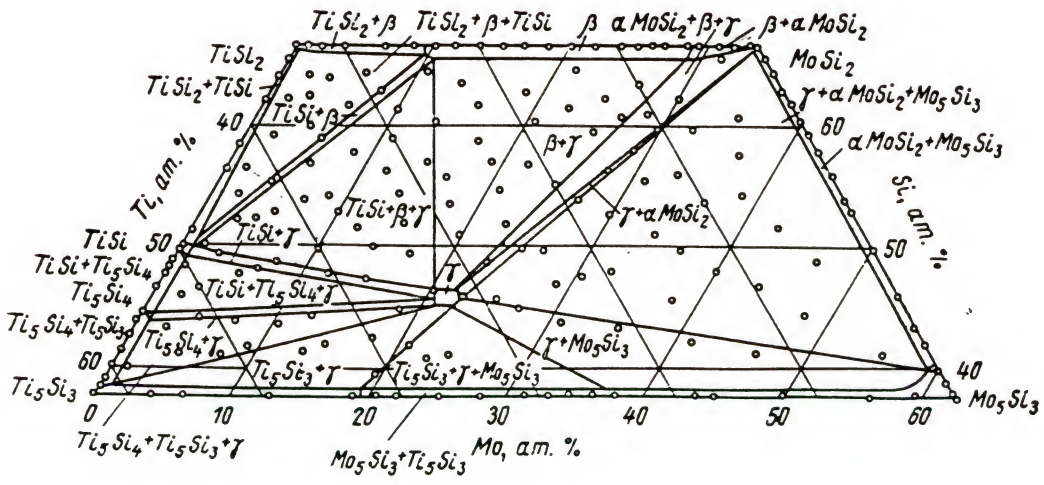


Figure 2.16 Partial 1250°C isotherm of the Mo-Ti-Si system [149, 150].

Table 2.6 Structural Information of Some Relevant Phases in the Mo-Si-C System.

| Phase | Strukturbericht Designation | Space Group | a nm | c nm | Reference |
|---|---|---|---|---|---|
| $Mo_{\leq 5}Si_3C_{\leq 1}$ | $D8_8$ | $P6_3/mcm$ | 0.7286* | 0.5046* | [154] |
| α-SiC | B4 | $P6_3mc$ | 0.3073 | 1.508 | [155] |
| β-SiC | B3 | F43m | 0.43596 | | [152] |

* These values vary considerably with carbon content.

Ternary isotherms. There is general agreement that only one ternary phase exists in this system, namely $Mo_{\leq 5}Si_3C_{\leq 1}$ , a Nowotny phase [154]*. There are two proposed isotherms for this system, which differ basically in the proposed phase relations in the composition region delimited by $MoSi_2$, SiC, $Mo_5Si_3$ and $Mo_5Si_3C$**. The first was proposed by Nowotny and coworkers in 1954 [45] after investigating the phase relations at 1600°C in the Mo-Si-C system via powder sintering followed by X-ray diffraction (XRD). The resulting isotherm, which was supported subsequently by Brewer and Krikorian [156], is presented in Figure 2.17a. Van Loo and collaborators [157] examined the phase relations at 1200°C using two different techniques: (1) arc melting followed by heat treatment and XRD, and (2) diffusion couples evaluated by electron microprobe and XRD. Figure 2.17b presents the 1200°C isotherm proposed by van Loo. As can be seen from Figure 2.17, there are several points of coincidence between both isotherms outside the composition range delimited by $MoSi_2$, SiC, $Mo_5Si_3$ and $Mo_5Si_3C$. It should be noted that Nowotny's isotherm presents MoC at 1600°C in disagreement with the presently accepted Mo-C diagram and $Mo_3Si_2$ instead of $Mo_5Si_3$ as presented in Section 2.1.

---

* The stoichiometries of the phases in the Mo-Si and Mo-Si-C systems proposed by Nowotny and coworkers [Nowotny, 1954 #340] and by Brewer and Krikorian [Brewer, 1956 #59], are not those presented in this work. The stoichiometries of these phases were only established later in the 1950's. For more details see [Parthe, 1965 #365] and the review by Gokhale and Abbaschian [Gokhale, 1991 #160].

** We refer to the ternary phase as $Mo_5Si_3C$ without explicitly mentioning its variable composition.

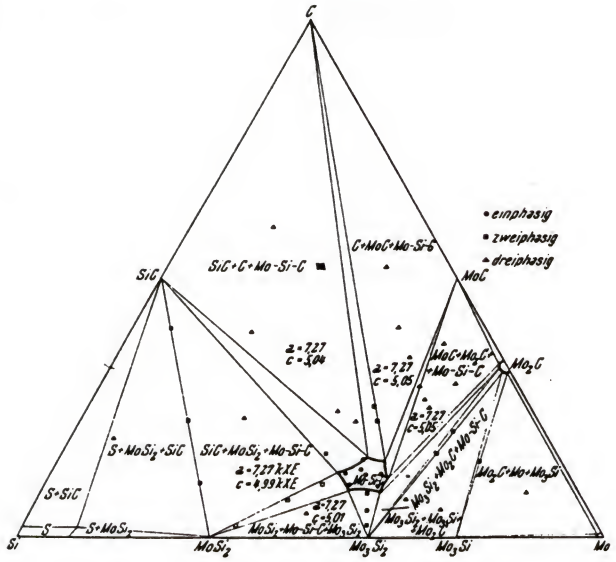


(a)

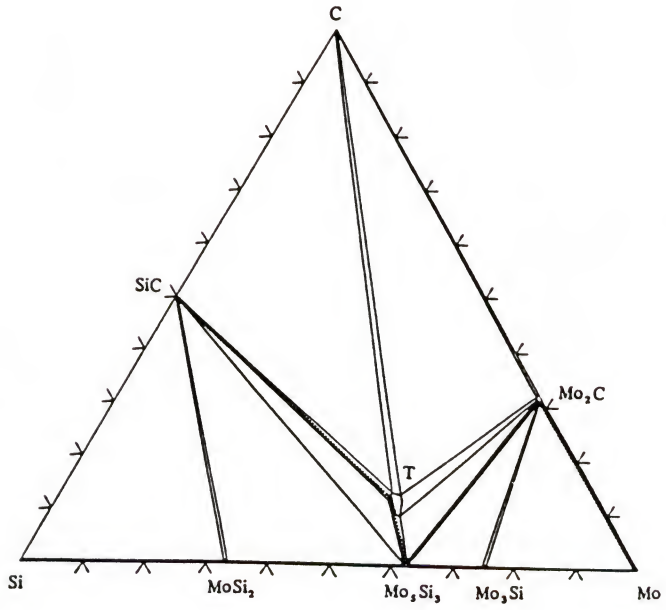


(b)

Figure 2.17 Proposed isotherm for the Mo-Si-C system (a) 1600°C, by Nowotny et al. [45]. (b) 1200°C by van Loo et al. [157]

Data from coating experiments. Additional information concerning the phase equilibria in the Mo-Si-C system can also be derived from the work of Steinmetz, Roques and Pichoir [158]. The objective of their study was to improve the stability of $MoSi_2$ coatings used to protect molybdenum from oxidation. Specifically, they attempted to prevent the loss of these coatings, caused by diffusion of silicon into the molybdenum, by introducing an intermediate layer of $Mo_2C$ between the silicide and the metal. Their experiments consisted of (1) siliciding previously carburized molybdenum samples and subsequently heat treating these specimens, and (2) producing bulk diffusion couples. The resulting phase distributions were evaluated by electron microprobe. Their data in the temperature range of 1200-1300°C are in general agreement with the 1600°C Nowotny isotherm. For example, a bulk $Mo_2C$-$MoSi_2$ couple formed an intermediate layer of $Mo_5Si_3C$ with SiC precipitates close to and at the interface between $MoSi_2$ and the Nowotny phase when heat treated for 8 h at 1250°C. Furthermore, when a molybdenum sample was completely carburized to $Mo_2C$ and subsequently silicided, an outer SiC+$MoSi_2$ layer formed. An anneal of 4 h at 1300°C was sufficient to develop a layer of $Mo_5Si_3C$ between the $Mo_2C$ substrate and this SiC+$MoSi_2$ layer. When shorter carburizing cycles were used, i.e., when only an $Mo_2C$ layer was developed, the response to the siliciding/annealing treatment depended on the thickness of the $Mo_2C$ layer. Specifically, if a sufficiently thick layer of $Mo_2C$ was produced on the Mo substrate, siliciding and annealing treatments resulted in the same layer sequence described above for a completely carburized substrate. If, however, the molybdenum carbide layer was thin, different results were obtained: for short times (0.25-1 h at 1300°C) a $Mo_5Si_3C$ layer developed between the outer SiC+$MoSi_2$ layer and the $Mo_2C$. Longer times (51 h at 1300°C) resulted in the replacement of the $Mo_5Si_3C$ layer by a layer of $Mo_5Si_3$ which eventually grew into interpenetrating $Mo_2C$-$Mo_5Si_3$. Apparently, van Loo and coworkers interpreted this latter result as evidence of SiC-$Mo_5Si_3$ equilibrium. Steinmetz indicated, however, that SiC was not present at the $MoSi_2$-$Mo_5Si_3$ interface and that porosity was

formed at this interface probably due to the participation of the SiC in the diffusion process.

It should be noted that the work by Steinmetz and collaborators was not aimed at establishing equilibrium phase relations in the Mo-Si-C system. For this reason, some of their data represent what is probably metastable equilibria and it appears that, in some cases, not all phases shown in their micrographs were identified. Thus, it is not recommended that phase equilibrium relations be derived from their data although it is informative to consider.

There is no *a priori* reason why both the 1200°C (van Loo) and the 1600°C (Nowotny) isotherms cannot be correct. The only requirement would be a four-phase equilibrium of the type $\alpha + \beta = \gamma + \delta$ (Class II according to Rhines [91]) at some intermediate temperature. However, as mentioned before, Jayashankar and Kaufman's $MoSi_2$-SiC alloys with average compositions in the region of interest show no evidence of this transformation and $Mo_5Si_3C$ is consistently retained to room temperature. Finally, the results of Steinmetz and coworkers also seem to indicate that $MoSi_2$, SiC and $Mo_5Si_3C$ are in equilibrium at 1200-1300°C. These results indicate that the Class II equilibrium may be absent and that the phase relations proposed by Nowotny may extend to lower temperatures.

Thermodynamic properties. Table 2.7 summarizes the free energy data selected for the calculations in the Mo-Si-C system, as well as their sources.

Table 2.7 Gibbs Free Energy of Formation Data for Phases in the Mo-Si-C system.

| Compound | $\Delta H^0_{298}$ (J/mol) | $\Delta S^0_{298}$(J/K mol) | Reference |
|---|---|---|---|
| $Mo_{0.75}Si_{0.25}$ | -29100 | 0.42 | [128] |
| $Mo_{0.625}Si_{0.375}$ | -38700 | 1.0 | [128] |
| $Mo_{0.333}Si_{0.667}$ | -43900 | -0.42 | [128] |
| $\alpha$-$Si_{0.5}C_{0.5}$ | -35773 | - 4.0375 | [159] |
| $\beta$-$Si_{0.5}C_{0.5}$ | - 36610 | - 3.975 | [159] |
| $Mo_{0.667}C_{0.333}$ | * | * | [153] |
| $Mo_{0.5}C_{0.5}$ | -16492 | -1.25 | [153] |

All values referred to the elements in their stable form at 298 K. For Si (s) = Si (l) $\Delta H^0$=50.2 KJ/mol $\Delta S^0$=29.797 J/K mol [159].

* The Gibbs Free Energy of $Mo_{0.667}C_{0.333}$ was described as (1/3)(-48300-7.25T-326000/T) according to the assessment of [153] .

# CHAPTER 3

# EXPERIMENTAL PROCEDURE

The samples used in this study were produced by arc melting and/or by vacuum hot pressing. When the liquid-solid equilibrium was to be studied molten alloys were held in contact with solid arc melted samples in refractory crucibles.

The starting materials for hot pressing were mixed by tumbling in glass or plastic vials or through the use of a high energy attritor (SPEX Mill) with a tool steel (AISI A2) vial and ball bearing steel (AISI 52100) balls, depending on the raw materials used and the desired results. All high energy milling was performed with a 0.05% addition of stearic acid as a milling aid. A ball-to-charge weight ratio of approximately 3.5 was used.

Vacuum hot pressing was performed in graphite dies, coated with boron nitride powder spray and lined with graphite paper, under a chamber pressure of less than 0.13 Pa. The hot pressing cycle consisted of a hold at 1400°C (+25, -20°C) for 1 h at a uniaxial compression stress of approximately 45 MPa. Typical heating time from room temperature was 0.5 h. Cooling was performed under vacuum, inside the hot press after the removal of the compacting stress. Cooling time to 700°C was around 0.5 h. After hot pressing, approximately 1 mm was removed from each surface to completely eliminate the region effected by the proximity of the die. All analyses were conducted after at least an additional 2 mm thickness was removed from the specimen surfaces. Except where otherwise indicated, hot pressing was performed in dies having an internal diameter of approximately 16 mm (5/8 in.).

The hot pressing temperature was monitored by measuring the die temperature with a two-color pyrometer. The pyrometer was calibrated by the manufacturer

(Capintec) and, in the range of temperatures in which the experiments were performed, its accuracy is +25 -20°C. To confirm the accuracy of this measuring technique, thermocouples calibrated by the manufacturer (Omega) were inserted in the die to within 3 mm from the sample and the temperature was simultaneously monitored using both techniques during hot pressing. In the temperature range of 780 to 1600°C, a linear correlation was found between the thermocouple and the pyrometer readings and the observed deviations did not show any bias and were within the experimental precision of the measuring and recording instrumentation used. To cover the different temperature ranges, Types K, C (W-5% Rh- W 26% Rh) and S thermocouples were used. Special care was taken to prevent the interaction between the thermocouple shielding and the graphite die. These experiments were conducted when hot pressing pre-reacted $MoSi_2$.

To verify if there were substantial temperature differences between the die and the *in-situ*-reaction samples, fine wire (250 μm dia.) Type C thermocouples were inserted in selected samples through a hole drilled in the bottom punch as shown in Figure 3.1. In order to prevent reaction of the sample with the thermocouple as well as the extrusion of the sample and thermocouple through the bottom punch during hot pressing, an alumina tube (3.2 mm dia.) was passed through the sample and into a hole drilled in the top punch; this minimized the resulting axial force on the thermocouple. The thermocouple joint was positioned inside the alumina tube in a position corresponding to the center of the final hot pressed sample. The thickness of the alumina wall separating the sample from the thermocouple was less than 500 μm. All surfaces exposed to the sample were coated with boron nitride while graphite paper was used as described previously. Due to some extrusion of the sample material into the gap between the alumina tube and the graphite punches, the thermocouple, as well as the punches, could be used only once with this arrangement.

The starting materials for arc melting were cleaned by mechanical grinding and chemical etching. Coarse raw materials (rods, lumps, etc.) were used to minimize oxygen

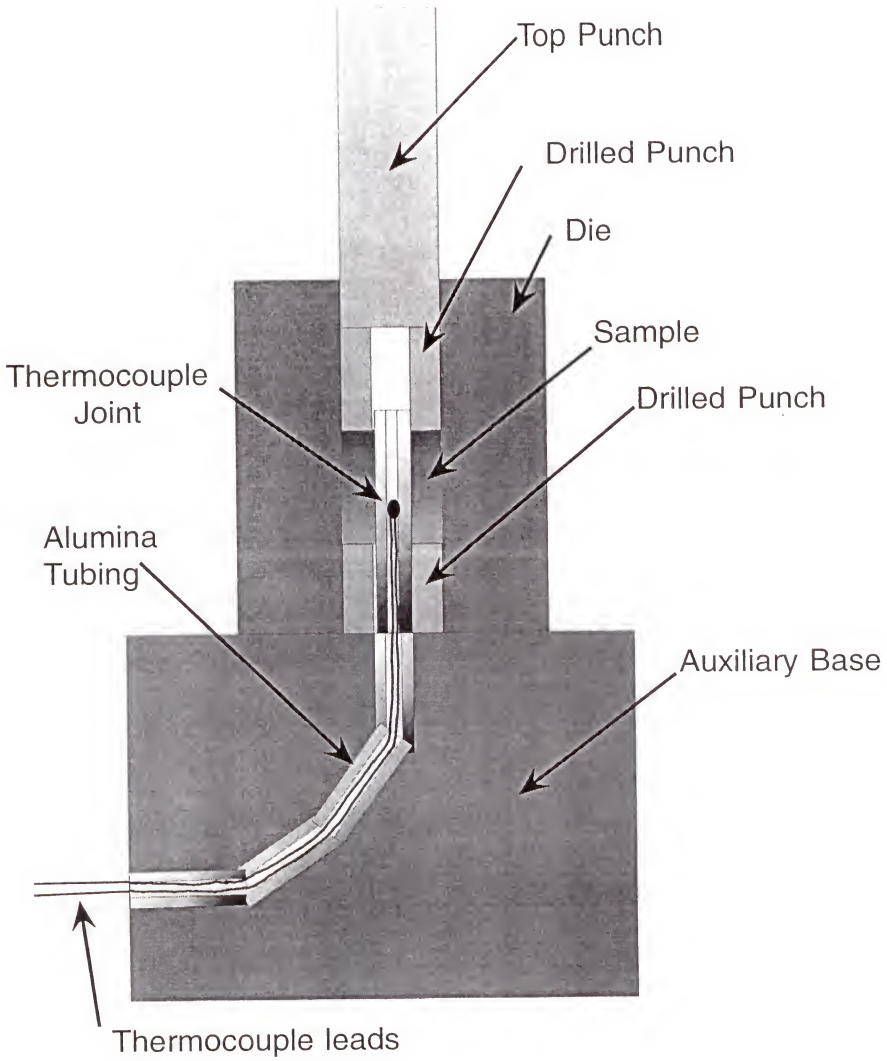


Figure 3.1 Schematic of the hot press die assembly for sample temperature measurement ("instrumented hot-pressing").

The starting materials for arc melting were cleaned by mechanical grinding and chemical etching. Coarse raw materials (rods, lumps, etc.) were used to minimize oxygen pick-up from surface oxides. Arc melting was performed under approximately 53.3 kPa (400 mm Hg) pressure argon gettered by flowing over a titanium charge heated to 900°C. Each sample was melted four to five times to ensure complete homogenization. Weight losses after five cycles of arc melting were less than 1%.

## 3.1 Raw Materials

Table 3.1 summarizes the relevant information on the raw materials used in this study.

Table 3.1 Characteristics of Raw Materials Used.

| Raw Material | Size | Purity (weight %) | Supplier |
|---|---|---|---|
| $MoSi_2$ (powder) | < 325 mesh | 99.9 | Johnson Matthey |
| Al (powder) | < 325 mesh | 99.5 | Johnson Matthey |
| Al (shot) | < 10 mm | 99.7 | Aesar |
| Mo (powder) | 4-7 μm | 99.5 | Johnson Matthey |
| Mo (rod) | 3 mm dia. | 99.7 | Johnson Matthey |
| Si (lumps) | < 10 mm | 99.9995 | Aesar |
| B (powder) | < 10 mm | 99 | Alfa |
| Ti (sponge) | < 5 mm | 99.5 | Johnson Matthey |
| Zr (powder) | < 325 mesh | 99 | Johnson Matthey |
| Nb (strips) | 1 mm thickness | > 98.5 | Teledyne |
| Nb (wire) | 250 μm dia. | > 98.5 | Teledyne |
| αSiC (powder) | < 325 mesh | 99.8 | Johnson Matthey |

## 3.2 Sample Production

### 3.2.1 Silica Modification

Samples for silica modification studies were prepared by mixing the reducing agent (Al or Zr) in powder form with commercial $MoSi_2$ powder. When large quantities of aluminum were added, molybdenum powder was introduced in order to maintain the proper Mo/(Si+Al) ratio of 1/2 in the matrix. The powders were mixed in plastic containers for at least 10 h. In the case of aluminum, samples were also prepared by mixing for 5 h in a SPEX mill.

### 3.2.2 Development of Second-Phase Reinforcements

Samples for the evaluation of the development of boride reinforcements via *in-situ* displacement reactions were prepared using boron powder, commercial $MoSi_2$ powder and arc-melted $Mo_5Si_3$, $Mo_3Si$ and $Ti_5Si_3$, as required. The powders were mixed in the SPEX mill for 5 h, except when the effect of milling time was to be evaluated. When elemental powders were used to produce equivalent compositions for comparison of microstructures, all other conditions were kept constant.

To prepare silicide-boron diffusion couples, pure $Mo_5Si_3$ was hot pressed, ground flat and put in contact with boron powder (<270 mesh) and again hot pressed. All hot pressing cycles were as previously described, except when longer holding times were used to evaluate the interaction kinetics. Finally, a sample was produced by mixing boron and $Mo_5Si_3$ powders (ground to approximately 50-70 μm) for 10 hours in a plastic container followed by hot pressing.

### 3.2.3 Equilibrium in the Mo-Si-Al System

Samples were arc melted with compositions in two- and three-phase fields of the proposed 1600°C isotherm and subjected to a first heat treatment of 50 h at 1400°C under flowing gettered argon, followed by air quenching. Portions of these samples were then subjected to a second heat treatment of 60 h at 1000°C, followed by air quenching. To verify if equilibrium had been achieved, two criteria were used, namely (a) that there were no measurable composition gradients in the different phases and (b) that for each phase the deviation between the results obtained in different portions of the sample were comparable to the deviation when the same region was analyzed several times. When equilibrium with the liquid phase was studied, either pure aluminum or arc-melted 60 % Al- 40% Si alloy were melted and held in contact for 5 to 10 h at 1000°C (+-10°C) with samples arc melted in the single phase $Mo(Si,Al)_2$ -C40 field.

3.2.4 *In-situ* Production of Second Phases from Glass-Fiber Precursors

E and S2 type glass fibers (Owens Corning) were used as precursors. Their characteristics are given in Table 3.2. Strands of these fibers were cut in short lengths and mixed with the appropriate powders for 10 h in plastic containers, to guarantee dispersion of the fibers in the powder.

Table 3.2 Characteristics of glass fibers used in this study.

| Composition ( at. %) | E Glass | S2 Glass |
|---|---|---|
| Al | 6.0 | 9.5 |
| Si | 20.4 | 21.5 |
| Ca | 7.2 | 0.0 |
| Mg | 0.2 | 4.2 |
| O | 66.2 | 64.8 |
| Diameter(μm) | 14-15 | 9-10 |

3.2.5 Production of *In-situ* Coatings in Nb fibers

Niobium strips or wire were oxidized under flowing oxygen at 500-600 $^{o}$C for 300-900 s following the procedure described by Lu and coworkers [160] and Doty and Abbaschian [161] to produce a typical $Nb_2O_5$ layer of approximately 5μm of thickness. Samples for evaluating the *in-situ* coating were prepared by dispersing approximately 20-30 pieces of the previously oxidized niobium wire with lengths of approximately 4-6 mm in a plane inside the powder to be hot-pressed. Typically, 8-12 fibers were found in each cross section prepared for metallography. Diffusion couples were produced by introducing the previously oxidized niobium strips into the powder mixtures before hot pressing.

## 3.3 Analytical Techniques

Samples were examined by optical metallography, scanning electron microscopy (SEM) equipped with an energy dispersive x-ray analysis system (EDS), electron microprobe, x-ray diffraction (XRD) and transmission electron microscopy (TEM) also equipped with an EDS system. Electron microprobe analysis (EMPA) was conducted using $Al_2O_3$, SiC, Mo, Nb, B and Ti as standards and a quantitative PRZ (PROZA) correction program. Only analyses resulting in a total weight percent (non-normalized) in the 98-102% range were considered acceptable for quantitative purposes. These values were then normalized to a total of 100%. For phase identification, results in the 97-103% range were accepted. When EMPA of carbon was performed, the results were used only for phase identification purposes, since the accuracy of this type of analysis for carbon limits its use for the establishment of phase boundaries in the phase diagram.

XRD phase identification was accomplished using both the JCPDS database[***] and diffraction patterns generated using the DIFFRACT II and the Desktop Microscopist softwares[****].

### 3.3.1 Metallographic Preparation (SEM and EDS)

Standard metallographic techniques were used to prepare samples for SEM and EDS. For all samples except those containing borides, grinding was done using silicon carbide papers up to 600 grit. Samples containing borides were ground on diamond wheels up to 12 μm grinding medium size. Polishing was accomplished with 6 μm diamond paste (or water suspension) followed, in most cases, by final polishing in colloidal silica. Samples were ultrasonically cleaned in a deionized water + detergent

---

[***] PC-PDF Card Retrieval/Display System and PDF-2 Data Base by JCPDS-ICDD, Swarthmore, PA.

[****] DIFFRACT II is a software written by M. E. Schlienger, J. T. Stanley and H.L. Fraser and distributed by MICRODEV Software, Evergreen, CO.

mixture after the final grinding and polishing steps, as well as in between all polishing steps. No etchants were used.

For the poorly-densified samples which were too fragile to withstand metallographic preparation (i.e., those obtained when hot pressing at lower temperatures for short times by "interrupted hot pressing"), impregnation with acrylic resin was performed prior to cutting and polishing. The acrylic resin was not removed after metallographic preparation.

### 3.3.2 Sample Preparation (XRD)

Mechanical alloyed powders were subjected to XRD without further comminution. Hot pressed samples were examined by XRD either as 1 mm thick slices cut with parallel faces from the hot pressed disks and ground to 400 grid (or 12 mm in the case of boride containing samples) or comminuted to finer than 200 mesh using mullite or alumina mortar and pestils. The former was the preferred method for boride containing samples, to reduce contamination from the comminution process.

### 3.3.3 Sample Preparation (TEM)

Slices 1 mm thick were cut from the hot-pressed disks either using an electric discharge machining unit (EDM) or a diamond saw. These slices were thinned down to 200-400 μm using the grinding techniques described above for metallographic sample preparation. Disks of 3 mm diameter were then cut from these slices and further thinned down to approximately 100 μm, using either 600 grit paper or 12 μm diamond grinding wheel as required. When required, a last thinning to 100 μm was accomplished with 6 μm diamond paste using a cylindrical tool in the dimpler. Final mechanical thinning was accomplished by dimpling using 6 μm paste to produce a thickness of 20 μm in the center of the dimple. The samples were then ion-milled until perforation using argon gas either

at constant current of 1 mA or at constant gun tension of 5 kV and a milling angle of 15-12°. The best results as far a homogeneity of thickness in the thinned region were obtained when the milling was done at constant voltage.

### 3.4 Room Temperature Hardness and Indentation Crack Fracture Toughness

Hardness and indentation crack fracture toughness were measured using 5, 7 and 10 kgf loads with a Vickers indenter on samples subjected to metallographic preparation. The hardness and fracture toughness were calculated in accordance with the formulae summarized in [162]. A linear dependence between the 1.5 power of the crack size ($c^{3/2}$) and load (P) was observed and the $c^{3/2}$ versus P plot went through the origin of the graph satisfying the criterion recommended by Sakai and Bradt [163]. Thus, the results were considered significant as an indication of $K_c$ .

# CHAPTER 4

# RESULTS AND DISCUSSION

## 4.1 The Third Phase in $MoSi_2$-SiC Composites

### 4.1.1 Thermodynamic Calculations

In order to evaluate which of the proposed isotherms (Nowotny or van Loo, as discussed in Section 2.4.4) is correct, the method described in Section 2.4.1 was extended to the ternary system Mo-Si-C. Values for the free energy of formation are available for all the compounds in this system, except $Mo_5Si_3C$. Using the methodology described, one can establish minimum and maximum limits for the magnitude of the free energy of formation of $Mo_5Si_3C$ and evaluate the consistency of these values with those required to support a given isotherm construction. Under the simplifying assumption that $Mo_5Si_3C$ can be considered as a line compound, two types of relations can be derived from the phase equilibria presented in a given isotherm. First, when a two-phase field exists between $Mo_5Si_3C$ and another phase such as graphite, all the other crossing two-phase fields (e.g. $Mo_2C$-SiC), shown as dotted lines in Figure 4.1a, are metastable with respect to this equilibrium. Since the thermodynamic functions for all the other compounds are known, one can calculate the minimum magnitude of the free energy of formation of $Mo_5Si_3C$, as indicated in Figure 4.1b. This follows from the application of the "taut string" concept to the ternary system.

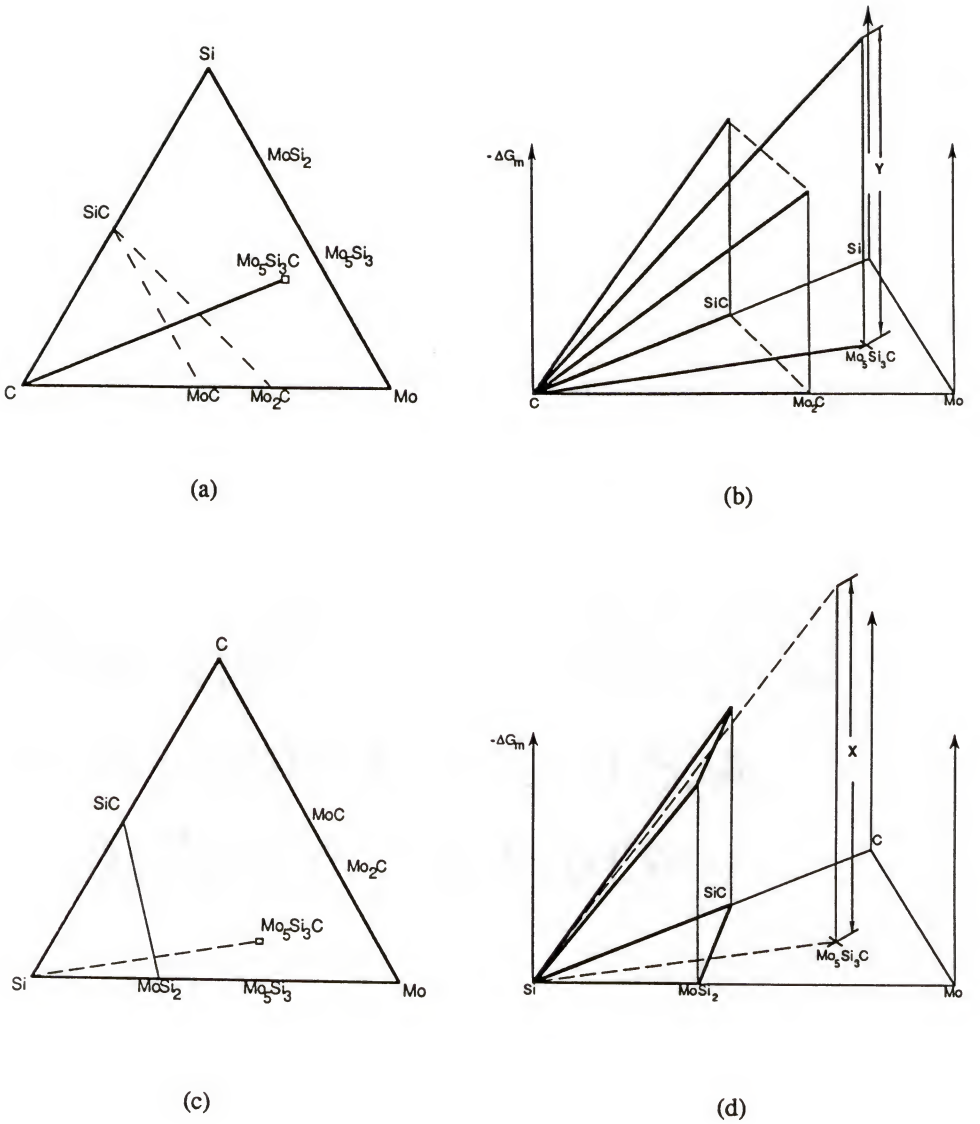


Figure 4.1 Schematic ternary isotherms and corresponding free energy plots illustrating the conditions for stability and metastability between phases. $-\Delta G_m$ is plotted along the vertical axis to make the visualization easier. If C and $Mo_5Si_3C$ are in equilibrium at a given temperature, the equilibria between SiC and MoC (or $Mo_2C$) must be metastable (a). The magnitude of the molal free energy of formation of $Mo_5Si_3C$ cannot be less than Y as indicated in (b). If SiC and $MoSi_2$ are in equilibrium at a given temperature, the equilibrium between Si and $Mo_5Si_3C$ must be metastable (c). The magnitude of the molal free energy of formation of $Mo_5Si_3C$ cannot exceed X as indicated in (d).

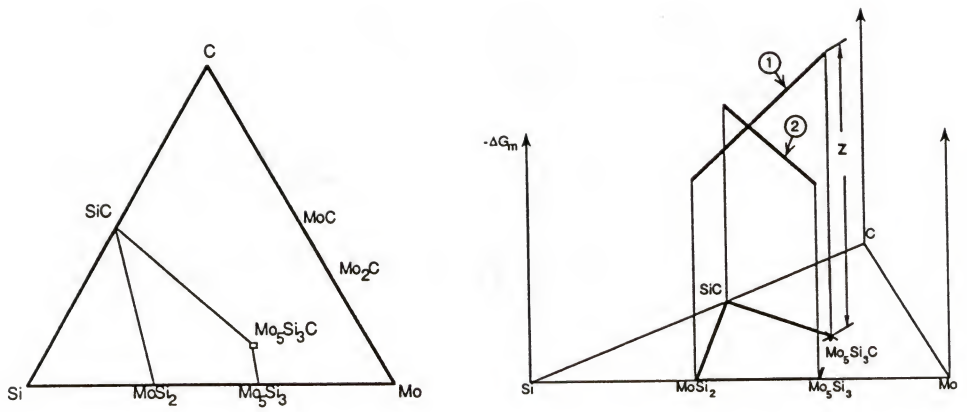


Figure 4.1 (continued) A critical magnitude of the molal free energy of formation of $Mo_5Si_3C$ for which SiC, $MoSi_2$, $Mo_5Si_3$, and $Mo_5Si_3C$ would be in equilibrium at a given temperature (e) can be derived when lines 1 and 2 intercept as indicated in (f).

On the other hand, if a possible two-phase field between $Mo_5Si_3C$ and another phase such as silicon does not exist, it is because it is metastable with respect to another two-phase equilibrium such as $MoSi_2$-SiC (see Figure 4.1c). By the same argument presented above, this leads to the calculation of a maximum magnitude for the free energy of formation of $Mo_5Si_3C$ (Figure 4.1d).

The application of this concept to all the independent possible equilibria (stable and metastable) in this system allows the establishment of maximum and minimum limits

for the magnitude of the free energy of formation of $Mo_5Si_3C$. These values can be derived as a function of temperature as presented in Figure 4.2. This figure was generated based on the data presented in Section 2.4.4. It is important to keep in mind that the results presented in Figure 4.2 are influenced by this data and its quality.

Additionally, one can define a critical value for the magnitude of this function that will discriminate between the 1200°C (van Loo) and the 1600°C (Nowotny) isotherms. This critical value is the magnitude of the free energy of formation of $Mo_5Si_3C$ that results in lines 1 and 2 intersecting as indicated in Figure 4.1f. If the actual magnitude of the free energy of formation equals this critical value, a Class II equilibrium exists between SiC, $Mo_5Si_3$, $MoSi_2$ and $Mo_5Si_3C$ at that temperature. If the actual magnitude exceeds this critical value, $MoSi_2$ and $Mo_5Si_3C$ will be in equilibrium, whereas in the opposite case, SiC and $Mo_5Si_3$ will coexist. This critical value is also plotted in Figure 4.2. Again, the derivation of this value is completely equivalent to the analysis of the viability of the reaction:

$$SiC + 8/7\ Mo_5Si_3 = 5/7\ MoSi_2 + Mo_5Si_3C \qquad (4.1)$$

The comparison of the maximum and minimum values established for the magnitude of the free energy of formation of $Mo_5Si_3C$ with this critical value for the four-phase equilibrium can lead to two results: (1) either the critical value falls within the possible range of values and nothing can be said about the equilibrium in question, or (2) it falls outside of that range, thus indicating that only one of the constructions is viable, i.e. either $MoSi_2$ coexists with $Mo_5Si_3C$ or SiC is in equilibrium with $Mo_5Si_3$, depending on whether the critical value is smaller than the minimum or larger than the maximum values established for this compound. Finally, this type of analysis provides a rough estimate of the free energy of formation of the Nowotny phase.

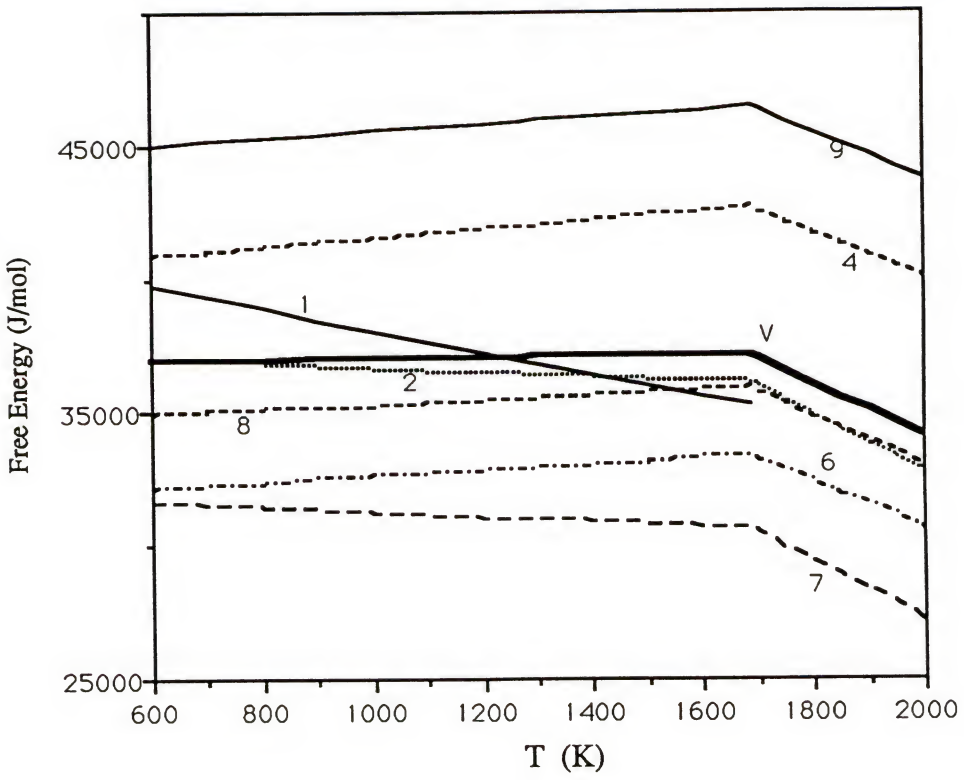


| Legend | Observed | Absent | Type of Limit |
|---|---|---|---|
| 7 | C-$Mo_5Si_3C$ | SiC-$Mo_3Si$ | Lower |
| 6 | C-$Mo_5Si_3C$ | $Mo_2C$-$MoSi_2$ | Lower |
| 8 | C-$Mo_5Si_3C$ | C-$Mo_5Si_3$ | Lower |
| 2 | C-$Mo_5Si_3C$ | SiC-$Mo_2C$ | Lower |
| 1 | C-$Mo_5Si_3C$ | SiC-MoC | Lower |
| 4 | $Mo_2C$-$Mo_5Si_3$ | Mo-$Mo_5Si_3C$ | Upper |
| 3* | SiC-$MoSi_2$ | Si-$Mo_5Si_3C$ | Upper |
| 9 | $Mo_2C$-$Mo_3Si$ | Mo-$Mo_5Si_3C$ | Upper |
| V | | | ** |

*Not shown in graph due to scale selection.
** This value is calculated for the hypothetical four phase equilibrium $Mo_5Si_3C$- SiC-$Mo_5Si_3$-$MoSi_2$. If the actual value is higher, the Nowotny construction is valid; the opposite case supports the van Loo isotherm.

Note: The slope changes at 1685 K correspond to the melting point of silicon.

Figure 4.2 Limits of the magnitude of the molal free energy of formation of $Mo_5Si_3C$ derived from equilibria observed and absent from the phase diagram.

Figure 4.2 shows that for temperatures above approximately 1000°C, the critical value falls between all calculated maximum and minimum limits. Thus both constructions are acceptable, as is the possibility of a Class II reaction. Below this temperature, the only equilibrium possible is $MoSi_2$- $Mo_5Si_3C$ since the critical value falls below a minimum limit. This indicates three possibilities:

1. There is no Class II reaction in the system and the Nowotny 1600°C isotherm is valid for all lower temperatures.

2. There are two Class II reactions in the system. There are two possible ways this can occur:

2.1 The Nowotny construction is valid at 1600°C and below to some temperature between 1600 and 1200°C, where the first Class II equilibrium occurs, as described by reaction 4.1. From this temperature down to some temperature between 1200 and approximately 1000°C the van Loo construction is valid. At this lower temperature the second Class II equilibrium occurs and again the Nowotny construction becomes valid.

2.2 Our basic assumption was that there is no other Class II reaction in this system and all the equilibria for which there is agreement between Nowotny and van Loo hold for all temperatures. If, however, we relax that condition, a second option is available. Specifically, the lower limit which is crossed at approximately 1000°C is established by the metastability of the SiC-MoC equilibrium with respect to the graphite-$Mo_5Si_3C$ equilibrium (further down at approximately 300°C the same happens with SiC-$Mo_2C$). If reaction 4.2 occurs somewhere above 1000°C, the limitation for the van Loo construction at lower temperatures disappears and both constructions can be valid at all temperatures (reaction 4.3 is equivalent to reaction 4.2 for $Mo_2C$).

$$7\ C + Mo_5Si_3C = 5\ MoC + 3\ SiC \qquad (4.2)$$

$$^9/_2\ C + Mo_5Si_3C = {}^5/_2\ Mo_2C + 3\ SiC \qquad (4.3)$$

Although the first possibility above is the simplest, one cannot, based on the thermodynamic arguments only, exclude the other possibilities. Consequently, experiments were conducted to evaluate the phase equilibria at 1550°C and 1200°C.

4.1.2 Equilibration Experiments

For the equilibration experiments at 1550°C, samples were hot pressed at 1550°C for 0.5 h. Since it was not possible to achieve densification via hot pressing at 1200°C for reasonable hot pressing times, the evaluation of the phase relations at 1200°C was performed on samples hot pressed at 1550°C and reheated to 1200°C (±15°C) for 50 or 100 h under flowing purified argon. A small number of samples was produced by arc melting selected compositions in the proposed three-phase fields.

Two types of powder mixtures were used, namely, a mixture of arc-melted $MoSi_2$ and $Mo_5Si_3C$ and one of arc-melted $Mo_5Si_3$ and commercial α-SiC powder. The first mixture should be in equilibrium at 1600°C according to the Nowotny isotherm and should react when the isotherm proposed by van Loo is applicable. The $Mo_5Si_3$ + SiC mixture should behave in the opposite way.

The microstructure and compositional data for the $Mo_5Si_3$ + SiC mixture after hot pressing are shown in Figure 4.3 and Table 4.1, respectively. The formation of $Mo_5Si_3C$ at the interfaces between $Mo_5Si_3$ and SiC is clearly evident as is the presence of some $MoSi_2$. These results were confirmed by XRD. Thus, it is clear that the time at the hot pressing temperature was sufficient for appreciable reaction. This result supports the validity of the Nowotny isotherm (Figure 2.17a) at the hot pressing temperature (1550°C).

There was no significant reaction after hot pressing the $MoSi_2$ + $Mo_5Si_3C$ sample although some small islands of $Mo_5Si_3$ were observed. These can be attributed either to some heterogeneity in the initial arc melted material or to the fact that the composition of

the $Mo_5Si_3C$ used was not in equilibrium with $MoSi_2$, i.e. was Mo-rich. This result is also in agreement with the Nowotny isotherm (Figure 2.17a).

Table 4.1 EPMA Results of Hot Presssed Samples with or without Subsequent Heat Treatment.

| Start Sample Material | Condition a) | Phase | Element (at%, normalized) | | |
|---|---|---|---|---|---|
| | | | Mo | Si | C |
| $Mo_5Si_3$ + SiC | HP | $Mo_5Si_3C$ | 54.6 | 34.5 | 10.9 |
| | | $Mo_5Si_3$ | 62.7 | 37.3 | 0.0 |
| $MoSi_2$ + $Mo_5Si_3C$ | HP | $Mo_5Si_3C$ | 56.9 | 36.8 | 6.3 |
| | | $Mo_5Si_3$ | 61.1 | 38.9 | 0.0 |
| $Mo_5Si_3$ + SiC | HP +HT | $Mo_5Si_3C$ | 57.0 | 34.9 | 8.1 |
| | | $Mo_5Si_3$ | 63.2 | 36.8 | 0.0 |
| $MoSi_2$ + $Mo_5Si_3C$ | HP +HT | $Mo_5Si_3C$ | 57.2 | 38.0 | 4.8 |
| | | $Mo_5Si_3$ | 61.4 | 38.6 | 0.0 |
| see note b) | HP or HP+HT | $MoSi_2$ | 32.0-34.5 | 65.5-68.0 | 0.0 |
| | | SiC | 0.0 | 48.0-51.5 | 48.5-52.0 |

Notes: a) See text for exact hot pressing and heat treatment conditions.

b)Whenever $MoSi_2$ or SiC was present the EPMA results obtained were within these limits.

In most cases, the XRD results indicated the presence of four phases after 50 h treatments. Initially, it was speculated that this might indicate insufficient time to achieve complete equilibrium. This condition, however, persisted in samples heat treated for 100 h. Metallographic examination revealed that the phase distribution was not what would be expected if an incomplete four-phase (Class II) solid-state reaction had occurred. Figure 4.4 shows the microstructure of a sample that was initially composed of $Mo_5Si_3$ + SiC. Its microstructure after hot-pressing was similar to that shown in Figure 4.3, i.e., $Mo_5Si_3$ surrounded by the Nowotny phase, formed by carbon pick-up from the SiC, and some $MoSi_2$. The corresponding EMPA results are presented in Table 4.1.

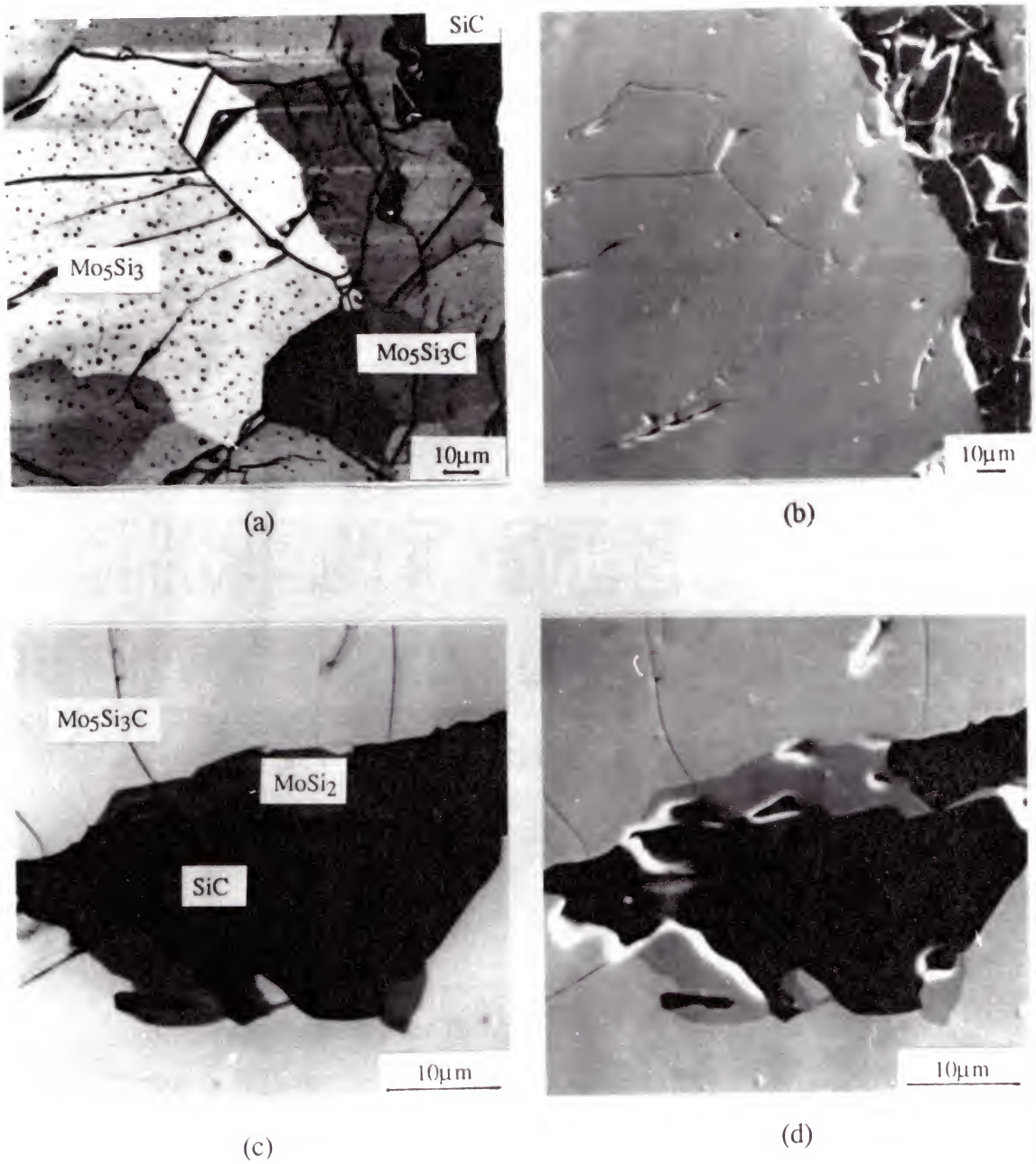


Figure 4.3 Microstructure of $Mo_5Si_3$-SiC mixture hot pressed at 1550°C for 0.5 h. (a) Backscattered electron image (BEI) (some light streaking is present due to the high contrast setting used). (b) Scanning electron micrograph (SEM) of the same area as in (a). (c) BEI of different region of the same sample. (d) SEM of same area as (c).

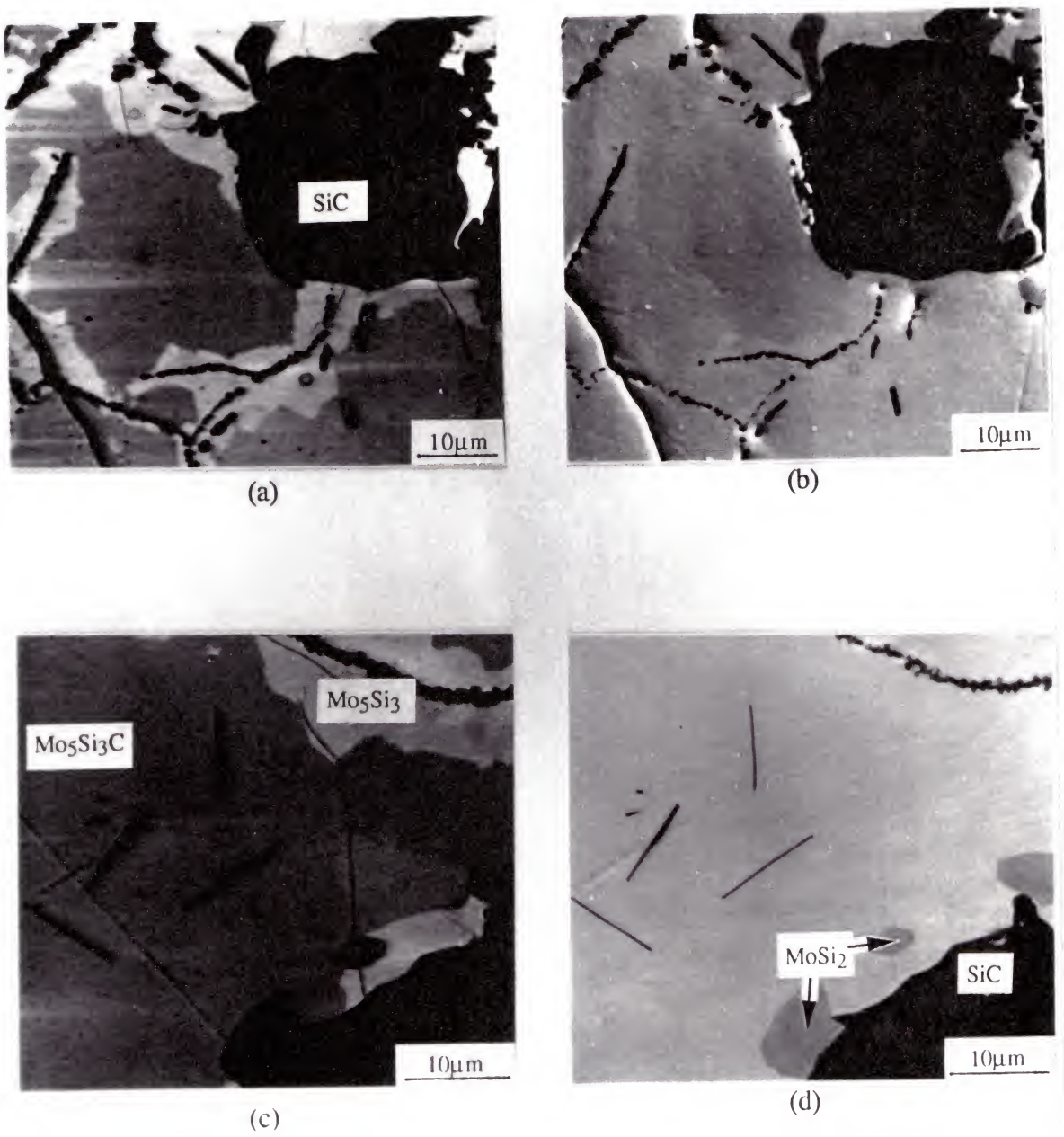


Figure 4.4 Microstructure of $Mo_5Si_3$-SiC mixture hot pressed at 1550°C for 0.5 h and heat treated at 1200°C for 100 h. (a) BEI (some light streaking is present due to high contrast setting used); black constituent is SiC or $MoSi_2$ (see (b)); gray constituent is $Mo_5Si_3C$ and liqht constituent is $Mo_5Si_3$ (see (c)); (b) SEM of same area as in (a); (c) BEI of different region of the same sample (Platelets are SiC); and (d) SEM of the same area as (c).

When analyzing the possible reactions, it is important to recall that the Nowotny phase is not of rigid stoichiometry as was assumed to simplify the thermodynamic calculations. Rather, a significant range of compositions can be expected, as discussed in Section 2.4.3 and confirmed by microprobe analysis. After heat treating at 1200°C, the microstructure changed significantly (Figure 4.4) and consisted mostly of the Nowotny phase, SiC, some $MoSi_2$ and, in regions corresponding to cracks, porosity or previous grain boundaries, SiC precipitates in $Mo_5Si_3$. This distribution of phases is not what would be expected if $Mo_5Si_3$ was being formed via reaction (4.1). Rather, the apparent concentration of $Mo_5Si_3$ along cracks and the presence of considerable porosity strongly suggest that the use of flowing purified argon for these long times results in carbon loss from the $Mo_5Si_3C$ promoting its transformation to $Mo_5Si_3$.[*****] The SiC precipitates are believed to have formed in the Nowotny phase as it adjusted its composition to the reduced homogeneity range at 1200°C and to have remained in the $Mo_5Si_3$ after decarburization probably due to its sluggish decomposition kinetics. It is possible that a thin intermediate layer between SiC and $Mo_5Si_3$ is present although this is not necessary due to the possibility of metastable equilibrium between these phases.

The microstructure and composition of a sample initially composed of $MoSi_2$ + $Mo_5Si_3C$ after hot pressing and heat treating at 1200°C for 100 h are shown in Figure 4.5 and Table 4.1 respectively. As described previously, the as-hot-pressed sample consisted of $MoSi_2$ and $Mo_5Si_3C$ with a small amount of $Mo_5Si_3$. After the 1200°C heat treatment, a considerable volume fraction of the $Mo_5Si_3$ phase was observed as was evidence of SiC precipitation in the $Mo_5Si_3C$ and $Mo_5Si_3$ phases. The distribution of the SiC precipitates indicates they formed from a single phase and not from both $Mo_5Si_3C$ and $Mo_5Si_3$ independently. Again, it is noted that the $Mo_5Si_3$ is present close to cracks and porosity in the sample probably due to carbon loss during the heat treatment. Finally, it is clear

---

[*****] Similar decarburization effects were observed in $Mo_2C$ samples which transformed to Mo+$Mo_2C$ after an equivalent heat treatment. [164]

that there are regions of contact between $MoSi_2$ and $Mo_5Si_3C$ everywhere in the sample; such would not be expected if these phases were not in equilibrium and reaction (4.1) was operating to form SiC and $Mo_5Si_3$, i.e., if the van Loo diagram was correct.

Thus, for the region delimited by $MoSi_2$, SiC, $Mo_5Si_3$ and $Mo_5Si_3C$ in the Mo-Si-C system the results of this study confirm the phase relations proposed by Nowotny at 1600°C. The results also show that $MoSi_2$ and the Nowotny phase $Mo_5Si_3C$ are in equilibrium at 1200°C, in agreement with the published data of Steinmetz and coworkers [158] and in disagreement with the isotherm proposed by van Loo and coworkers [157]. Again, it is noted that the $Mo_5Si_3$-SiC equilibrium in the latter diagram was proposed based on the XRD results of only one arc melted specimen which had been heat treated at 1200°C for at least 64 h. Since the specimen microstructure was not reported, it is neither possible to further compare their results to those of the present study nor to offer the reason for this disagreement.

Based on the observations, and assuming that the phase relations observed at high temperatures do not change during cooling, the data in Figure 4.2 can be used to estimate the Gibbs free energy of formation of the idealized compound $Mo_5Si_3C$ as -40.2 KJ/mol at 298 K. Assuming $\Delta S^0_{298}=0$ when all reactants and products are solid, the heat of formation can be estimated as $\Delta H^0_{298}$=-40.2 KJ/mol (compare with -30.77±3 KJ/mol for $Mo_4Si_3C$ given by [156]). The accuracy of this estimate, as in the case of the one given by Brewer and Krikorian [156], depends directly on the quality of the thermodynamic data used.

These results indicate that the phase relations in the system Mo-Si-C between 1200 and 1600°C are as proposed by Nowotny and coworkers, except for the fact that MoC should be absent above 1150°C [153, 156] and below 1659°C, the lower stability limit for η $MoC_{1-x}$ [153, 156]. The thermodynamic calculations suggest that these phase relations should extend to lower temperatures, at least for the range of compositions investigated.

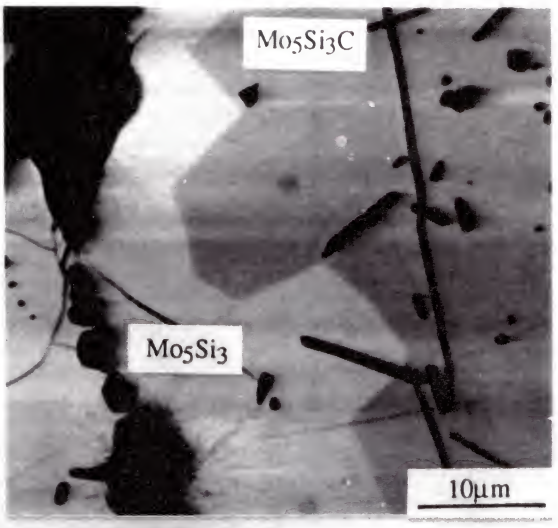


(a)

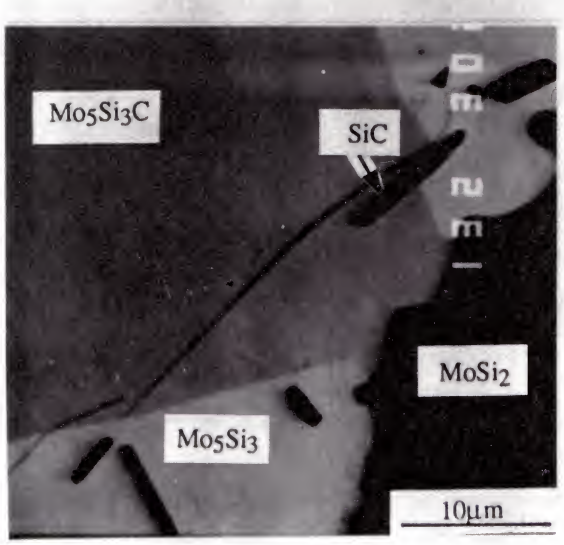


(b)

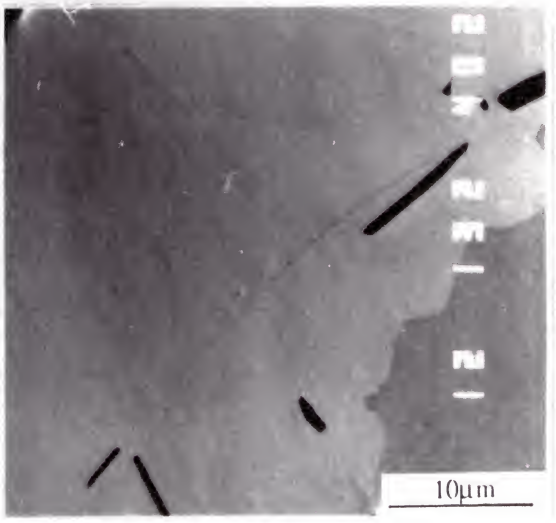


(c)

Figure 4.5 Microstructure of $MoSi_2$-$Mo_5Si_3C$ mixture hot pressed at 1550°C for 0.5 h and heat treated at 1200°C for 100 h. (a) BEI (some light streaking is present due to the high contrast setting used); black constituent is SiC or $MoSi_2$ (see (c)); gray constituent is $Mo_5Si_3C$ and light constituent is $Mo_5Si_3$ (see (b)) and platelets are SiC. (b) BEI of different region of the same sample. (c) SEM of same area in (b).

## 4.2 Silica Modification with Aluminum

Samples were produced with different levels of aluminum addition (2.5, 4.1 and 8.1% wt.) following the methods outlined in Section 3.2.1. The microstructure of the sample resulting from an addition of 2.5% wt. Al is shown in Figure 4.6. The matrix is homogeneous $MoSi_2$ containing approximately 0.8% at. dissolved aluminum. All second-phase inclusions examined had an Al/O atomic ratio of 2/3; in some of the smaller inclusions, silicon contents of up to 3% at. were measured. This is most likely due to the limited spatial resolution of the microprobe, and is consistent with the TEM observations in which all inclusions examined had diffraction patterns corresponding to $\alpha$-$Al_2O_3$ which does not have a significant solubility for silica. XRD analysis indicated the presence of tetragonal $MoSi_2$ ($C11_b$) and $\alpha$-$Al_2O_3$ only.

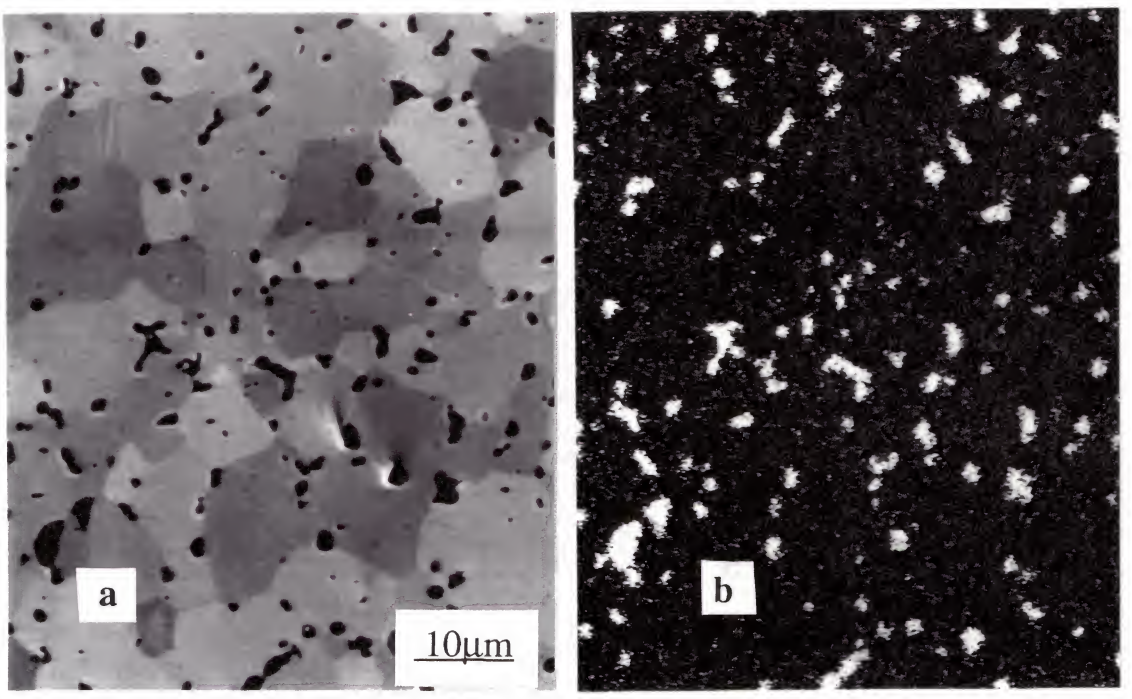


Figure 4.6 Microstructure of $MoSi_2$ + 2.5% wt. Al mixture hot pressed at 1400°C for 1 h. (a) Scanning electron micrograph. (b) Al $K_\alpha$ x-ray map of the same region.

With an increase in the aluminum addition to 4.1% wt., the microstructure was not significantly altered. The matrix was also homogeneous $MoSi_2$ ($C11_b$) with a larger amount of dissolved aluminum (approximately 1.8% at.). The atomic ratio (Si+Al)/Mo corresponded closely to 2/1 as expected from the ternary isotherms. While only $MoSi_2$ ($C11_b$) and $\alpha$-$Al_2O_3$ were present in detectable quantities in the XRD analysis and alumina inclusions were predominant, sparse silicon inclusions could be found; these inclusions are probably due to an excess of Si+Al over that required for a mixture of $MoSi_2$ and $Al_2O_3$. In view of the very narrow solubility ranges involved, the correct definition of the amount of aluminum to be added requires an accurate knowledge of the composition of the raw materials. For instance, if a final structure containing only $MoSi_2$ ($C11_b$) and $Al_2O_3$ is desired, one must know the initial oxygen content in both raw materials and the Mo/Si ratio of the silicide powder, i.e., the phases composing the powder (e.g. $MoSi_2$, $Mo_5Si_3$, $SiO_2$ ) as well as the fraction of each phase. Given this information, the aluminum addition can be determined so that the following conditions are satisfied:

$$Al_T \geq 2/3\ O_T + Al_R \qquad (4.4)$$

$$(Si + Al_R)/Mo = 2 \qquad (4.5)$$

$$Al_R \leq Al_S \qquad (4.6)$$

In these equations, $Al_T$ is the total aluminum addition, $Al_S$ is the solubility limit derived from the phase diagram, $Al_R$ is the residual aluminum in solution in $MoSi_2$, and Si and Mo are the total amounts of these elements, all expressed in gram-atoms. Evidently, $Al_R$ should be such that the aluminum activity is sufficient to satisfy the conditions required for silica reduction, but should not exceed $Al_S$. As discussed in section 2.4, Brukl, Nowotny and Benesowsky [116, 165] did not report the solubility of

aluminum in $MoSi_2$, and the only value available is the result of the measurements of Yanigihara and coworkers [117].

A simplified estimation of the activity of aluminum in solution in the silicide necessary to maintain the reaction:

$$Al\ (a_{Al}\ \text{in solution}) + SiO_2 = Al_2O_3\ (a_{Al_2O_3}) + Si\ (a_{Si}\ \text{in}\ MoSi_2) \qquad (4.7)$$

in equilibrium can be made, assuming that the activity of silicon in binary $MoSi_2$ ($C11_b$) can be used as a first approximation. This is justified since the low solubility of aluminum in this phase should not have a pronounced effect on the behavior of silicon. Thus, the activity of silicon in $MoSi_2$ can be estimated considering the two possible equilibria in the binary system, namely (a) $MoSi_2$-Si, and (b) $MoSi_2$-$Mo_5Si_3$. Using the free-energy of formation data assessed by Chart (see section 2.4), one can estimate $a_{Si}$ to be in the range of 0.03-1 at 1400°C. Taking these values and the free energy of formation for the oxides given in [96], the activity of aluminum required to maintain reaction (4.7) in equilibrium can be estimated to be in the range of $2 \times 10^{-5}$ to $4 \times 10^{-4}$, assuming the formation of pure $Al_2O_3$. Since, as discussed in section 2.4, there are no thermodynamic data for the behavior of aluminum in solution in $MoSi_2$ (nor for the C40-$Mo(Si,Al)_2$ phase), it is not possible to calculate the required amount of aluminum ($Al_R$) necessary to reach this activity.

For practical purposes, condition (4.5) can be substituted by $(Si + Al_R)/Mo \approx 2$; deviations must be such that the overall composition is slightly molybdenum rich in order to prevent the occurrence of lower melting phases, such as silicon in this case.

An addition of 8.1% wt. of aluminum produced the microstructure shown in Figure 4.7. The XRD analysis of this sample indicated the predominance of the hexagonal $Mo(Si,Al)_2$ (C40) phase, with $MoSi_2$ ($C11_b$) and $\alpha$-$Al_2O_3$ also present. This is confirmed by the microprobe analysis as evidenced by the aluminum x-ray map (Figure 4.7). Aluminum to silicon ratios of approximately 0.12 were observed in the C40 phase.

This ratio falls within the range of the C40 phase proposed by both isotherms discussed in section 2.4.

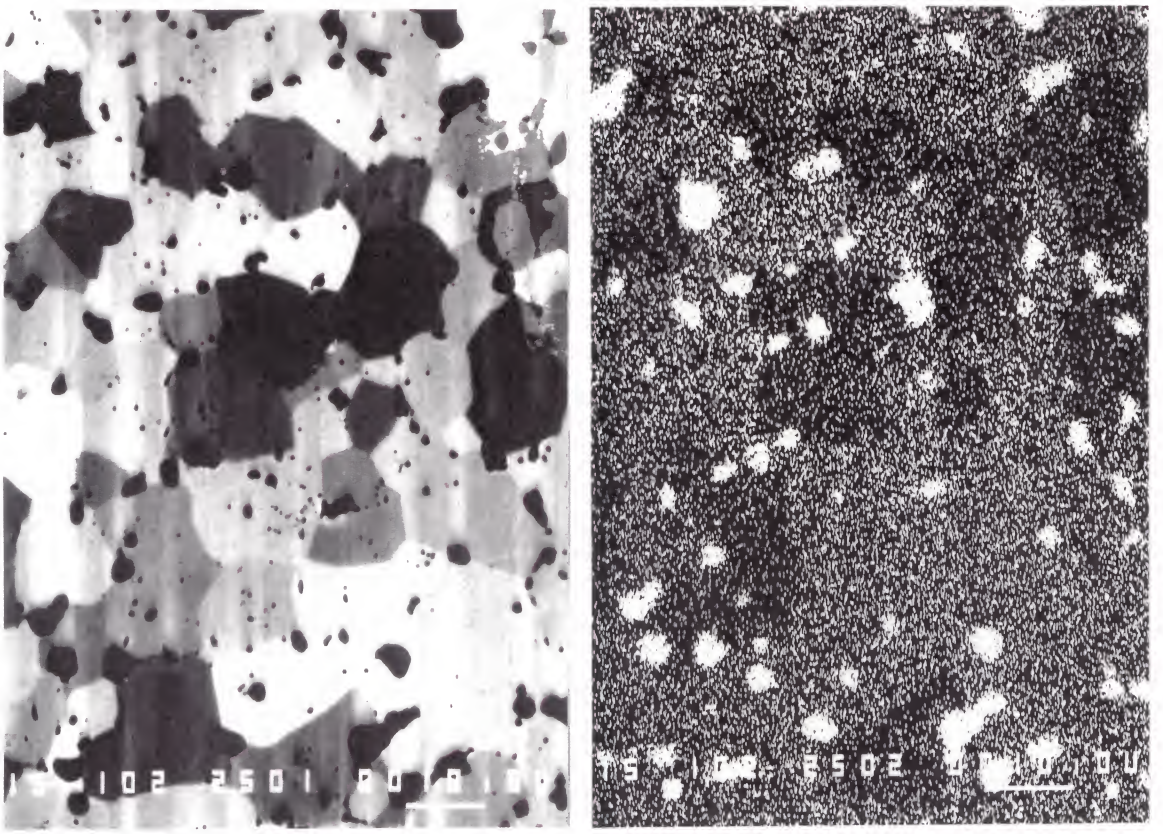

Figure 4.7 Microstructure of $MoSi_2$ + 8.1% wt. Al mixture hot pressed at 1400°C for 1 h. (a) Backscattered electron image (some light streaking is present due to the high contrast setting used). (b) Al $K_\alpha$ x-ray map of the same region.

For a preliminary evaluation of the mechanical properties of these composites, hardness and indentation crack fracture toughness tests were performed; these results are presented in Table 4.2. Although the data scatter is high, there appears to be a trend to lower hardness with the increase in aluminum in the $C11_b$ phase. The sample containing the hexagonal C40 phase appears to have a higher fracture toughness than those samples consisting of the $C11_b$ phase, regardless of the type of oxide present. Since the effects of grain size, morphology and volume fraction of the different phases were not quantified,

these observations are provisional but sufficient to recommend further examination of these properties. A significant fact is that, for a given oxygen content, the volume of alumina formed is approximately 75% of that of the initial silica; this is expected to result in larger grain sizes in the structures in which silica is modified using this processing scheme, due to the lower pinning power of the alumina particles. It is expected that the *in-situ* process can be optimized to produce the desired grain sizes and morphologies, together with the desired silica modification.

Table 4.2 Hardness and Indentation Fracture Toughness of Hot Pressed $MoSi_2$ with and without Aluminum Additions.

| Nominal Al addition. % wt. | Microstructure | Hardness GPa | | $K_C$ MPa$\sqrt{m}$ | | |
|---|---|---|---|---|---|---|
| | | Aver. | σ (n) | Aver. | σ (n) | Crack size[a)](μm) |
| 0 | $C11_b + SiO_2$ | 8.62 | 0.30 (5) | 3.6 | 0.2 (5) | 415 |
| 2.5 | $C11_b + Al_2O_3$ | 8.34 | 0.14 (12) | 3.6 | 0.27 (5) | 416 |
| 4.1 | $C11_b + Al_2O_3$ | 7.35 | 0.12 (15) | 3.7 | 0.3 (5) | 435 |
| 8.1 | $C11_b$+C40+$Al_2O_3$ | 7.91 | 0.3 (11) | 4.3 | 0.34 (5) | 385 |

[a)]For 10 Kgf load. Averages of five measurements per sample.

## 4.3 Silica Precursors for Alumina Reinforcement Formation

Based on the favorable results obtained with the displacive reduction of silica through aluminum additions, it was speculated that alumina could be generated as a second phase using a deliberate addition of a silica precursor. Glass fibers were selected as precursors due to their availability, morphology and small diameter which should favorably influence the overall kinetics of the displacive process. Thus, E and S2 type glass fibers were added to $MoSi_2$-10.4% wt. aluminum before hot pressing. In this stage of the investigation, the objective was to demonstrate the feasibility of the approach from

the physico-chemical point of view and no attempts were made to measure or optimize mechanical properties.

The microstructures of samples containing E and S glass fibers after hot pressing are shown in Figure 4.8.

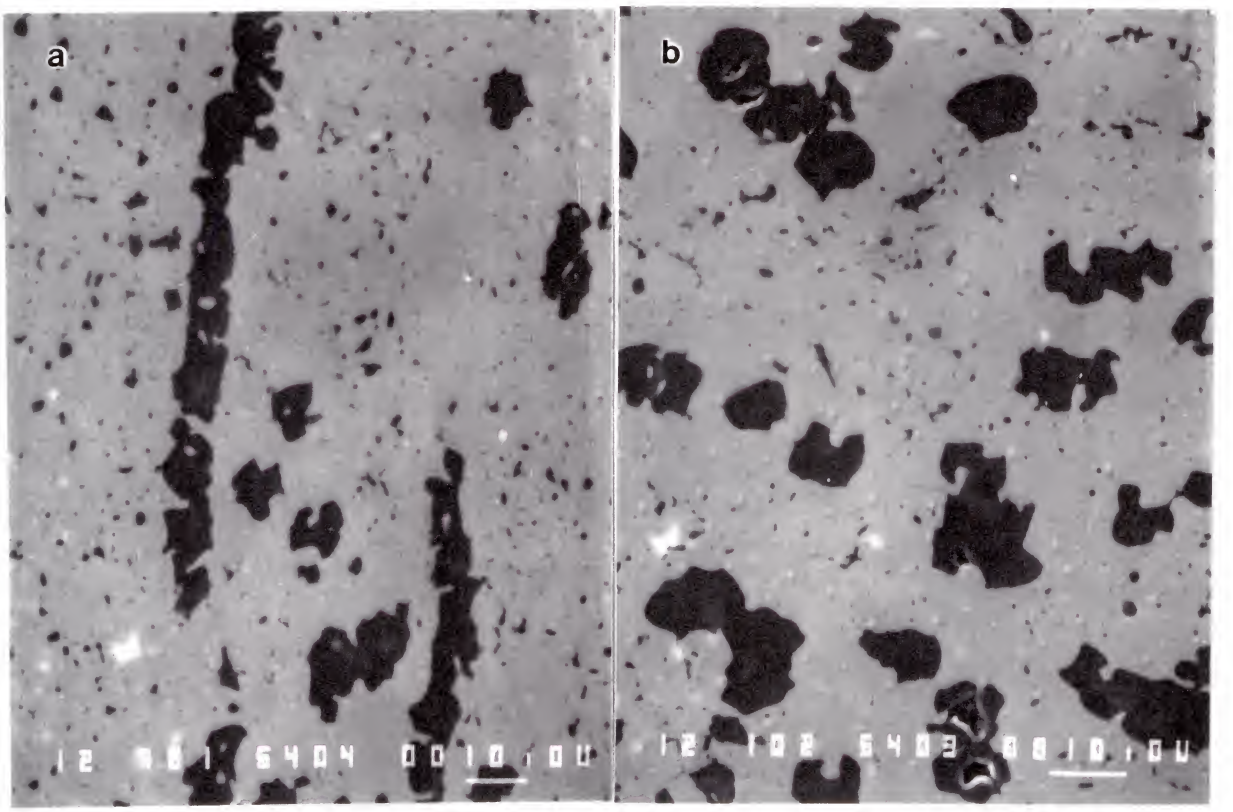


Figure 4.8 SEM of *in-situ* formed alumina-rich elongated second phase from glass fiber precursors. (a) Longitudinal section from sample produced using E glass in a mixture of $MoSi_2$ + 10.4 % wt. Al and (b) transverse section from sample produced using S2 glass in the same mixture.

As before, all $SiO_2$ inclusions were converted to $\alpha$-$Al_2O_3$ and the matrix is composed of both $Mo(Si,Al)_2$ (C40) and $MoSi_2$ ($C11_b$). However, larger aluminum-rich oxide regions with Al/O ratio corresponding closely to that of alumina (Table 4.3) are

also present. These oxides are the product of the reduction of the less stable oxide in the glass fibers by aluminum in accordance with reaction (4.7). It is speculated that calcium and magnesium were either lost during vacuum processing due to their high vapor pressures or dissolved in the matrix in levels below the EMPA detection limit for these elements (0.1% wt.). The resulting morphology is considerably less uniform than the originally cylindrical fibers. Besides, some cavities, due to the reduction in volume (≈ 25%) associated with the conversion of $SiO_2$ to $Al_2O_3$, and increased tortuosity of the fiber-matrix interface is also evident. Such tortuosity could be beneficial in cases where a strong bond between matrix and reinforcement is desired. In some regions, especially when multiple precursor fibers bundled together, silicon-rich regions were observed between the large alumina particles. These are present either due to insufficient time to dissolve them in the matrix or to inadequate stoichiometry control in these regions leading to saturation of the matrix with silicon. This would probably be detrimental for high temperature mechanical behavior since it could lead to liquid phase formation. From the point of view of the reactions occurring, there is no significant difference between the precursors used and only further characterization, including mechanical testing, may prove otherwise.

Table 4.3. Characteristics of Oxide Derived from Glass Fibers via *In-situ* Reaction.

| | | Oxide derived from glass fiber | |
|---|---|---|---|
| | | E glass | S2 glass |
| Composition: (normalized atomic %) | Al | 38.9 | 38.3 |
| | Si | 0.4 | 0.1 |
| | Ca | 0.0 | 0.0 |
| | Mg | 0.0 | 0.0 |
| | O | 60.7 | 61.6 |
| Diameter: | μm | ≈10 | ≈7-8 |

## 4.4 *In-situ* Formation of Coatings in Niobium

As discussed in Section 2.3, the use of refractory metals for toughening $MoSi_2$ composites is limited by their interaction and formation of intermediate silicides. The use of conventional coating techniques to prevent this interaction has cost limitations and imposes a severe constraint on the handling of the fibers prior and during composite manufacture to prevent coating damage. *In-situ* alumina coatings have been successfully applied to refractory metals in $NbAl_3$ and NiAl [160, 161] using pre-oxidized niobium fibers. In this section, the attempts to achieve similar results using an aluminum-modified $MoSi_2$ are described.

The concept of producing an *in-situ* coating in a pre-oxidized niobium fiber presupposes the occurrence of reaction (4.8) and formation of a dense alumina layer before any further significant interaction between the fiber and the matrix occurs.

$$2\ Al\ (a_{Al}\ \text{in the matrix}) + 3/5\ Nb_2O_5 = Al_2O_3 + 6/5\ Nb \qquad (4.8)$$

To determine the feasibility of producing a protective layer, experiments were performed using different compositions with a constant $x_{Mo}=1/3$ and variable $x_{si}/x_{Al}$ ratios. For high $x_{si}/x_{Al}$ ratios, no protection was observed, as shown in Figure 4.9 for a sample produced with a 10.4% wt. addition of aluminum to $MoSi_2$. A discontinuous alumina layer is present at radial positions of 150-300 μm from the center of the original fiber. In order to further clarify the phase relations in the interaction between pre-oxidized niobium and aluminum-containing $MoSi_2$, a planar diffusion couple was produced using a mixture containing 4.1% wt. aluminum. The resulting diffusion path is shown in Figure 4.10, superimposed on the applicable ternary isotherms. These phase relations were typical of the samples in which interaction was observed, except for the

facts that: (a) for high aluminum contents, the matrix did not contain $C11_b$ $MoSi_2$, and (b) for longer interaction times the niobium "core" was absent from the reacted fiber.

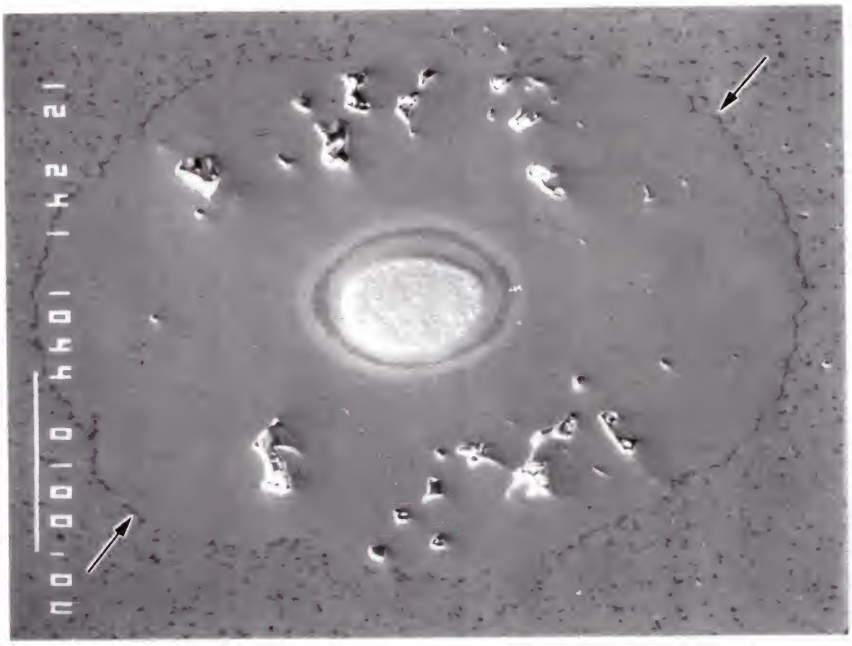

Figure 4.9 SEM of a niobium fiber that interacted with the matrix. Initial fiber diameter, approximately 250 μm. Matrix is C40 ($Mo(Si,Al)_2$) with alumina inclusions. A discontinuous layer of alumina particles mark the original fiber-matrix interface.

Protective layers were formed when $x_{Si}/x_{Al} \approx 1$ in at least 80% of the fibers, as shown in Figure 4.11. The alumina layers formed had thicknesses in the range of 2-3 μm. When protective layers were formed, the phase sequence did not follow that observed in the diffusion couple; only a thin layer composed of $Nb_2Al$ and $Nb_3Al$ was present between the niobium fiber and the alumina layer, as shown in Figure 4.11 and indicated by the EMPA results of Table 4.4. While both aluminides appear to be in equilibrium with alumina [166], only $Nb_3Al$ is stable in contact with niobium, in accordance with available binary and ternary phase diagrams. Thus, the observed layer arrangement is in accordance with the predicted phase equilibria.

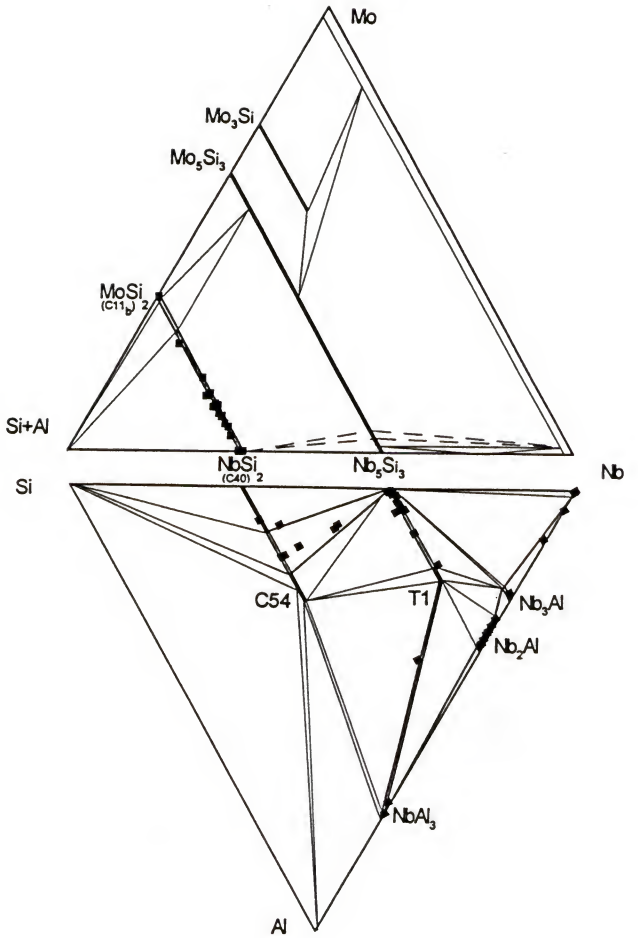


Figure 4.10 Diffusion path for a flat diffusion couple between pre-oxidized niobium and aluminum containing $MoSi_2$ superimposed on the applicabe isotherms. See text for details.

The following factors probably control the formation of a dense and protective alumina layer in accordance with reaction (4.8): (a) the presence of aluminum in the matrix with an activity, $a_{Al}$, sufficient to cause significant completion of the displacement reaction, (b) the volume changes associated with the displacement reaction and (c) the competition between the kinetics of silicon and aluminum transport into the niobium and the kinetics of the displacement reaction itself.

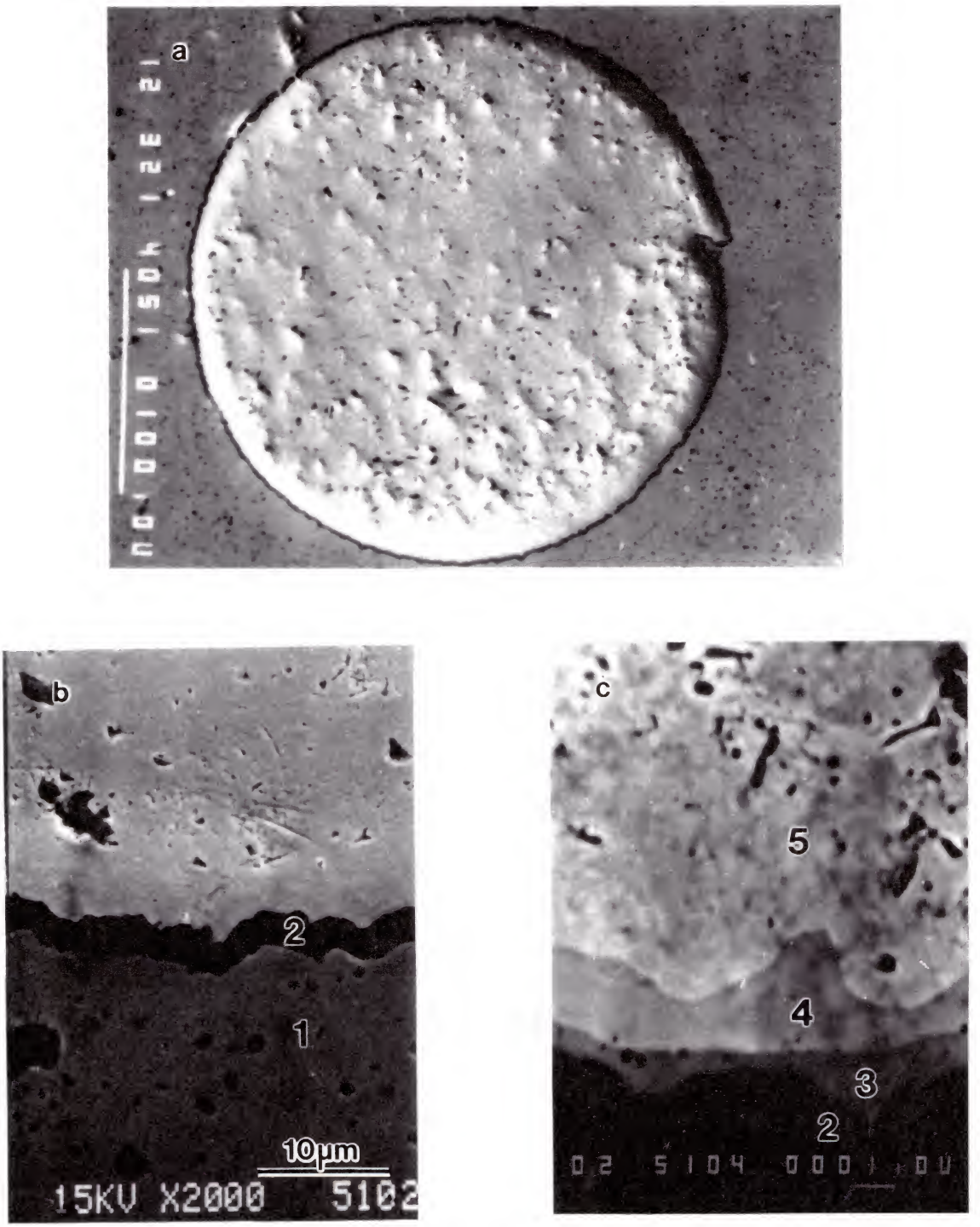


Figure 4.11 (a) Typical microstructure (SEM) of a niobium fiber surrounded by alumina layer formed *in-situ* in a C40 plus alumina matrix. (b) Higher magnification (SEM) and (c) BEI of the interface region. EMPA analyses of indicated areas are given in Table 4.4.

Table 4.4: EMPA Analysis of Areas Indicated in Figure 4.11.

| Position (Figure 4.11) | Element (atom %) | | | | | Phase |
|---|---|---|---|---|---|---|
| | Si | Nb | Mo | Al | O | |
| 1 | 35.2 | 0.0 | 34.2 | 30.6 | - | $Mo(Si, Al)_2$ |
| 2 | 0.1 | 0.0 | 0.0 | 39.0 | 60.9 | $Al_2O_3$ |
| 3 | - | 69.7 | - | 30.3 | - | $Nb_2Al$ |
| 4 | - | 80.3 | - | 19.7 | - | $Nb_3Al$ |
| 5 | - | 100.0 | - | - | - | Nb |

Note: Results corresponding to points 3 and 4 are within the solubility ranges of the indicated phases but are subject to errors due to layer thickness being comparable to the spatial resultion of the microprobe.

In a previous section, the minimum aluminum activity necessary to cause the reduction of pure silica in $MoSi_2$ ($C11_b$) was estimated as approximately $2 \times 10^{-5}$ at 1400°C. Assuming the oxides taking part in reaction (4.8) are at unit activity and that $a_{Nb} \approx 1$, the equilibrium value of $a_{Al}$ is estimated as $10^{-7}$ at 1400°C. Thus, there does not seem to exist a thermodynamic limitation to the formation of the barrier. The volume change when niobium oxide is converted to alumina according to reaction (4.8) is in the range of -16.6 to -28%. This is based on room temperature density data, since thermal expansion data for the niobium oxide is scant. Lu and coworkers [160], however, have shown that a dense alumina layer can be formed during the displacement reaction with the aluminides they analyzed. They observed the presence of fine Nb particles inside the alumina layer as well as a significant thickness reduction in the oxide layer, in agreement with the present observations. Interestingly, Lu has noted that the $Nb_2O_5$ layer is porous; it may be speculated that this may enhance the transport of aluminum and favor the growth of a dense alumina layer. Since both silicon and aluminum diffuse in niobium, it seems probable that the relative rates of transport of these elements and the reactions occurring (not only the displacement reaction but also the formation of the intermediate compounds) will control the overall ability of forming a dense, protective oxide layer at

the interface. It is conceivable that if silicon was immobile and the displacement reaction is assumed faster than the transport of aluminum through $Nb_2O_5$, aluminum would be transported from the matrix to convert the oxide layer until completion of this reaction. If the assumptions above are somewhat relaxed, it could be expected that some of the aluminum could be transported through the reaction zone interacting either with the niobium being generated in the reduction process or with the original fiber. Furthermore, since silicon has a considerable mobility in the silicides [6, 167, 168], superimposed on this process, silicon transport occurs. Thus, it is concluded that, at least for the processing cycle used, the limitation for the formation of the protective layer is kinetic. Furthermore, at least when fracture occurs at room temperature, the *in-situ* coated Nb-C40 $Mo(Si,Al)_2$ composites exhibit substantial fiber debonding at the alumina interface, a condition considered essential for obtaining toughening of brittle matrices with ductile reinforcements.

## 4.5 An Estimation of the Ternary Mo-Si-Al System

### 4.5.1 Criteria for Preliminary Estimation of Mo-Si-Al Phase Equilibria

As discussed in Chapter 2, the data available on the Mo-Si-Al is scant. Actually, not even the binary Mo-Al can be regarded as well established. However, it was considered justifiable to perform a first estimation of this ternary system, at least to define the areas where the uncertainty is largest and more experiments are necessary and to have some estimates of aluminum activities in the $C11_b$ $MoSi_2$ and C40 $Mo(Si,Al)_2$ phases.

As can be seen on both available isotherms, most experimental exploration has been performed in the range of $X_{Si}/X_{Al} > 2.33$ and $X_{Mo} > 0.33$, except for the pseudo-binary $Mo_3Si$ - $Mo_3Al$. Thus, the present estimate has been restricted to this range as much as possible. In order to clarify some of the conflicting information presented in the

two isotherms as well as to have more data to verify the results of the estimation, equilibration experiments were performed following the techniques described in Chapter 3.

Two aspects must be considered in the estimation of a ternary system. First, it is necessary to have good and consistent descriptions of the binaries. While the recent description of the Al-Si system by Chakraborti and Lukas [139] was considered satisfactory, some problems were found with the other two binaries. This is discussed in detail in the next section. Second, a model for those phases that extend into the ternary systems must be adopted. In the present case, the Muggianu model was adopted for the ternary solutions (liquid and BCC) while the models adopted for the ternary phases are discussed in the subsequent section.

### 4.5.2 An Estimation of the Binary Mo-Si

In order to fit the enthalpy of mixing in the liquid phase reported for silicon-rich mixtures by Sudavtosva and coworkers [133] and that of Arpaci and Froberg [132] for molybdenum-rich liquids, Vahlas and coworkers [169] introduced significant temperature dependence terms in their first and second-order Redlich-Kister coefficients. As a result, increasing the temperature some 100K above the melting point of molybdenum is sufficient to cause the appearance of a miscibility gap in the silicon-rich region of the liquid. It was felt that it would be advantageous to use a simpler description of the liquid, especially in view of the intention of using this data as a starting point for the description of the ternary system. Thus, a new description of the Mo-Si system was attempted in which (a) the assessed data of Chart were accepted for the silicides [131], (b) the phase diagram data summarized by Brewer [2] and Gokhale and Abbaschian [3] were used and (3) the only data considered for the liquid were those of Arpaci and Froberg [132], i.e. the data of [133] were not used. As usual, the Gibbs energy of each phase was described

separately with the solutions being treated as substitutional solutions using a Redlich-Kister polynomial to describe the excess free energy, as discussed below.

Elements. The free energy of a pure element *i*, ${}^{o}G^{T}_{i,\Phi}$, referred to the enthalpy of its stable state $\Phi$ at 298.15K ($H^{298.15K}_{i,\Phi}$) is denoted as GHSER*i* (the superscript T indicates that G is a function of temperature). The expressions for GHSER*i* as a function of temperature are given in the SGTE database [102]. The free energy of element *i* in a different structure $\Pi$ (${}^{o}G^{T}_{i,\Pi}$) can be expressed in the same way, and is also given in [102]. The difference between ${}^{o}G^{T}_{i,\Pi}$ and ${}^{o}G^{T}_{i,P}$ is frequently referred to as the lattice stability of element *i* in phase $\Pi$.

Solution phases. Complete miscibility was assumed for both the BCC and the liquid phase. The diamond cubic phase was assumed to have no solubility for molybdenum. Thus, the molal free energy for the BCC phase, for instance, is given as:

$$G^{T}_{BCC} = x_{Mo}\,{}^{o}G^{T}_{Mo,BCC} + x_{Si}\,{}^{o}G^{T}_{Si,BCC} + R\,T\,(x_{Mo}\ln x_{Mo} + x_{Si}\ln x_{Si}) + {}^{E}G^{T}_{BCC}$$

A similar expression is obtained for the liquid.

The excess Gibbs free energies were described using the following expressions:

$${}^{E}G^{T}_{BCC} = x_{Si}\,x_{Mo}\,[\,L^{0}_{Mo,Si,BCC}]$$

$${}^{E}G^{T}_{Liq} = x_{Si}\,x_{Mo}\,[L^{0}_{Mo,Si,Liq} + (x_{Si} - x_{Mo})(\,L^{1}_{Mo,Si,Liq})]$$

where the $L^{i} = A + BT$ are the Redlich-Kister polynomial coefficients of order *i* and A and B are the constants determined through the optimization process.

Stoichiometric compounds. All stoichiometric compounds were described using a two-sublattice model with Mo in one and Si in the other sublattice. This does not allow for the description of solubility ranges. In this case, the Gibbs energy of each phase is written in a form in which the right-hand side of the equation can be interpreted as the Gibbs free energy of formation of that phase:

$$G^{T}_{Mo_pSi_q} - p\,{}^{o}G^{T}_{Mo,BCC} - q\,{}^{o}G^{T}_{Si,DIA} = A + BT$$

The liquid phase was optimized first, and then the other phases were added in sequence and their parameters optimized. Finally, all variables were optimized

simultaneously in order to minimize the total error of the adjustment. The results of the optimization are given in Table 4.5 and the estimated phase diagram presented in Figure 4.12.

Table 4.5 Results of the Optimization of the Mo-Si System

(a) Coefficients and Phase Description.

| Phase | $i$ in $L^i$ | A (J/mol) | B (J/K mol) |
|---|---|---|---|
| Liquid | 0 | -150180 | 0 |
| | 1 | 5340 | 0 |
| BCC | 0 | -98950 | 0 |
| $MoSi_2$ | - | -137000 | -12.76 |
| $Mo_5Si_3$ | - | -313380 | -45.93 |
| $Mo_3Si$ | - | -127000 | -10.00 |

(b) Special Points in the Calculated Mo-Si Binary.

| Reaction | Temperature (°C) | Reaction Type | Composition (at% Si) |
|---|---|---|---|
| $L = Mo_3Si + Mo(BCC)$ | 2035 | Eutectic | L=19.8, BCC= 6.2 |
| $L=Mo_3Si$ | 2061 | Congruent | |
| $L = Mo_5Si_3$ | 2187 | Congruent | |
| $L = Mo_5Si_3 + Mo_3Si$ | 2060 | Eutectic | L=26.0 |
| $L = MoSi_2 + Mo_5Si_3$ | 1919 | Eutectic | L=54.3 |
| $L = MoSi_2$ | 2032 | Congruent | |
| $L = MoSi_2 + Si(DIA)$ | 1368 | Eutectic | L=94.3 |

4.5.3 An Estimation of the Binary Mo-Al

Since Kaufman's model [143, 170] for this binary uses quite unrealistic values for the thermodynamic functions of the different solid phases, it was decided that it could not be used in the evaluation of the ternary system and a more reasonable estimation of this system was necessary. As the experimental data are extremely scant as reviewed before, the following criteria were followed for this estimation. No compound richer in

aluminum than $Mo_3Al_8$ was used in this estimation, as discussed previously. This is justified by (a) the lack of experimental thermodynamic data for this compounds, and (b) the uncertainty in the phase relations in this region of the diagram. Furthermore, the solid phases in this composition range are not relevant for the compositions and temperatures of interest in the present study and, using the Muggianu model, this portion of the liquid phase only effects the region close to the aluminum-rich corner of the ternary.

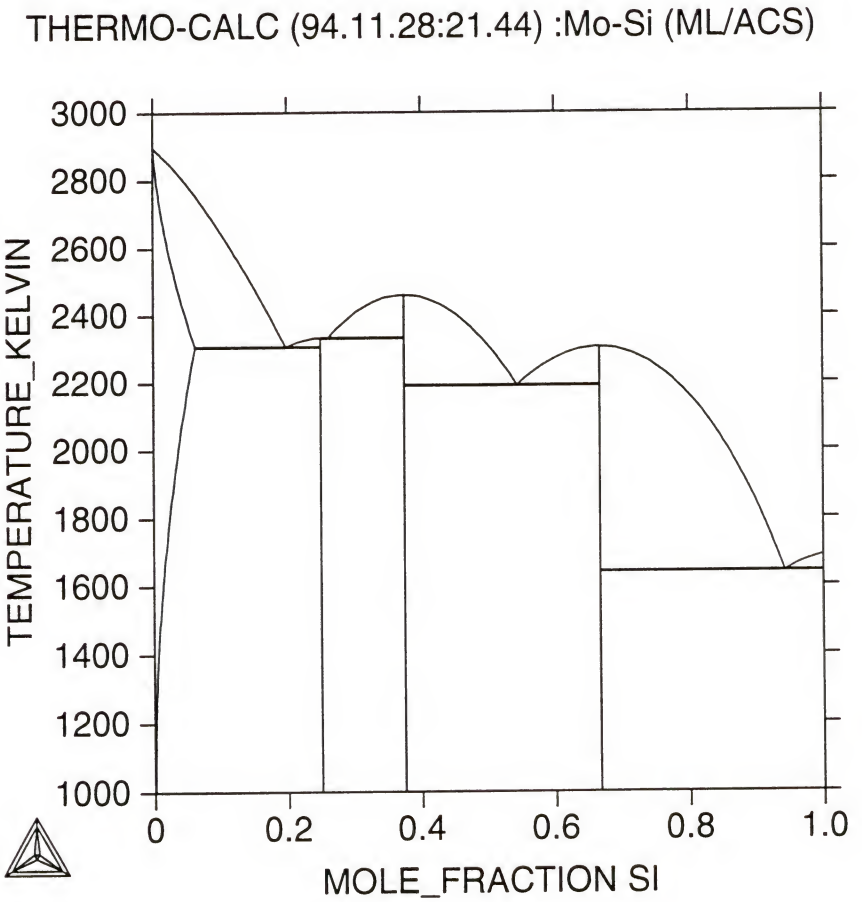


Figure 4.12 Calculated Mo-Si Phase Diagram.

The enthalpies of formation for the aluminides between $Mo_3Al_8$ and $Mo_3Al$ were taken from the calorimetric measurements of Meschel and Kleppa [137] when available

or from Shilo and Franzen [136]. The values suggested by Brewer [2] based on somewhat older data were not used in view of their significant discrepancy with these more recent experimental values. For the compound MoAl the molar enthalpy of formation was obtained by linear interpolation of Meschel and Kleppa's and Shilo and Franzen's data as a function of composition, following the suggestion of Kubaschewski [96]. This method may not be justified in view of the apparent differences in stabilities and melting points of the aluminides, but was used in view of the absence of experimental data. To estimate the variation of the free energy of formation with temperature, the correlation between heats of formation and excess entropies of formation suggested by Chart [128] was used. The values obtained from this correlation were used as starting values for the phase descriptions, together with the experimental heats of formation.

Since no thermodynamic data are available for the liquid and most of the liquidus lines are not established, it was decided to use a simple regular solution model for this phase. For consistency, a regular solution model was also used for the BCC phase. Shilo and Franzen's data for aluminum vapor pressure over BCC Mo-Al alloys and Rexer's [171] BCC-$Mo_3Al$ phase boundaries were used to adjust the description of the BCC phase. It was found that the stability of $Mo_3Al$ derived using the method described above was incompatible with this data so that, in order to increase the stability of this phase, its free energy variation with temperature was changed until the solubility of aluminum in BCC Mo-Al was compatible with the accepted peritectic point between BCC and $Mo_3Al$. The temperature dependence of the free energy of MoAl was adjusted based on the aluminum vapor pressure measurements of Shilo and Franzen in the $Mo_3Al$- MoAl range. An attempt at adjusting the liquid-phase description using the data for the two peritectics proposed by Saunders [172] and the congruent melting of $Mo_3Al_8$ was unsuccessful. Thus, the regular-solution parameter of the liquid and the temperature coefficient of $Mo_3Al_8$ were adjusted together, using the $Mo_3Al$ peritectic, the congruent melting points

of MoAl (proposed by Brewer [2]) and $Mo_3Al_8$ and the aluminum vapor pressure measurements of Shilo and Franzen in the $Mo_3Al$- $Mo_3Al_8$ range. The phase $Mo_{37}Al_{63}$ was not included in this estimation for two reasons: (a) it is not expected to have any significant influence in the Mo-Si-Al ternary and (b) there is no thermodynamic data that can be used to verify any adjustment to the proposed lower-temperature eutectoid and high-temperature peritectic occurring in an interval of less than 100K in the proposed phase diagrams -- this makes any adjustment a futile exercise. The results of the optimization are given in Table 4.6 and the estimated phase diagram presented in Figure 4.13.

Table 4.6 Results of the Optimization of the Mo-Al System

(a) Coefficients and Phase Description.

| Phase | $i$ in $L^i$ | A (J/mol) | B (J/K mol) |
|---|---|---|---|
| Liquid | 0 | -72330 | - |
| BCC | 0 | -46600 | - |
| $Mo_3Al$ | - | -89200 | 4.0 |
| MoAl | - | -22250 | -18.52 |
| $Mo_3Al_8$ | - | -363000 | 36.43 |
| $Mo_{37}Al_{63}$ | | - | - |

(b) Special Points in the High-Molybdenum Range of the Calculated Mo-Al Binary.

| Reaction | Temperature (°C) | Reaction Type | Composition (at% Mo) |
|---|---|---|---|
| $L + Mo = Mo_3Al$ | 1897 | Peritectic | L=0.69 BCC=0.85 |
| $L = MoAl + Mo_3Al$ | 1717 | Eutectic | L=0.56 |
| $L = MoAl$ | 1756 | Congruent | |
| $L = Mo_3Al_8$ | 1577 | Congruent | |
| $L= MoAl + Mo_3Al_8$ | 1537 | Eutectic | L=0.36 |
| $MoAl = Mo_3Al_8 + Mo_3Al$ | 1190 | Eutectoid | |

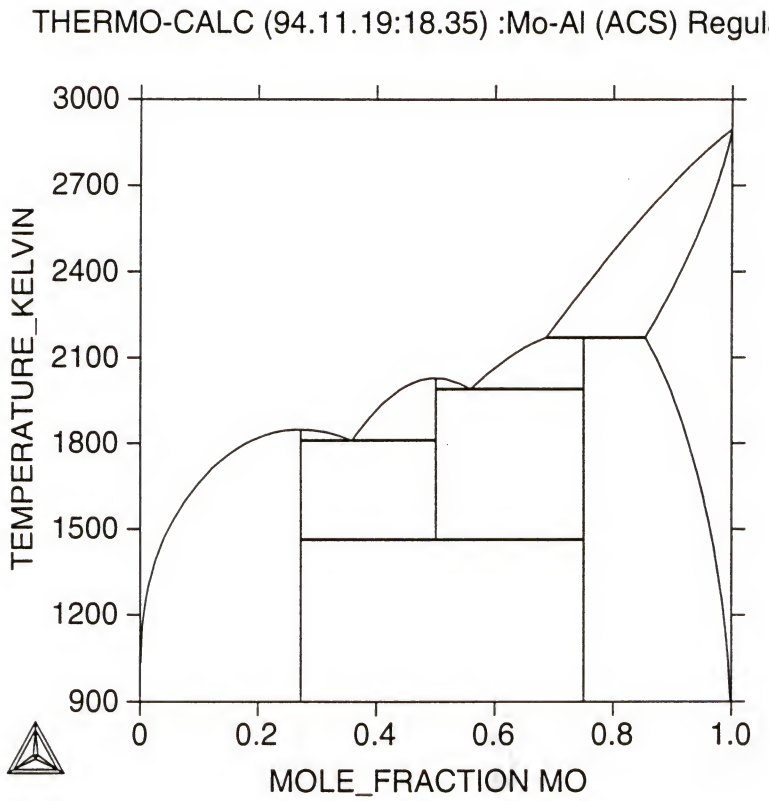


Figure 4.13 Calculated Mo-Al Phase Diagram.

4.5.4 Experimental Measurements in the Mo-Si-Al System

Two sets of equilibria were examined at 1000 and 1400°C in order to acquire more data for the estimation of the ternary system: (a) the C40-$C11_b$-T1($Mo_5Si_3$) three-phase equilibrium, and (b) tie-lines in the C40-T1($Mo_5Si_3$) two-phase field. Furthermore, the C54-T1-$Mo_3Al_8$ equilibrium was also examined at 1400°C. In addition, attempts were made at equilibrating the C40 phase with liquids in the Mo-Si-Al system at 1000°C but were unsuccessful. The results of the EMPA analysis of the various arc-melted and heat-treated samples are presented in the form of isotherms in Figure 4.14.

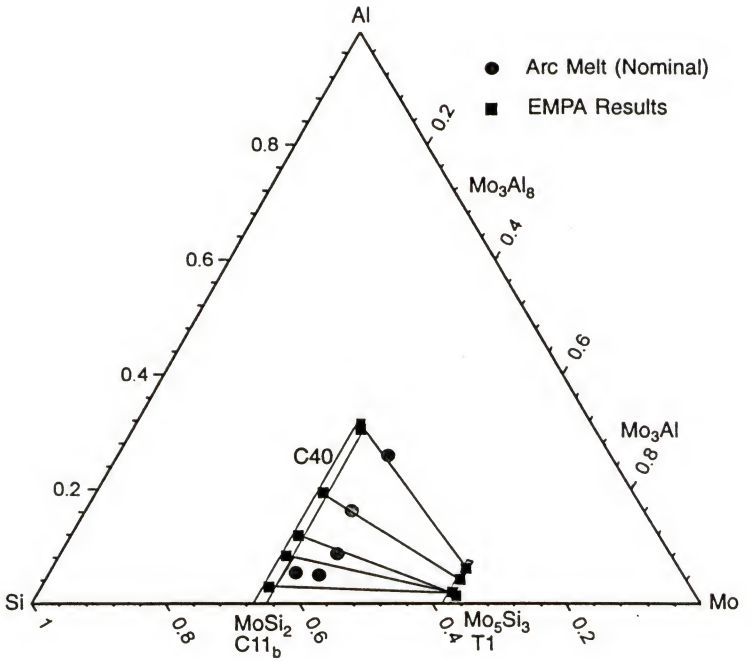


(a)

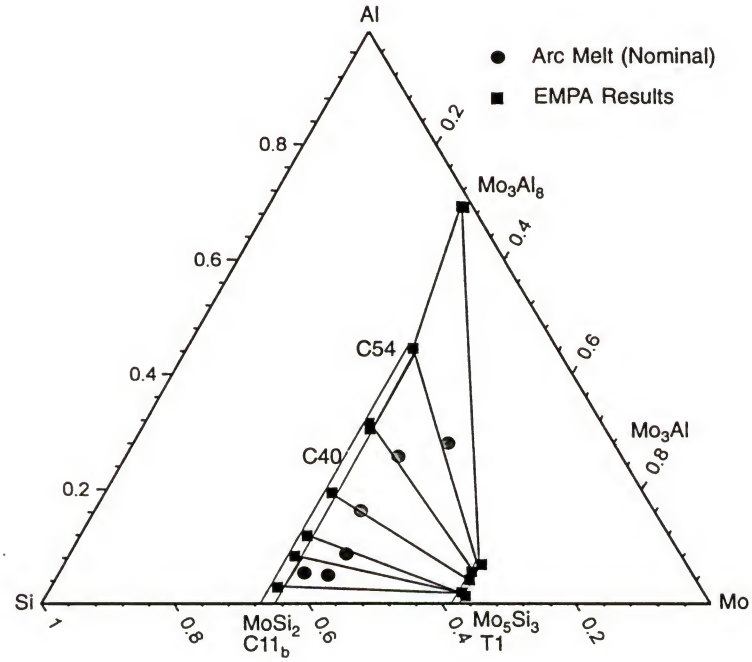


(b)

Figure 4.14 Experimental isotherms in the Mo-Si-Al system. (a) 1000°C. (b) 1400°C.

These results are averages of at least four analyses in different points of each phase. In contrast to the isotherm proposed by Brukl and in agreement with Yanigihara and coworkers [117], the composition of T1 in equilibrium with $C11_b$ and C40 has a low aluminum content. The most interesting result of these experiments is that there is a considerable range of compositions of T1 in equilibrium with C40 both at 1000 and 1400°C, as opposed to the single point from which all tie-lines emanate in the Brukl isotherm (1600°C). However, the range of values does not appear to be as extensive as sketched by Yanigihara and collaborators. The extent of the C40 field and the composition of the C54 phase are in good agreement with the diagram proposed by Brukl. Brukl and coworkers proposed that two three-phase fields emanate from the point of maximum solubility of aluminum in T1, namely the T1-$Mo_3(Si,Al)$-"$MoAl_2$" and the T1-C54-"$MoAl_2$" fields, and that there is a negligible difference between this solubility limit and the aluminum content of T1 in the T1-C40-C54 equilibrium. This construction is plausible if "$MoAl_2$" is taken to be $Mo_3Al_8$. Yanigihara and coworkers, conversely, proposed that the T1 field extends only to the T1-C40-MoAl and T1-$Mo_3(Si,Al)$-MoAl three-phase fields and assumed an aluminum solubility in T1 similar to the value given by Brukl. Although the presence of MoAl is plausible based on the Mo-Al diagram, the absence of C54 from the ternary diagram was not confirmed in the present investigation, at least at 1400°C. If it is accepted that the T1 ($Mo_5Si_3$) field extends only up to the three-phase field T1-C40-C54 or T1-C54-$Mo_3Al_8$ (the limits of the present investigation), the solubility of aluminum in T1 measured at 1400°C is around 8.1%at, lower than the value reported by Brukl at 1600°C (12.5%at).

### 4.5.5 Description of the Ternary Phases

Based on their constant molybdenum content, the ternary phases should, in principle, be described using a two sub-lattice model with one lattice occupied by

molybdenum and the other by silicon and aluminum. This was, indeed, the model adopted for $Mo_3(Si,Al)$ which has the A15 structure and complete miscibility across the diagram. In view of its narrow homogeneity range, the C54 phase would be better described as a "line compound" with three sub-lattices and a fixed ratio of $X_{Si}/X_{Al}$ equal to 3/2. This is in good agreement with both the Brukl isotherm and the experimental results of the present work. For the C40 and the T1 phases, however, two approaches can be adopted: (a) these phases can be assumed to extend across the complete range of $X_{Si}/X_{Al}$ with their absence on the Mo-Al side of the diagram being caused by the fact that they have lower stabilities at these compositions than the phases observed in the stable binary phase diagrams, and (b) in order to minimize extrapolation errors associated with values of the free energy of "$MoAl_2$" and "$Mo_5Al_3$", following a suggestion of Sundman, the maximum aluminum content of these phases can be fixed to agree with the experimentally observed values by the ratio of lattice sites. Thus, in this approach, the C40 phase is described as existing between $X_{Al}=0$ and $X_{Al}=0.33$ with a constant ratio $(X_{Si}+X_{Al})/X_{Mo}=2$, i.e. from "metastable" C40-$MoSi_2$ to MoSiAl. Practically, this is modeled as three sub-lattices, with the site ratio of 1/ 1/ 1, containing Mo, Si and Si+Al, respectively. The $Mo_5Si_3$ phase is also modeled with three sub-lattices in this case, and with a range of existence between $Mo_5Si_3$ and $Mo_5(Si,Al)_3$ with $X_{Al}=0.081$, based on the experimental measurements of the present work. This translates in a Mo, Si, Si+Al sub-lattice ratio of 5/ 2.35/ 0.65.

### 4.5.6 Results of the Estimations

#### 4.5.6.1 The model extending to "$MoAl_2$" and "$Mo_5Al_3$"

The main difficulty in this model was found in the estimation of the free energy of C40 and $C11_b$ "$MoAl_2$" as well as T1 "$Mo_5Al_3$". As initial values, Miedema's [97] estimations of the heats of formation for these hypothetical compounds were used, in

conjunction with entropies of formation estimated using Chart's correlation, as described before. In view of the similar structures of $C11_b$ and C40, it can be argued that their thermodynamic functions should not be very different . Thus, while the estimated values on the Mo-Al side were kept constant for $C11_b$, the deviation from Miedema's estimation was optimized for C40 using the experimental data. On the Mo-Si side, the temperature coefficient of the free energy of C40 was taken to be equal to that of $C11_b$ and only the heat of formation of C40 was optimized. For the T1 phase, only the deviation from Miedema's estimation for the heat of formation of T1 "$Mo_5Al_3$" was optimized. These selections limited to three the number of variables to be optimized in this ternary. The limited data available did not justify adjusting the free energy of the C54 phase although at least minimum values for this phase could be fixed based on the knowledge of its presence in the various isotherms using a concept similar to the one applied previously in the Mo-Si-C system to $Mo_5Si_3C$ (Section 4.1). This would result in more variables to be adjusted and little improvement in the estimates of the region of interest in the diagram.

Table 4.7 summarizes the optimized description of the ternary phases in this model. The calculated 1400°C isotherm is presented in Figure 4.15. It displays a larger solubility of aluminum in $C11_b$ than measured but shows good overall agreement with the experimental isotherms in the regions of interest. Figure 4.16 shows the activity of aluminum along a section of constant $X_{Mo}$=0.33. Since $C11_b$ and C40 are modeled as line compounds with a fixed $X_{Mo}$, a very slight deviation towards molybdenum-rich compositions is necessary to define the activity in the absence of the liquid phase.

Calculations were made at higher temperatures, with the following results. The stability range of C40 is not reduced considerably at 2000K and, along the constant $X_{Mo}$=0.33 line, C40 is in equilibrium with the liquid phase above $X_{Al}$=0.15. However, the liquid-C40 equilibrium starts at 2180K ($X_{Al}$=0.15), which was somewhat lower than expected for this phase.

Table 4.7 Summary Description of Phases in the Mo-Si-Al Ternary

| Phase | Comp. | Term in Thermocalc Description | Coefficients | | |
|---|---|---|---|---|---|
| | | | A [a] (J/mol) | Miedema's Estimate for A | B [a] (J/K mol) |
| $C11_b$ | $MoAl_2$ | G($MoSi_2$,Mo:Al;0) | -60000 | -60000 | 0.42 |
| | $MoSi_2$ | G($MoSi_2$,Mo:Si;0) | -137000 [b] | - | -12.758 [b] |
| T1 | $Mo_5Al_3$ | G(T1,Mo:Al;0) | -183400 | -176000 | 2.24 |
| | $Mo_5Si_3$ | G(T1,Mo:Si;0) | -313400 [b] | - | -45.93 [b] |
| C40 | $MoAl_2$ | G(C40,Mo:Al;0) | -68030 | -60000 | 0.42 |
| | $MoSi_2$ | G(C40,Mo:Si;0) | -136290 | - | -12.758 [c] |

Notes:

a) From $G^T_{Mo_pSi_qAl_r} - p\,{}^oG^T_{Mo,BCC} - q\,{}^oG^T_{Si,DIA} - r\,{}^oG^T_{Al,FCC} = A + BT$

b) From the estimated Mo-Si binary.

c) Fixed as the same as for $C11_b$-$MoSi_2$.

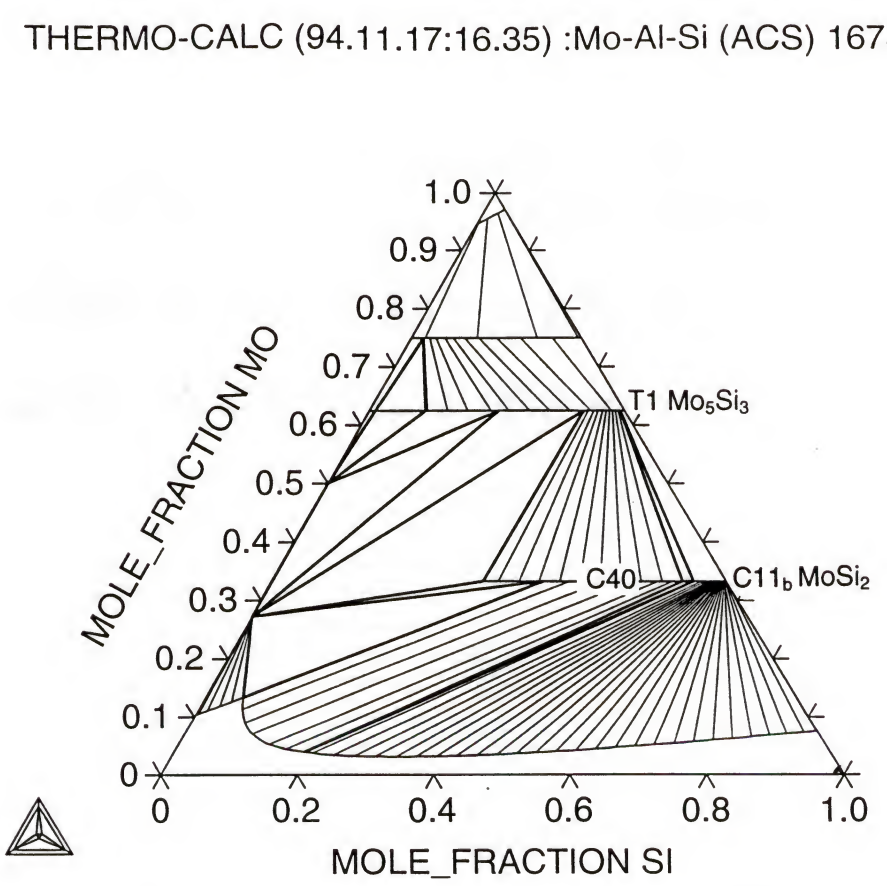


Figure 4.15 Isotherm calculated for the Mo-Al-Si system at 1673K. See text for discussion.

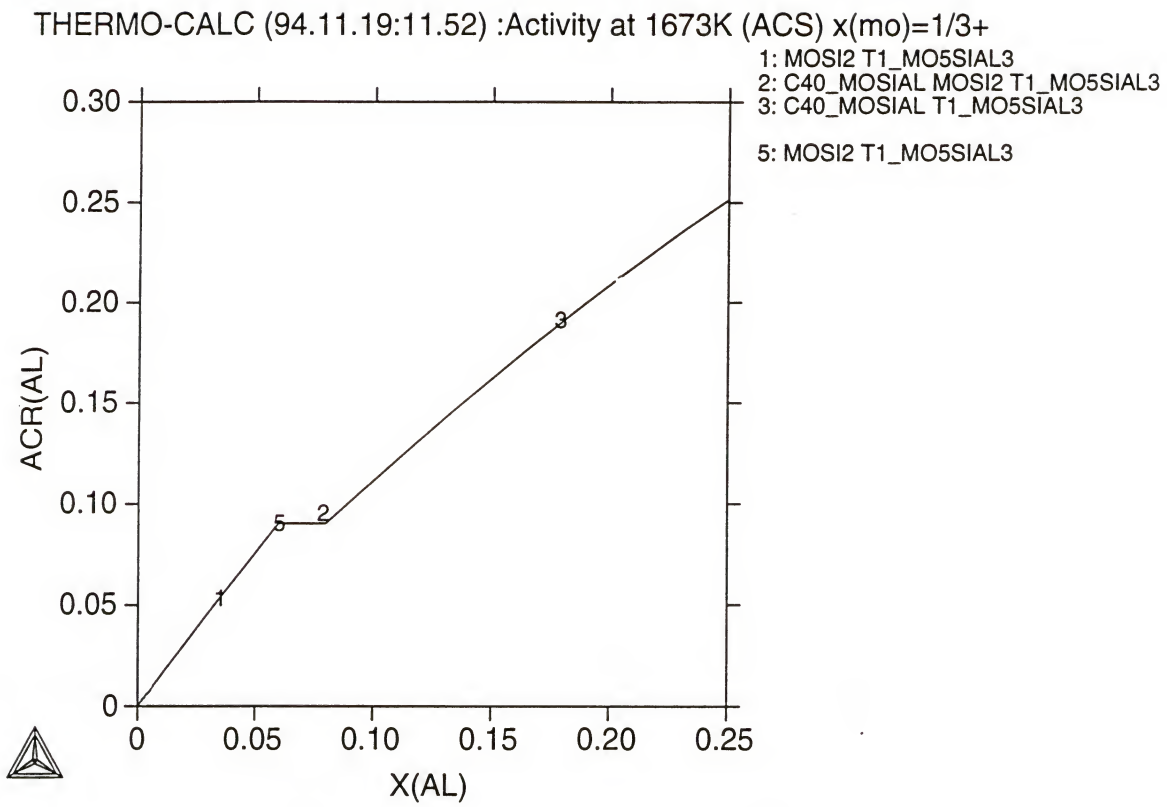


Figure 4.16 Calculated aluminum activity (reference state: pure liquid aluminum at 1673K, 1 atm) along an $X_{Mo}$=0.33 isopleth at 1673K. See text for discussion.

4.5.6.2 The model with limited solubility of aluminum in C40 and T1

In this model, the following phases must have their free energies optimized in a first stage: (a) the metastable C40 $MoSi_2$ and the corresponding MoSiAl and (b) the T1 $Mo_5(Si,Al)_3$ with $X_{Al}$=0.081. This simplifies the optimization process by keeping the solubility of aluminum in $C11_b$ $MoSi_2$ as non-existent and thus avoiding the need to include an additional set of variables in the initial stages of the calculation, when initial values must be established for MoSiAl and the maximum-aluminum containing T1. Once these first values are optimized, aluminum solubility in $C11_b$ can be introduced following the same procedure used in the previous model. The assumption of constant maximum possible aluminum contents in C40 and T1 reduces the degrees of freedom of

the estimate so that in this model, no temperature dependence was introduced for optimization on the ternary phase descriptions. Also in this model, C54 was not introduced, for the same reasons discussed before. Table 4.8 summarizes the optimized description of the ternary phases in this model. The calculated 1400°C isotherm is presented in Figure 4.17a. It displays good agreement with the experimental isotherms in the regions of interest, especially in the three-phase field C40-$C11_b$-T1. Figure 4.17b shows the activity of aluminum along a section of constant $X_{Mo}$=0.33. As before, a very slight deviation towards molybdenum-rich compositions is necessary to define the activity in the absence of the liquid phase. Although calculations were also made at higher temperatures, the results are less reliable, since temperature variation was excluded from the description of the free energy of some of the ternary phases. This leads to a considerable reduction of the stability range of C40 at 2000K and, along the constant $X_{Mo}$=0.33 line, C40-liquid equilibrium does not occur over the composition range investigated ($X_{Al}$<0.3). The aluminum activity estimation at 1400°C, however, agrees well with that of the previous model.

Table 4.8 Summary Description of Phases in the Mo-Si-Al Ternary (Restricted solubility model)

| Phase | Composition | Term in Thermocalc Description | Coefficients | |
|---|---|---|---|---|
| | | | A [a] (J/mol) | B [a] (J/K mol) |
| $C11_b$ | $MoAl_2$ | G($MoSi_2$,Mo:Al;0) | -57520 | - |
| | $MoSi_2$ | G($MoSi_2$,Mo:Si;0) | -137000 [b] | -12.758 [b] |
| T1 | $Mo_5Si_{2.35}(Si,Al)_{0.65}$ | G(T1,Mo:Si:Al;0) | -349570 | |
| | $Mo_5Si_3$ | G(T1,Mo:Si:Si;0) | -313400 [b] | -45.93 [b] |
| C40 | $MoSi_1Al_1$ | G(C40,Mo:Si:Al;0) | -133350 | - |
| | $MoSi_2$ | G(C40,Mo:Si:Si;0) | -155230 | - |

Notes:

a) From $G^T_{Mo_pSi_qAl_r} - p\,{}^oG^T_{Mo,BCC} - q\,{}^oG^T_{Si,DIA} - r\,{}^oG^T_{Al,FCC} = A + BT$

b) From the estimated Mo-Si binary.

4.5.7 Application to *In-situ* Reactions

Based on the modeling of the Mo-Si-Al system one can conclude that the amount of aluminum in solution in $C11_b$ required to equilibrate reactions (4.7) and (4.8) at 1400°C, under the conditions previously discussed, are quite small and in the range of $X_{Al} \approx 10^{-4}$. Thus, as in the case of the aluminum deoxidation of steel [41], the amount of aluminum to be added in order to convert silica to alumina will be defined to a larger extent by the amount of silica present and the eventual losses of aluminum to other sources of oxygen rather than by the soluble aluminum necessary to maintain the reaction equilibrium. It is implicitly assumed that the solubility of oxygen in $MoSi_2$ is negligibly small.

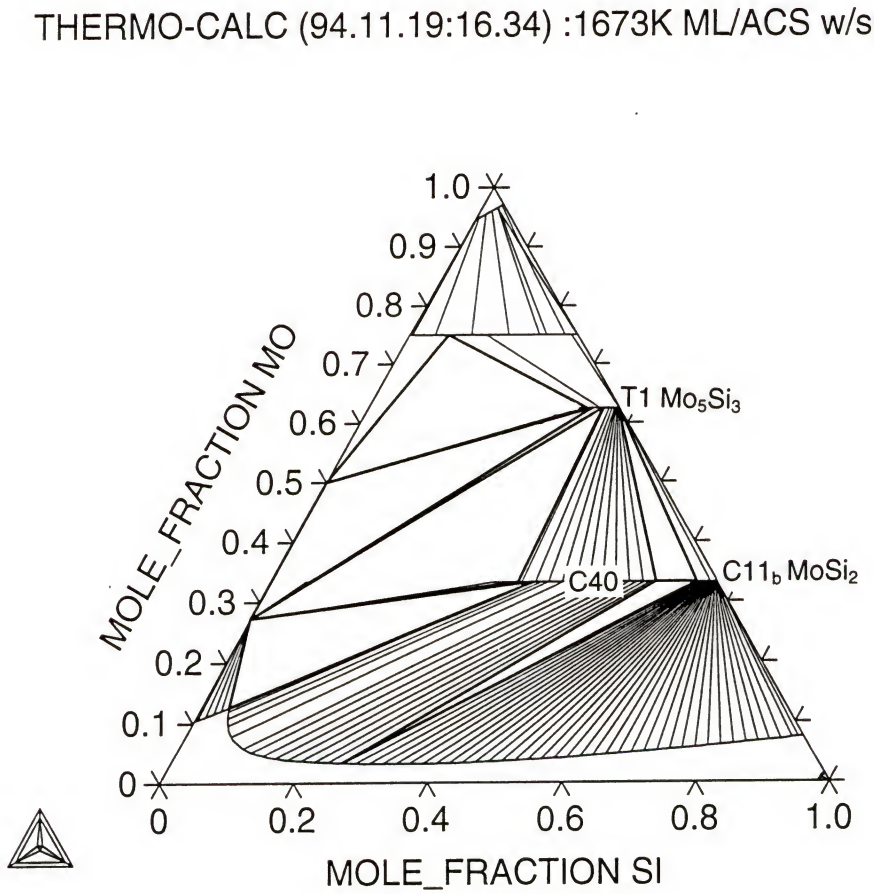


Figure 4.17 (a) Isotherm calculated for the Mo-Al-Si system at 1673K limiting the maximum solubility of aluminum in the C40 and T1 phases. See text for discussion.

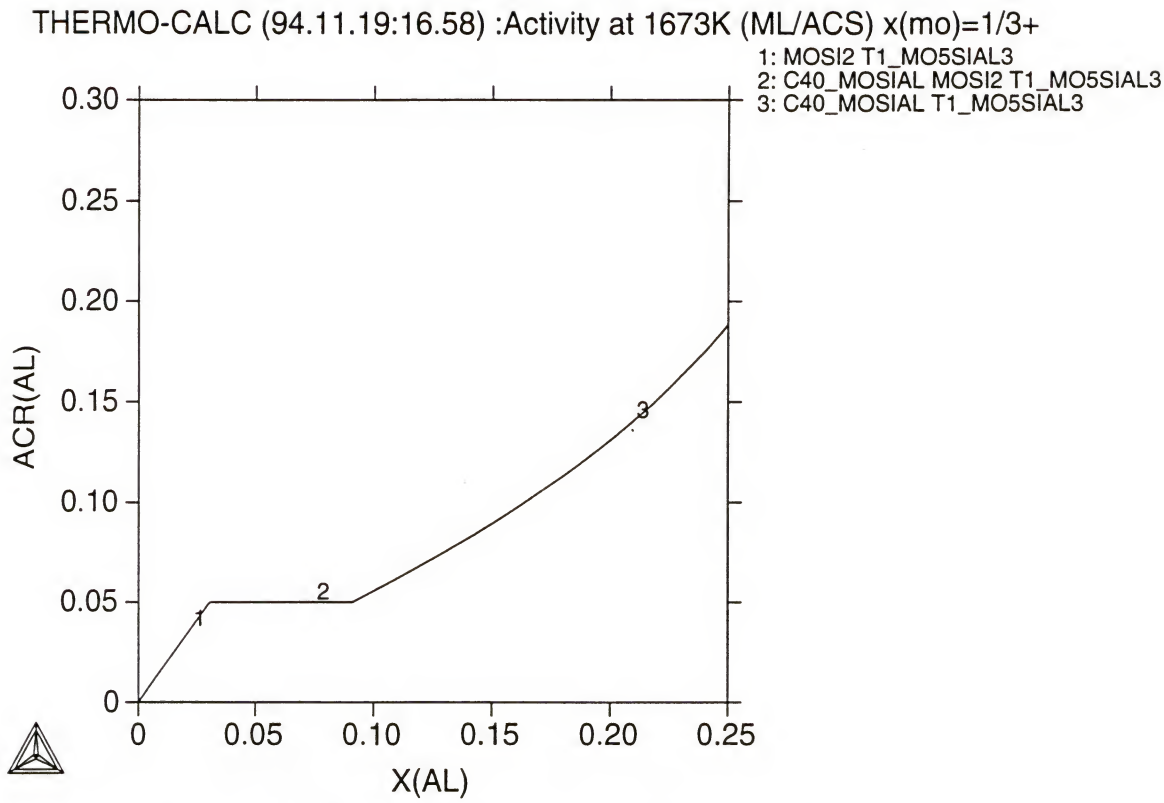


Figure 4.17 continued (b) Calculated aluminum activity (reference state: pure liquid aluminum at 1673K, 1 atm) along an $X_{Mo}$=0.33 isopleth at 1673K. See text for discussion.

## 4.6 Production of *In-situ* $MoSi_2$-Boride Composites

### 4.6.1 Mo-Si-B System

#### 4.6.1.1 Possible displacement reaction schemes

Examination of the 1400°C Mo-Si-B isotherm (section 2.4) [173] indicates that two basic approaches are available to produce $MoSi_2$ -molybdenum boride composites through *in-situ* displacement reactions: (a) reaction of molybdenum with one of the silicon borides ($SiB_4$ or $SiB_6$) and (b) reaction of boron with one of the molybdenum

silicides higher in molybdenum than $MoSi_2$, namely $Mo_3Si$ or $Mo_5Si_3$. The possible reactions are:

$$^2/_3\ Mo_5Si_3 + {}^7/_3\ B = MoSi_2 + {}^7/_3\ MoB \qquad (4.9)$$

$$^2/_3\ Mo_5Si_3 + {}^{35}/_6\ B = MoSi_2 + {}^7/_6\ Mo_2B_5 \qquad (4.10)$$

$$9\ Mo + 2\ SiB_4 = MoSi_2 + 8\ MoB \qquad (4.11)$$

$$^{21}/_5\ Mo + 2\ SiB_4 = MoSi_2 + {}^8/_5\ Mo_2B_5 \qquad (4.12)$$

$$13\ Mo + 2\ SiB_6 = MoSi_2 + 12\ MoB \qquad (4.13)$$

The reactions between boron and the silicides were preferred in view of the higher volume fractions of $MoSi_2$ that can be obtained with these reactions as opposed to those involving the silicon borides. The target composition for the various samples used in this study are indicated in Figure 4.18, together with the relevant reactions, superimposed on the proposed 1400°C isotherm.

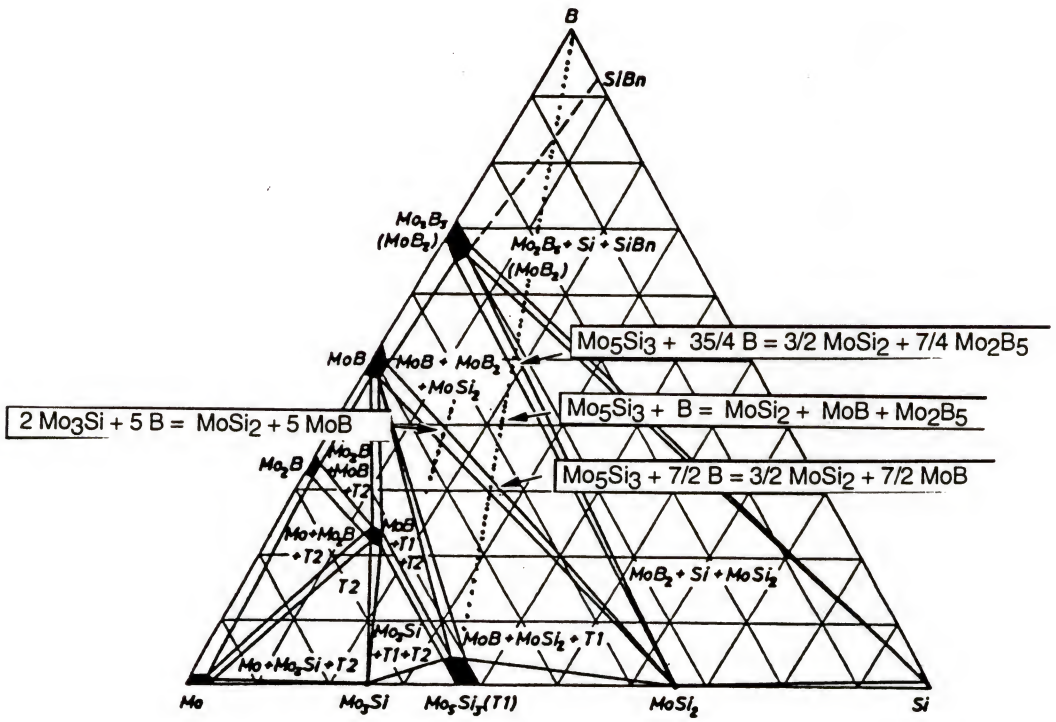
B
SiBn
Mo2B5 (MoB2)
Mo2B5 + Si + SiBn (MoB2)
Mo5Si3 + 35/4 B = 3/2 MoSi2 + 7/4 Mo2B5
Mo5Si3 + B = MoSi2 + MoB + Mo2B5
Mo5Si3 + 7/2 B = 3/2 MoSi2 + 7/2 MoB
2 Mo3Si + 5 B = MoSi2 + 5 MoB
MoB
MoB + MoB2 + MoSi2
Mo2B
Mo2B + MoB + T2
Mo + Mo2B + T2
MoB + T1 + T2
T2
MoB2 + Si + MoSi2
Mo3Si + T1 + T2
MoB + MoSi2 + T1
Mo + Mo3Si + T2
Mo
Mo3Si
Mo5Si3 (T1)
MoSi2
Si

Figure 4.18 Target composition for the various samples used in this study are indicated together with the relevant reactions, superimposed on the Mo-Si-B 1400°C isotherm.

4.6.1.2 Microstructures generated and properties obtained

In all samples, only the phases predicted by the 1400°C isotherm were observed in the XRD analysis after hot pressing. Representative microstructures are shown in Figures 4.19 and 4.20 for the samples containing $MoSi_2$ + MoB and $MoSi_2$ + $Mo_2B_5$. Besides these main phases, a small amount of porosity and a third phase were observed. This phase, which is present in considerable amounts, was identified as an amorphous oxide containing boron and silicon as shown in Figure 4.21. The most striking feature of these microstructures, however, is their fine scale. The grain sizes of the silicide and the boride are substantially finer in the $MoSi_2$ + MoB sample than in the $MoSi_2$ + $Mo_2B_5$ specimen. This difference was also observed when the milling time in the attritor was reduced from 5 to 2 h. In order to confirm that this difference was not caused by the milling process, the XRD patterns of the "as-milled" powders were compared. The peaks corresponding to the starting silicide are always clearly present, while the boron peaks disappear when longer milling times are used. It was observed, however, that the XRD spectrum of pure boron milled for 2 h showed a substantial broadening of the peaks with a corresponding reduction in intensity while 5 h milling was sufficient to cause the disappearance of all crystalline peaks. This may suggest that the changes occurring during milling could be associated with the "amorphization" or vitrification of crystalline boron, rather than with the formation of solutions or new phases. Since the processes ocurring when milling pure boron are probably not the same as those happenning when all powders are present in the attritor, this suggestion cannot be confirmed at this point.

Samples with compositions in the three-phase $MoSi_2$ + $Mo_2B_5$ + MoB field were also produced. These samples had grain sizes comparable to those of the $MoSi_2$ + $Mo_2B_5$ sample.

Table 4.9 presents hardness and toughness results for the different samples, compared to monolithic $MoSi_2$. As expected, the hardness values are substantially higher

than that of $MoSi_2$; the agreement with the values predicted by the rule of mixtures is reasonable. Although there is considerable scatter in the toughness results, all microstructures resulted in significant improvement over monolithic $MoSi_2$. This is especially interesting because the values reported in Table 4.9 are probably conservative estimates, since they were calculated using the elastic modulus of $MoSi_2$ which is significantly smaller than that of the borides.

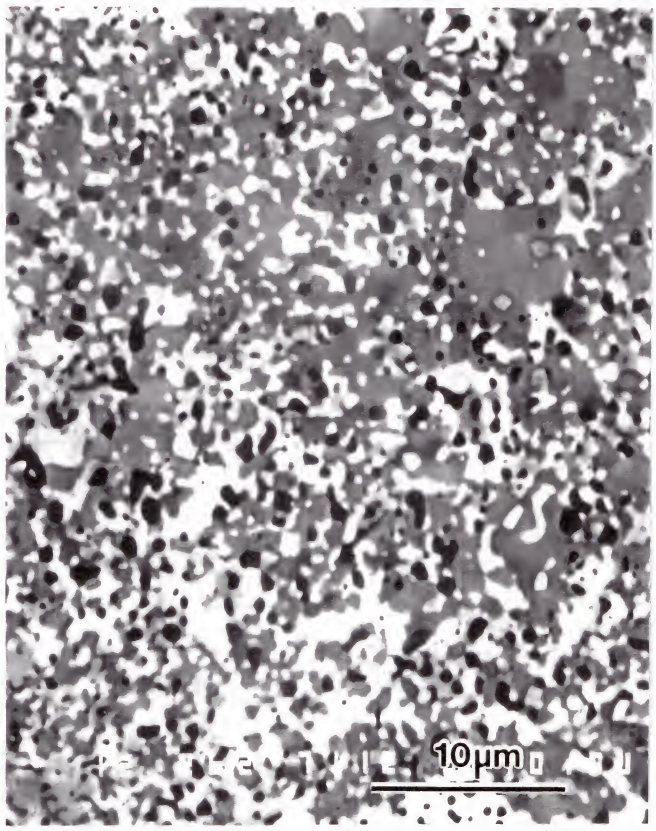


Figure 4.19 Microstructure (BEI) of *in-situ* $MoSi_2$ + MoB composites. Dark regions are oxide and small amount of porosity.

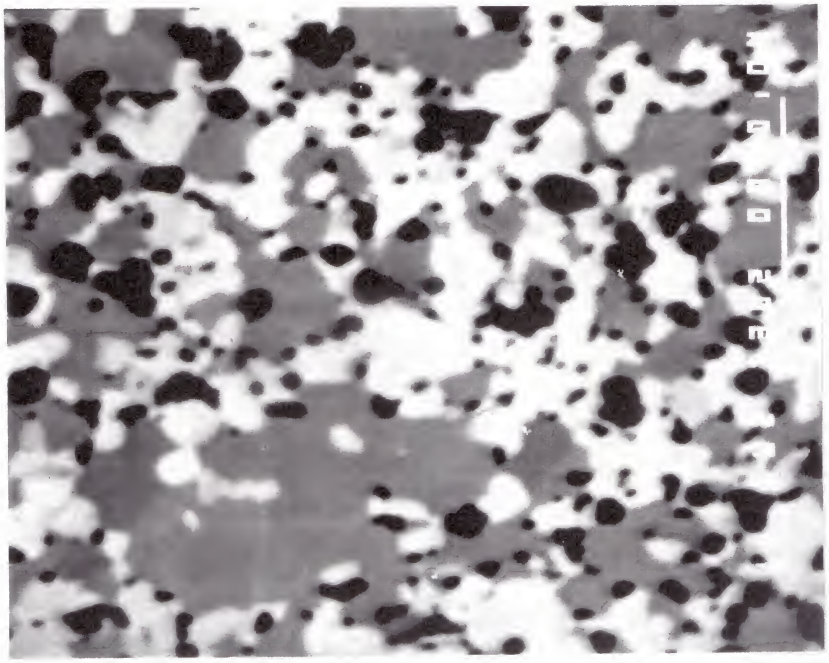

Figure 4.20 Microstructure (BEI) of *in-situ* $MoSi_2$ + $Mo_2B_5$ composites. Dark regions are oxide and small amount of porosity.

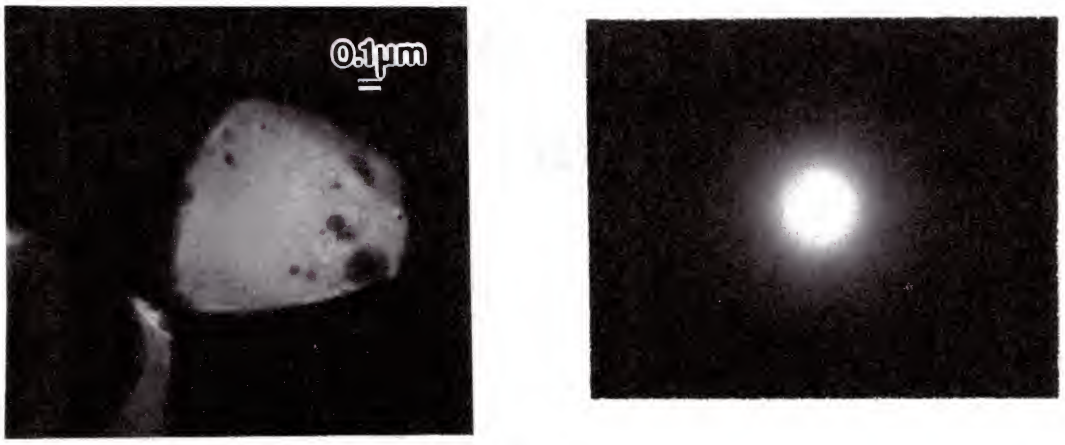


Figure 4.21 Transmission electron micrographs of amorphous oxide particles in *in-situ* $MoSi_2$ + MoB composites.

Table 4.9 Hardness and Indentation Fracture Toughness of Hot-Pressed $MoSi_2$ - Molybdenum Boride Composites.

| Microstructure | Theoretical volume fraction | Rule of mixtures estimates | | Hardness [a] (GPa) | | $K_C$ [a] (MPa$\sqrt{m}$) | | |
|---|---|---|---|---|---|---|---|---|
| | | Density ($g/cm^3$) | Hardness (GPa) | Aver. | σ | Aver. | σ | Crack size[b] (μm) |
| $MoSi_2$ | 1 | 6.31 | - | 8.6 | 0.3 | 3.6 | 0.2 | 208 |
| $MoSi_2$ + MoB | 0.44 / 0.56 | 7.65 | 16.4 | 17.3 | 0.6 | 3.9 | 0.3 | 199 |
| $MoSi_2$ + $Mo_2B_5$ | 0.44 / 0.56 | 6.96 | 16.6 | 15.6 | 0.6 | 4.5 | 0.4 | 187 |
| $MoSi_2$ + MoB + $Mo_2B_5$ | 0.44/0.26/ 0.28 | 7.14 | 16.2 | 15.2 | 0.5 | 4.9 | 0.3 | 180 |

[a] All values based on five measurements per load per sample.
[b] For 5 Kgf load.

4.6.1.3 The MoB-$MoSi_2$ microstructure

To better understand the processes occurring during the *in-situ* reaction, samples were prepared with a "well-defined" interface between the silicide and boron. This was accomplished by hot pressing diffusion couples with a relatively flat interface as well as coarse boron particles (2-3 mm) in a matrix of finely ground $Mo_5Si_3$. Figure 4.22 shows a typical interdiffusion zone of the B-$Mo_5Si_3$ couple. The phase sequence in the diffusion couple is B- $Mo_2B_5$ -($MoSi_2$ + $Mo_2B_5$)-MoB- ($MoSi_2$ + MoB)- $Mo_5Si_3$ and the loci of three-phase equilibria were non-planar, indicating that either the chemical potentials were not functions of a single variable (distance from the original interface) or the system was higher order than ternary. Due to the difficulties in preparing flat diffusion couples without preferred diffusion paths (e.g. particle surfaces), it was concluded that the former is the most plausible explanation. Furthermore a large portion of the growth of $MoSi_2$ + MoB into $Mo_5Si_3$ occurred as an agglomerate structure, as shown in Figure 4.23. Boron seems to be the fast moving species, in view of the apparent location of the initial interface. As expected, parabolic growth was observed, within the limits of the experimental conditions.

Figure 4.22 Typical interdiffusion zone in a B-$Mo_5Si_3$ couple. The phase sequence is B-$Mo_2B_5$-($MoSi_2$ + $Mo_2B_5$)-MoB-($MoSi_2$+MoB)-$Mo_5Si_3$.

In order to further explore the $MoSi_2$ + MoB agglomerate structure, a sample consisting of boron and $Mo_5Si_3$ powders (ground to approximately 50-70 μm) was hot pressed. The microstructure of this sample is shown in Figure 4.24. The agglomerate structure is the dominant feature of the microstructure. Furthermore, TEM analyses have shown that there is a simple orientation relationship between $MoSi_2$ and MoB, namely $(001)_{MoB}$ // $(001)_{MoSi_2}$ and $[110]_{MoB}$ // $[110]_{MoSi_2}$ as shown in Figure 4.25. This is not unexpected since both phases have tetragonal structures and similar lattice parameters in their (001) planes (as shown in Section 2.4.2). Besides, the (001) planes in both phases contain only Mo atoms and these are located in the same positions. These observations strongly suggest that $MoSi_2$ and MoB grow in a cooperative manner during these displacement reactions.

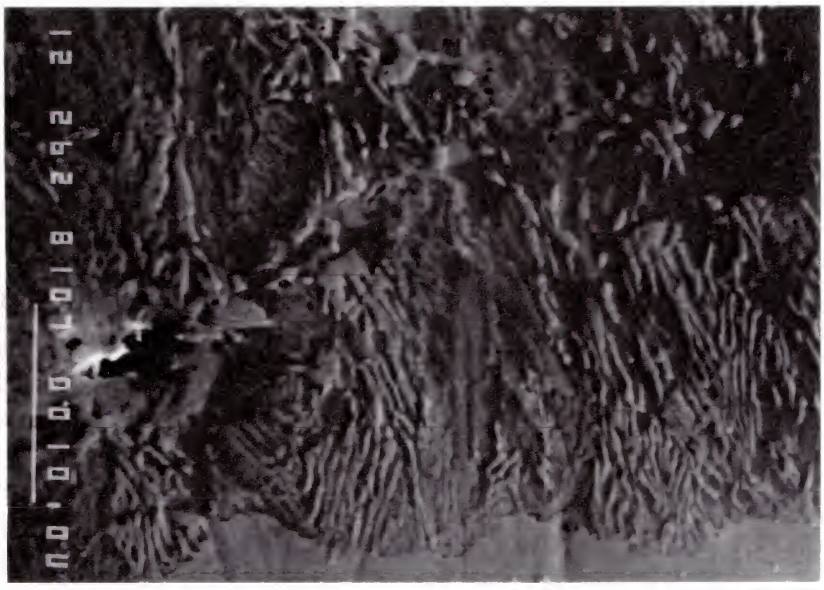

Figure 4.23 Microstructure (SEM) of the agglomerate $MoSi_2$-MoB structure growing in $Mo_5Si_3$ in a B-$Mo_5Si_3$ diffusion couple (bulk phase is $Mo_5Si_3$, dark phase is $MoSi_2$).

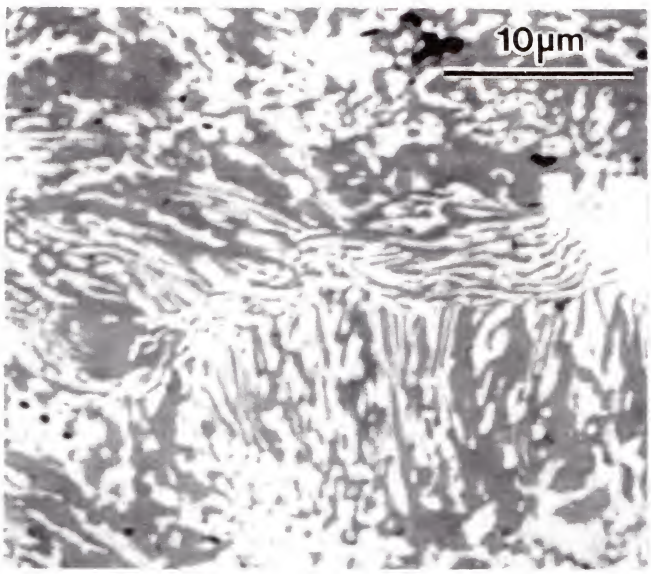


Figure 4.24 Microstructure (SEM) of the agglomerate $MoSi_2$-MoB structure growing in a hot pressed mixture of B and $Mo_5Si_3$.(light phase is MoB, dark phase is $MoSi_2$).

4.6.2 Mo-Si-B-Ti System

With the aim of evaluating the possibility of producing $MoSi_2$-$TiB_2$ composites through *in-situ* displacement reactions, the Mo-Si-Ti-B system was appraised at 1400°C. The data of Kaufman [143] were used to calculate the quaternary isotherm. In order to verify that his data were sufficiently accurate for this calculation, the following tests were performed: (a) the binary diagrams were verified to reproduce satisfactorily the experimental binaries (evidently, Kaufman's simplified model assumed that all intermediate phases were line compounds). In addition, the parameters used to describe the intermediate compounds were verified to agree reasonably well with tabulated $\Delta H^0_{298}$ and $\Delta S^0_{298}$ values for these compounds (in some cases, the adoption of simple descriptions for the liquid led to somewhat large deviations in melting points); (b) some of the 1400°C ternary isotherms were calculated using Thermocalc (using Redlich-Kister-Muggianu model) for the regions of interest.

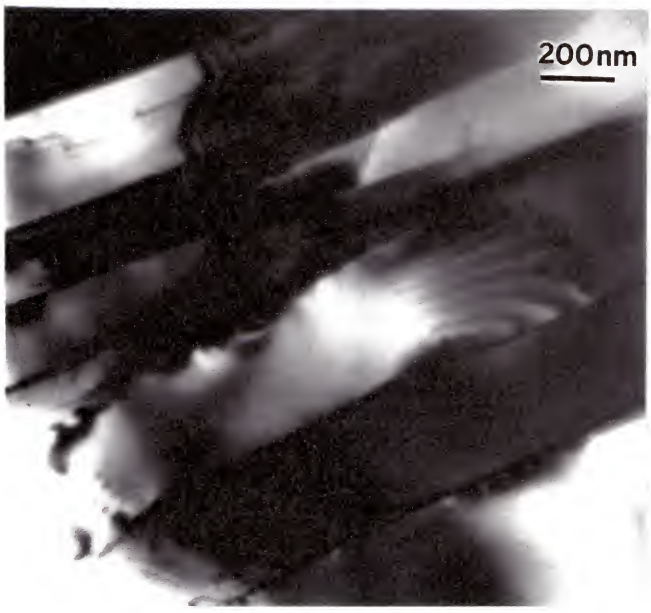


(a)

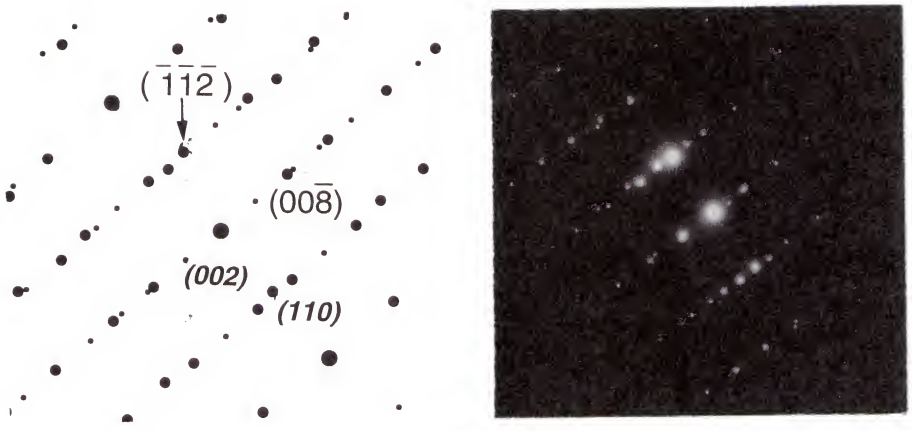


(b)

Figure 4.25 (a) Bright field (BF) TEM of MoB and $MoSi_2$ parallel plates from Figure 4.23. (b) Corresponding diffraction pattern and computer simulation of the diffraction pattern. In the simulated diffraction pattern, the italicized indices correspond to $MoSi_2$ and the normal indices to MoB. B=[$\bar{1}$10].

Thus, the Mo-Si-B and Mo-Ti-Si isotherms were calculated and compared to the available experimental isotherms, as shown in Figure 4.26 for the Mo-Si-B system. The agreement is satisfactory, considering that no ternary phases are described in this model and that it does not describe solubility of third elements in any of the intermediate compounds. These assumptions are justified since the ternary phases that occur in these systems are out of the region of interest for the *in-situ* composites and there are no data readily available to extend the description of the compounds in the ternary and quaternary systems. Furthermore, the existence of a liquid phase at the compositions and temperatures of interest is not anticipated.

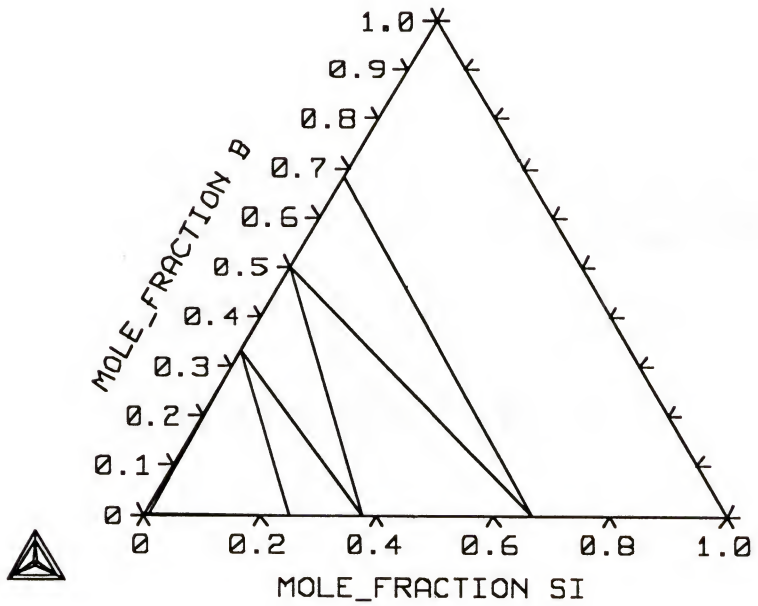


Figure 4.26 Calculated Mo-Si-B ternary 1400°C isotherm used to verify the simple model applied to the calculation of the quaternary Mo-Si-Ti-B system.

A portion of the calculated quaternary isotherm is shown in Figure 4.27. Two points deserving special attention are: (a) $MoSi_2$ and $TiB_2$ are in equilibrium at 1400°C, and (b) among the various four-phase fields (polyhedra) that surround the $MoSi_2$-$TiB_2$

two-phase field (here degenerated into a single tie-line, in view of the absence of composition variation of the compounds), one contains only high melting phases, namely $MoSi_2$, $TiB_2$, MoB and $Mo_2B_5$. Thus, in order to prevent lower-melting phases (such as some of the titanium silicides), deviations from the exact $MoSi_2$-$TiB_2$ composition should preferably be in the direction of this four-phase field.

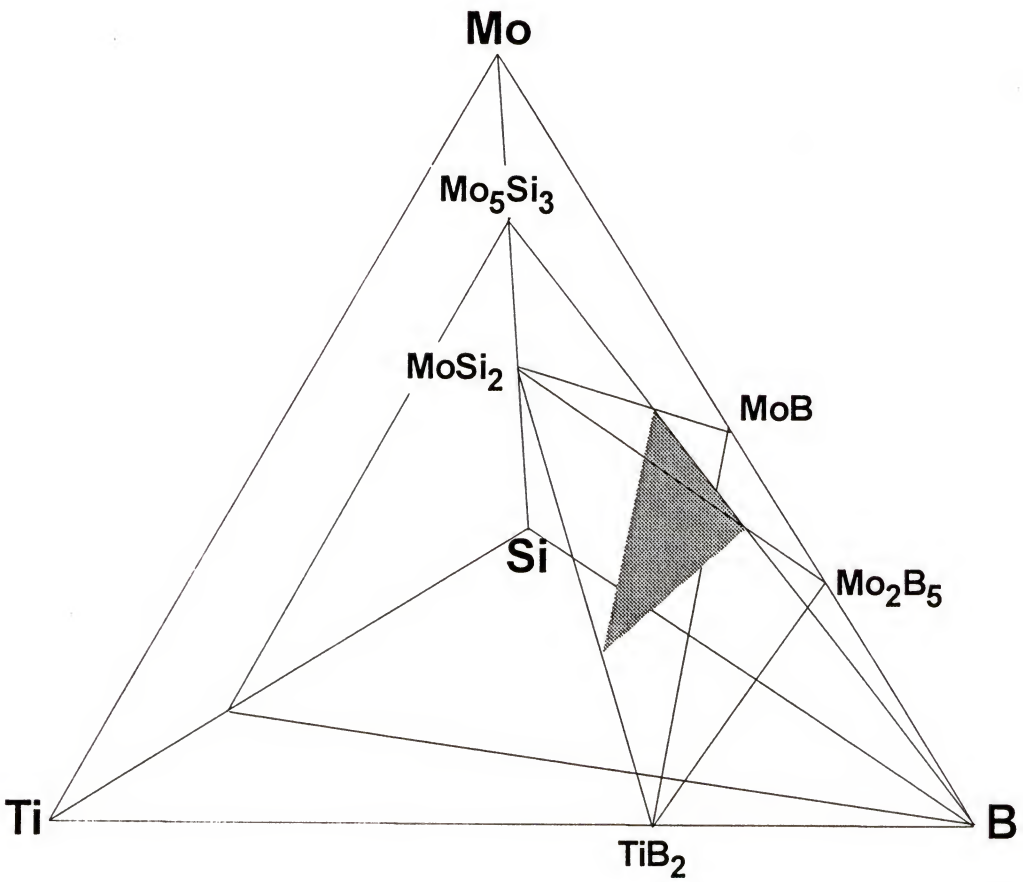


Figure 4.27 Schematic of a part of the calculated 1400°C isotherm in the Mo-Si-Ti-B phase diagram. The four-phase field $MoSi_2$-MoB-$Mo_2B_5$-$TiB_2$ is indicated, as well as the B-$Mo_5Si_3$-$Ti_5Si_3$ plane, locus of the compositions produced by *in-situ* displacement reactions in this study.

4.6.2.1 Proposed displacement reaction scheme

Extending the concept of reacting lower silicides with boron to form $MoSi_2$ plus a boride, both molybdenum and titanium silicides should be used, when titanium diboride is a desired reaction product. Obviously, this is not the only displacement reaction that will lead to these two phases in this quaternary system. As discussed for the case of the molybdenum borides, there is a number of combinations of the compounds present in this system that can react to achieve the desired overall composition. While the enumeration of all possibilities is viable, the experimental pursuit of all such candidate schemes was beyond the scope of this work.

The overall reaction scheme adopted in this investigation is analogous to the one applied to the $MoSi_2$-MoB composites and is described by:

$$^{3}/_{7}\ Mo_5Si_3 + Ti_5Si_3 + 10\ B = {}^{15}/_{2}\ MoSi_2 + 5\ TiB_2 \qquad (4.14)$$

This reaction can be represented by the intersection of the plane defined by $Mo_5Si_3$-$Ti_5Si_3$-B with the $MoSi_2$-$TiB_2$ line as schematically shown in the quaternary isotherm (Figure 4.27). The microstructure of the hot pressed samples prepared with the reactants according to reaction (4.14) is shown in Figure 4.28. As expected from the stoichiometry of reaction (4.14) and the theoretical densities, the volume fraction of $TiB_2$ is close to 60%. In order to adjust the microstructure and obtain a matrix of $MoSi_2$, an addition of pre-reacted $MoSi_2$ was made, to achieve a total volume fraction of $MoSi_2$ of 60%. The resulting microstructure was even finer than that of the material produced according to reaction (4.14), as shown in Figure 4.29.

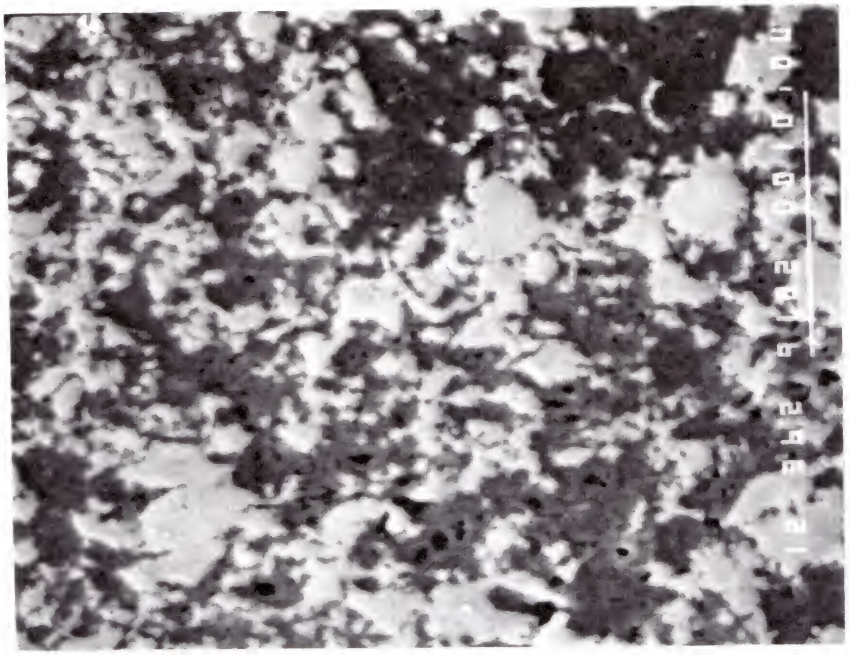

Figure 4.28 Microstructure (SEM) of $MoSi_2$-$TiB_2$ composites produced through *in-situ* displacement reaction, without any pre-reacted addition.

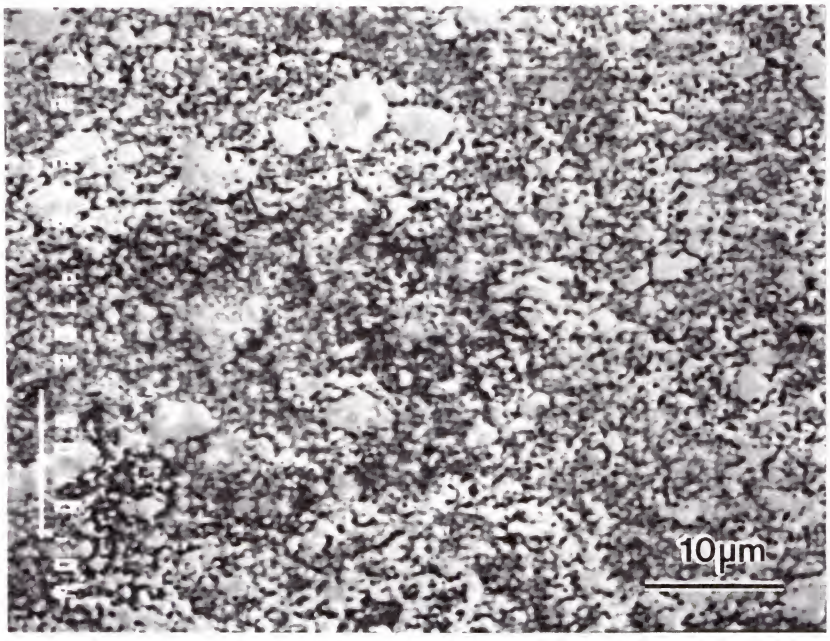


Figure 4.29 Microstructure (SEM) of $MoSi_2$-$TiB_2$ composites produced through *in-situ* displacement reaction, with the addition of pre-reacted $MoSi_2$.

4.6.2.2 *In-situ* vs. elemental powders

In order to investigate whether the fine structure obtained via the displacement reaction was a characteristic of the *in-situ* reaction or not, samples consisting of mixtures of the elemental powders (Ti, Mo, Si and B powders) were mixed using similar conditions and proportions required to produce the same final volume fraction of $MoSi_2$ and $TiB_2$ and hot pressed under the same experimental conditions. Figure 4.30 presents the resulting microstructure. Even though conversion to $MoSi_2$ and $TiB_2$ is complete as confirmed by XRD and EMPA, there is a substantial difference in the scale of this microstructure when compared with that produced by the *in-situ* process (Figure 4.29) which is considerably finer. In order to determine the sequence of events leading to these different microstructures, the following techniques were used: differential thermal analysis (DTA), interrupted hot pressing at different temperatures, and instrumented hot pressing in which a thermocouple was inserted in the powders during the densification cycle.

Comparison of microstructural evolution. DTA analysis of both loose MA powders and MA powders cold compacted at 20 MPa failed to reveal any significant peak, albeit a deviation in the exothermic direction was observed over the temperature range of 500-1200°C. XRD analysis of the samples after DTA to 1400°C indicated the presence of $MoSi_2$ and $TiB_2$ only, i.e., complete reaction. Thus, no detailed information concerning the temperature range at which the different reactions occurred was obtained using DTA. For this reason, the volume change during hot pressing was used as an indication of the reaction temperature. Information was obtained indirectly by monitoring the displacement required to keep a constant load during pressing. It was observed that the largest displacement under load in the pressing of the mixtures for the production of *in-situ* composites occurred above 1000°C. Thus, three temperatures between 1000 and 1400°C (the final hot pressing temperature) were selected for the performance of the

interrupted hot pressing tests. In these tests, the compression stress was maintained at 45 MPa after reaching 800°C, as in the case of the actual hot pressing cycle but the heating was stopped as soon as the desired temperature was attained. This may be substantially different from the DTA experiments even when the same cold compaction used in the hot pressing cycle is applied, since the volume reduction during heating is not accompanied by further compression. In fact, while the samples after DTA did not show substantial densification, the hot pressing interrupted at 1300°C resulted in a specimen with the same "metallic" appearance as those resulting from hot pressing at 1400°C.

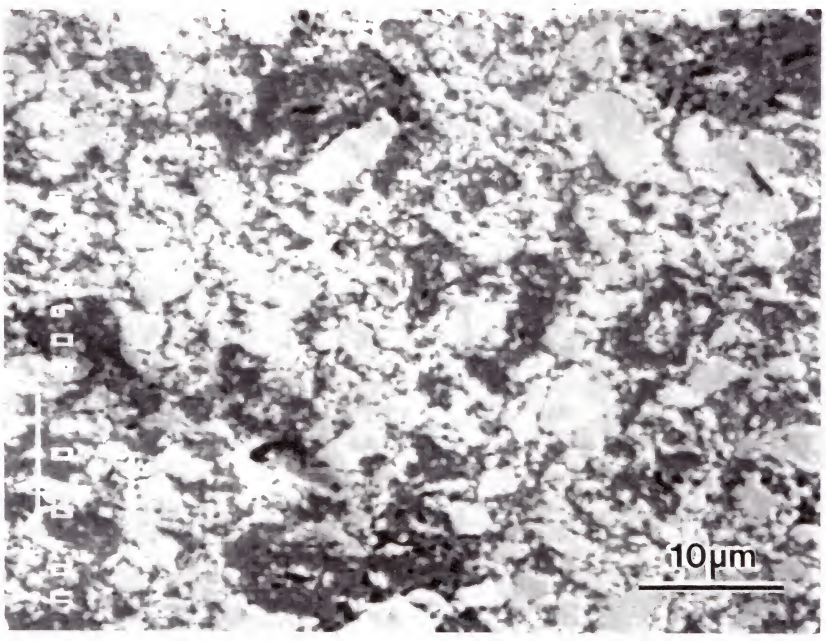


Figure 4.30 Microstructure (SEM) of $MoSi_2$-$TiB_2$ composite produced through reaction of elemental powders to result in the same volume fractions as the material in Figure 4.29.

The results of XRD analysis of the samples hot pressed at 1000, 1150 and 1300°C are presented in Figures 4.31 and 4.32. Comparison of the results obtained with

elemental powders and with the *in-situ* displacement reaction seems to indicate that significant $MoSi_2$ formation from elemental Mo and Si occurs at a lower temperature than the displacement reaction in accordance with the findings of Jayashankar and Kaufman [43] as discussed before. While this is somewhat masked by the presence of pre-reacted $MoSi_2$ in the normal composition used for the displacement reaction, it is evident from the results obtained using the exact stoichiometry for total conversion to $MoSi_2$ +$TiB_2$ (Figure 4.33).

For the embedded thermocouple tests, one sample consisting of the mixture of elemental powders and one containing the reactants used for the *in-situ* displacement reaction were hot pressed as described in Chapter 3, so that the actual sample temperature could be compared to the die temperature. In both cases, the sample temperatures lagged the die temperature by approximately 100K to around 1000°C with the temperature differences decreasing continuously from that point on and the hot pressing temperature being reached simultaneously (within the experimental uncertainties) by the sample thermocouple and the die. At no point in the cycle did the sample temperature exceed the die temperature, indicating that the exothermic processes eventually occurring do not do so in an explosive manner and, evidently, that the conditions inside the graphite die, are far from adiabatic in these processes. This supports the argument that the present conditions are inadequate for the occurrence of SHS, and the coarser $MoSi_2$ particle size is due to its earlier formation and longer growth time.

In an attempt to further elucidate the microstructural evolution of these samples, their microstructures were evaluated using SEM and EMPA. In order to preserve their integrity, the samples hot pressed at 1000 and 1150°C had to be impregnated with acrylic resin prior to metallographic preparation as described in Chapter 3. Low magnification micrographs of the three different powder compositions (elemental powders, displacement reaction, displacement reaction diluted with $MoSi_2$) pressed at 1000, 1150 and 1300°C are presented in Figure 4.34.

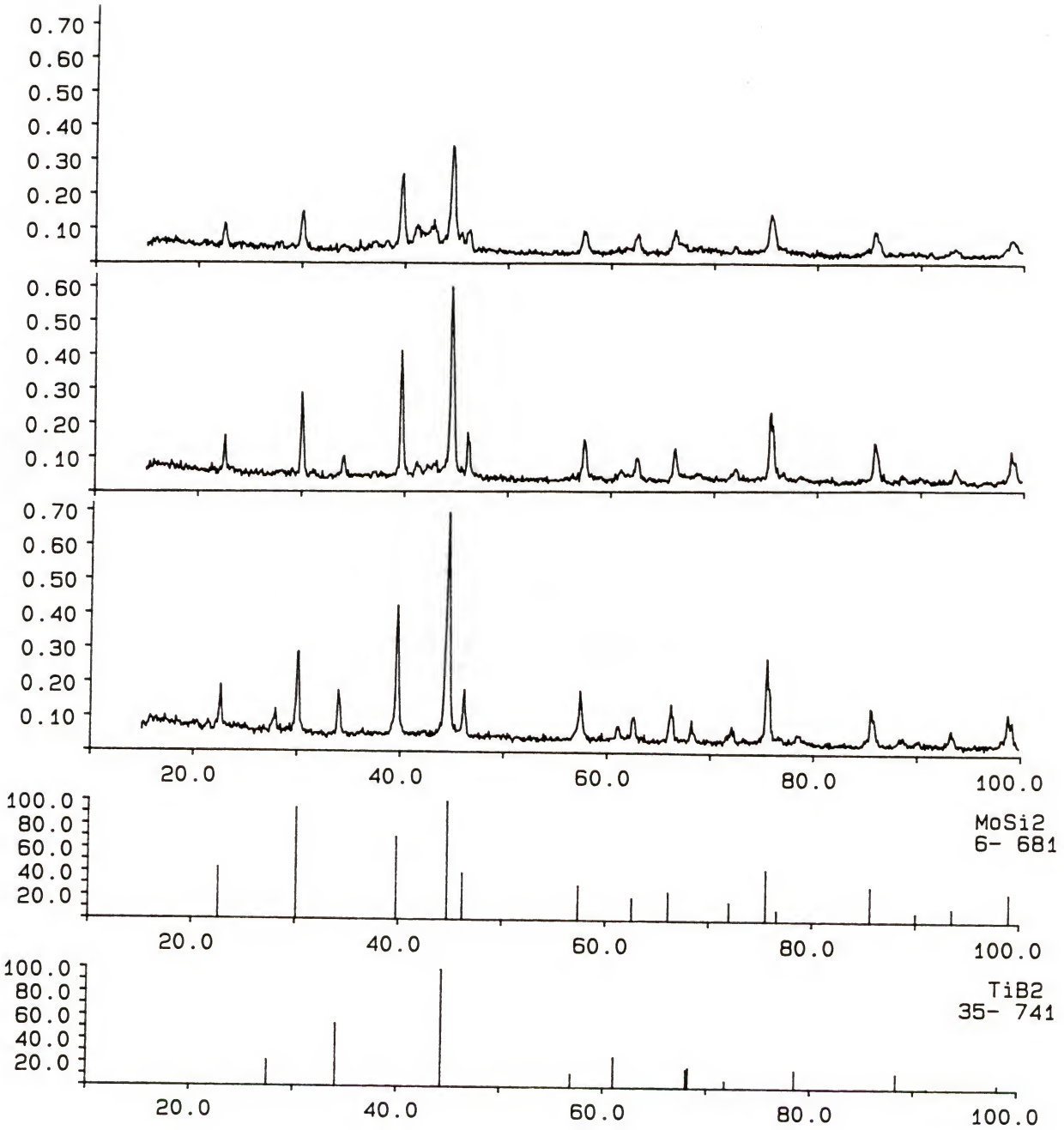


Figure 4.31 X-ray diffractograms of the *in-situ* formation of $MoSi_2$+$TiB_2$ interrupted at 1000, 1150 and 1300°C, compared with the JCPDS cards for these phases.

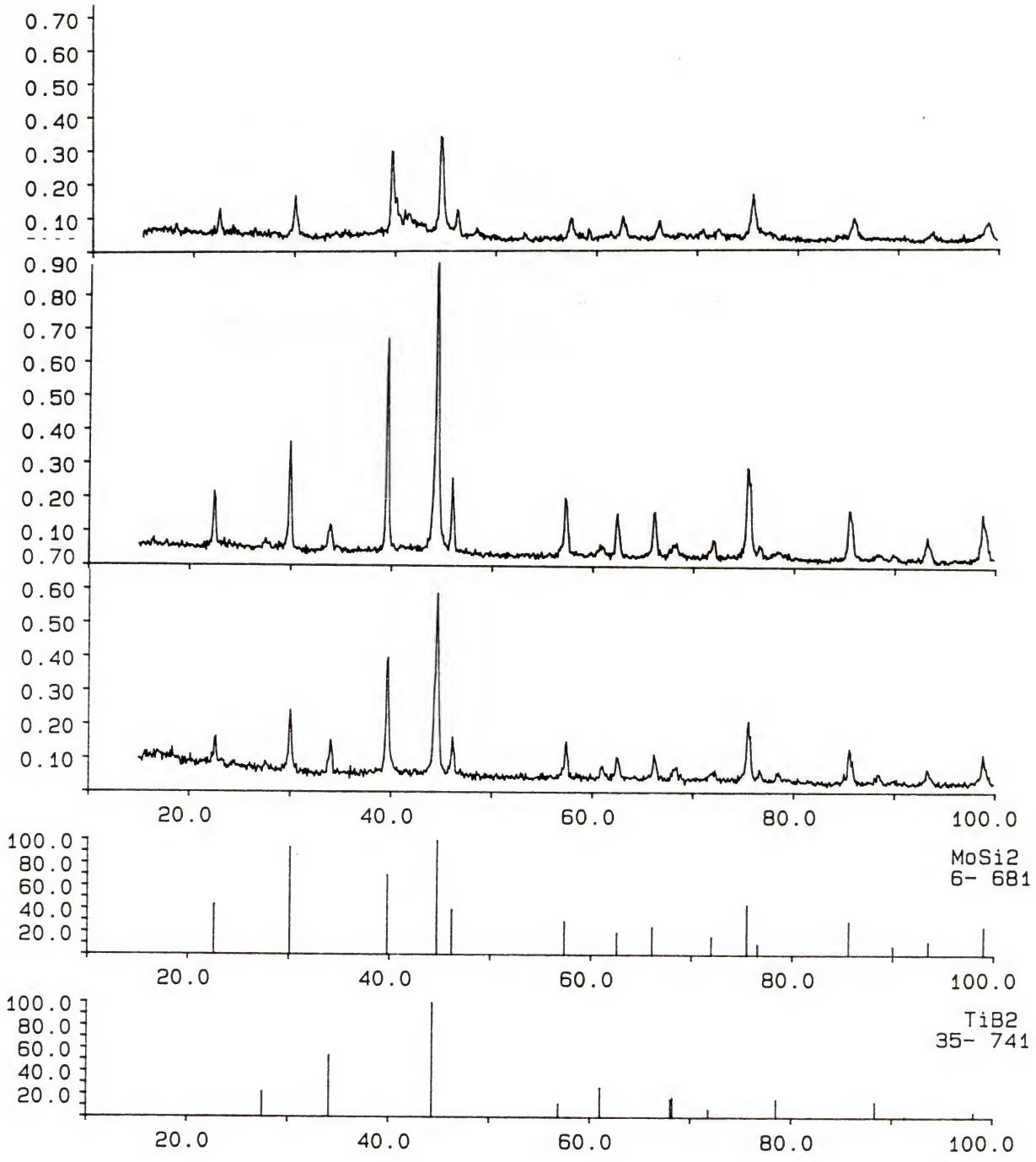


Figure 4.32 X-ray diffractograms of the formation of $MoSi_2$+$TiB_2$ from elemental powders interrupted at 1000, 1150 and 1300°C, compared with the JCPDS cards for these phases.

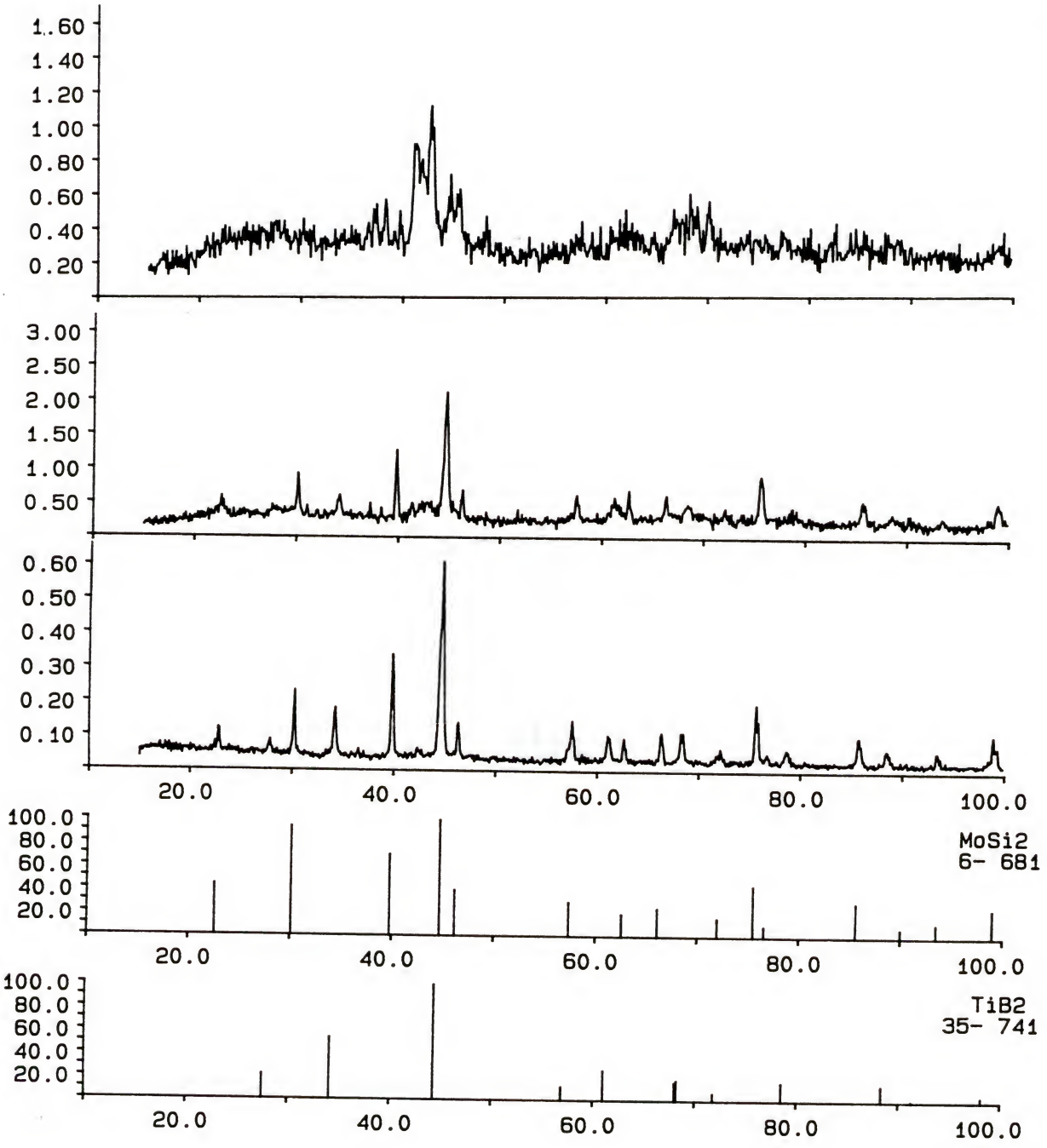


Figure 4.33 X-ray diffractograms of the *in-situ* formation of $MoSi_2$+$TiB_2$ without the addition of pre-reacted $MoSi_2$, interrupted at 1000, 1150 and 1300°C, compared with the JCPDS cards for these phases.

The salient feature of these microstructures is the relatively lower densification observed in the samples involving the displacement reaction up to 1150°C, and the presence of unreacted boron particles in all samples except two of those hot pressed to 1300°C. The EMPA indicated that the boron particles, in general, contained approximately 5 at % Si. Using TEM analysis, the presence of dissolved silicon was confirmed and the structure of the boron particles was determined to be that of the rhombohedral form of boron (α-B).

Phase identification in these samples was made difficult by two factors: (a) the small scale of the microstructure, which not only interfered with the spatial resolution of the EMPA but also limited the possibility of obtaining diffraction patterns from individual grains, and the low strength of these partially reacted samples, which, in most cases, prevented the preparation of samples for TEM. However, some results were obtained as described in the following paragraphs.

Elemental powders. It was possible to identify a considerable volume fraction of $MoSi_2$ in the elemental-powders sample hot pressed at 1000°C as well as some unreacted titanium as shown in Figure 4.35. This is consistent with the XRD patterns presented in Figure 4.31. An interesting feature of this sample is the presence of boron in contact with titanium. This supports the hypothesis that the activation energy for the Ti-B reaction is quite high, as previously discussed. Furthermore, the titanium particles contain molybdenum in solution, and a layer of $Ti_5Si_3$ can be observed to surround some of these particles, both at 1000 and 1150°C (Figure 4.36). Even though the amount of this silicide appears to be higher at 1150°C, it is still insufficient to produce peaks in the XRD spectrum from these samples. In the sample hot pressed at 1150°C, it is possible to detect the formation of $TiB_2$ at the interfaces between boron and titanium silicide (Figure 4.37).

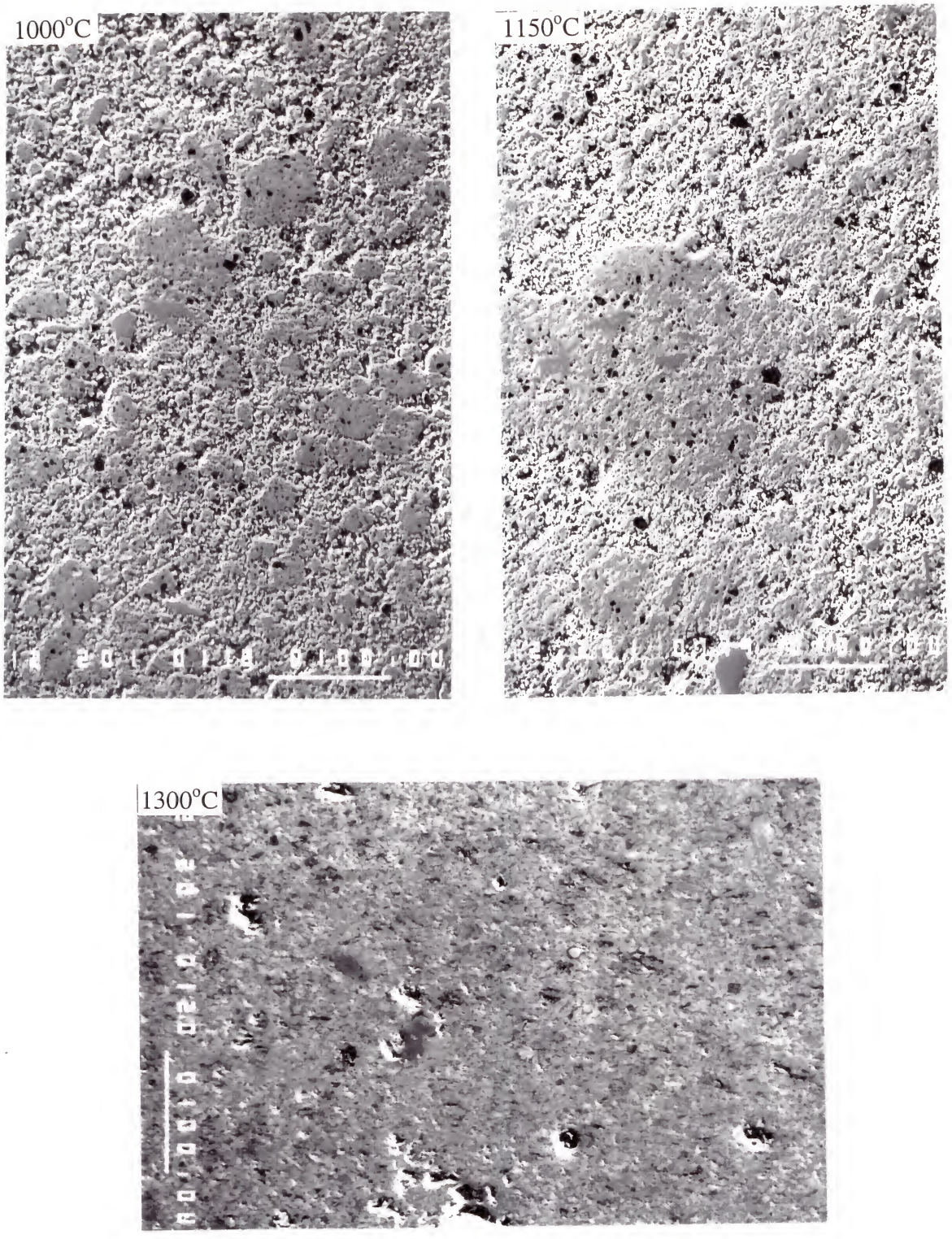


(a)

Figure 4.34 (a) SEM of elemental Mo-Si-Ti-B hot pressed at 1000, 1150 and 1300°C (as indicated) to produce $MoSi_2$+$TiB_2$ composites. See text for discussion.

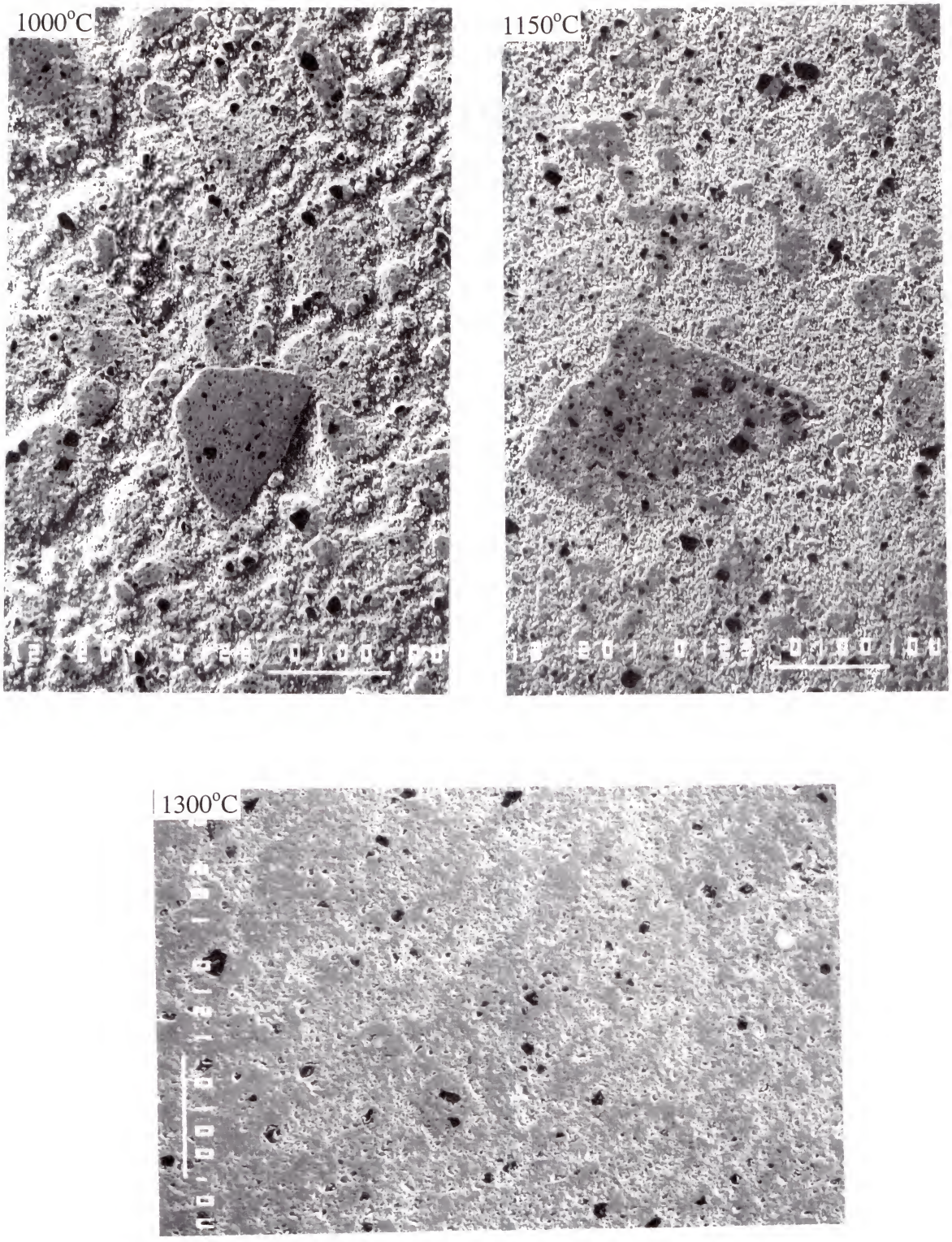


(b)

Figure 4.34 (continued) (b) SEM of $Ti_5Si_3$+$Mo_5Si_3$+B hot pressed at 1000, 1150 and 1300°C (as indicated) to produce $MoSi_2$+$TiB_2$ composites. See text for discussion.

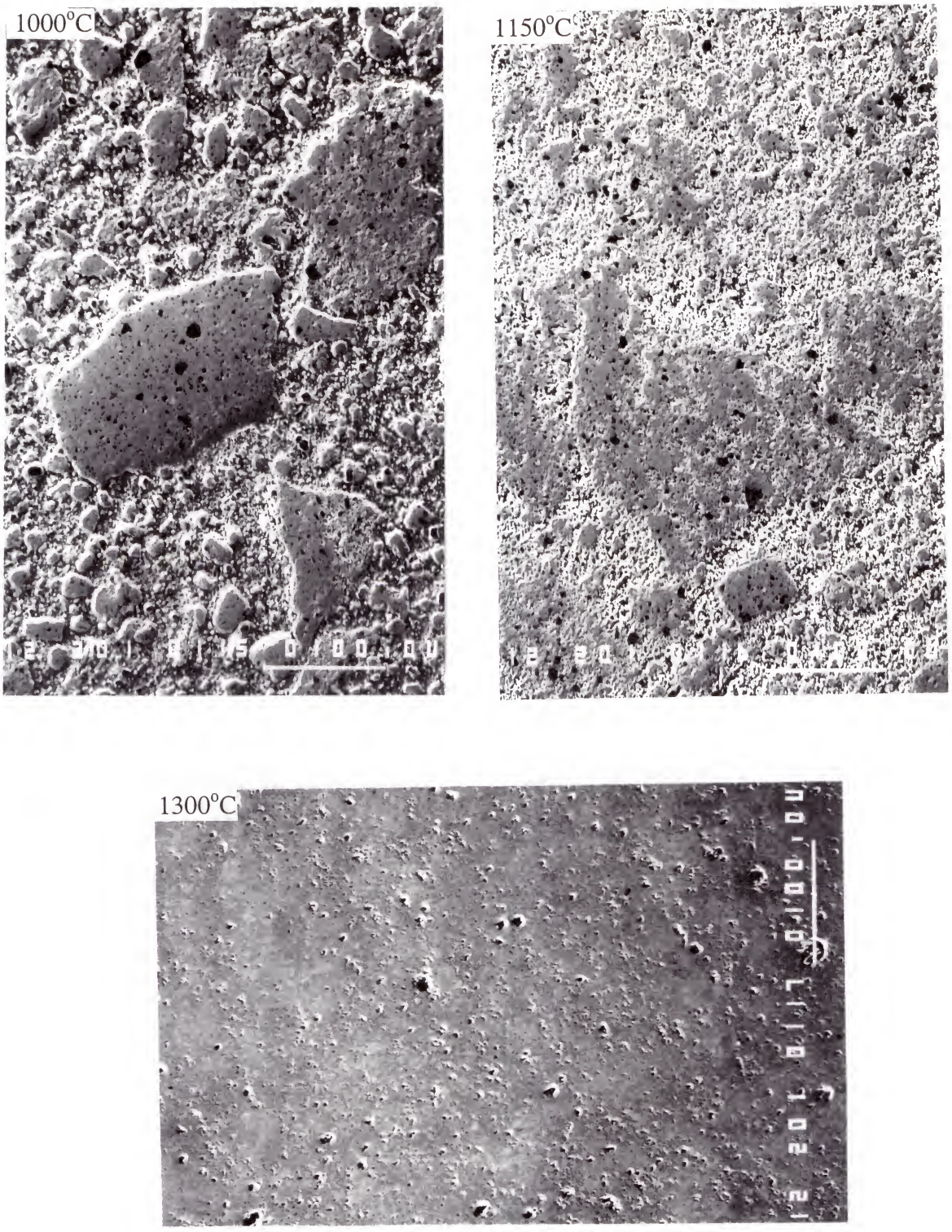


(c)

Figure 4.34 (continued) (c) SEM of $Ti_5Si_3$+$Mo_5Si_3$+B, diluted with pre-reacted $MoSi_2$, hot pressed at 1000, 1150 and 1300°C (as indicated) to produce $MoSi_2$+$TiB_2$ composites.

Interestingly, the few unreacted titanium areas that were large enough to be observed in this sample were not in contact with boron particles. Although this could be construed to indicate that the Ti + B reaction was concluded at this temperature in the regions where there was direct contact, one must be aware that the metallographic procedure is somewhat biased, since only the areas that could be satisfactorily polished were observed. The microstructure of the sample hot pressed at 1300°C is very similar to the one hot pressed at 1400°C for 1 h, except for a larger volume fraction of porosity.

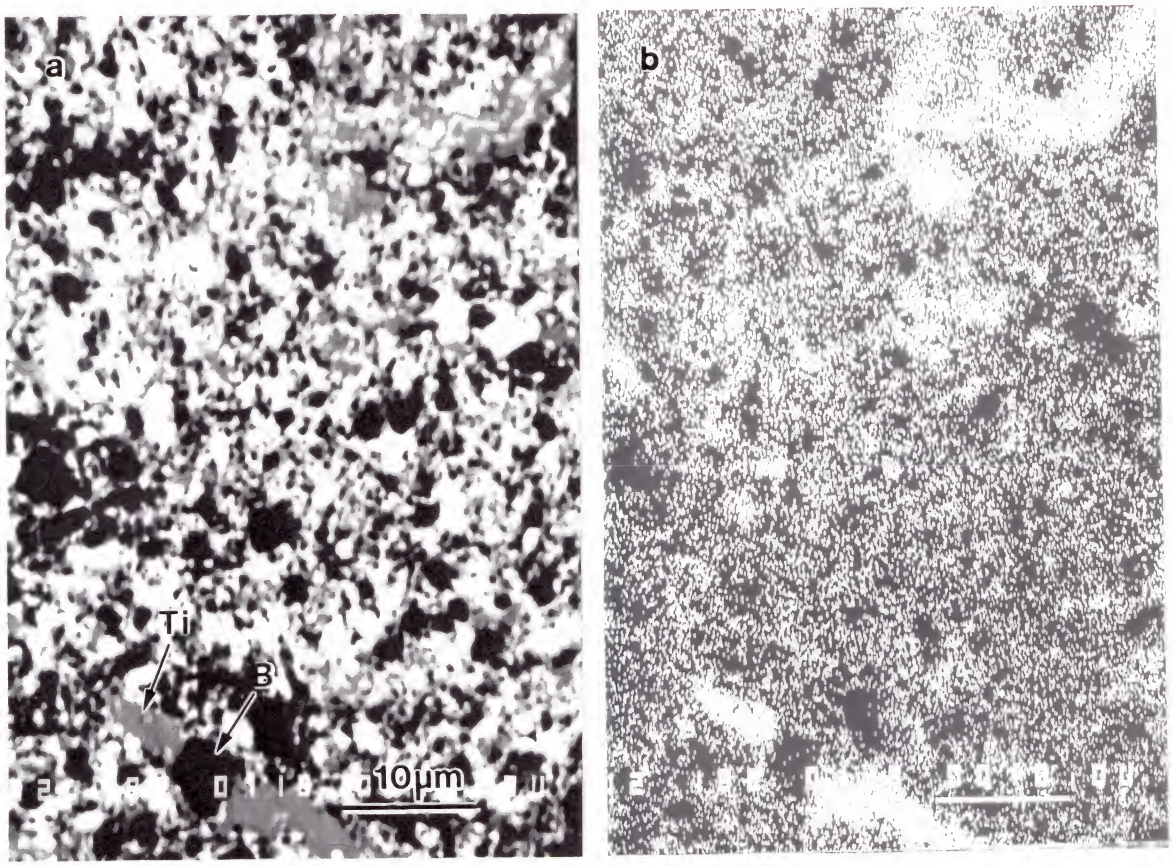


Figure 4.35 Microstructure of elemental powders hot pressed at 1000°C. (a) BEI: Large particle of boron in contact with titanium is marked with arrow. Most of the light phase is $MoSi_2$. (b) Ti $K_\alpha$ x-ray map of the same region.

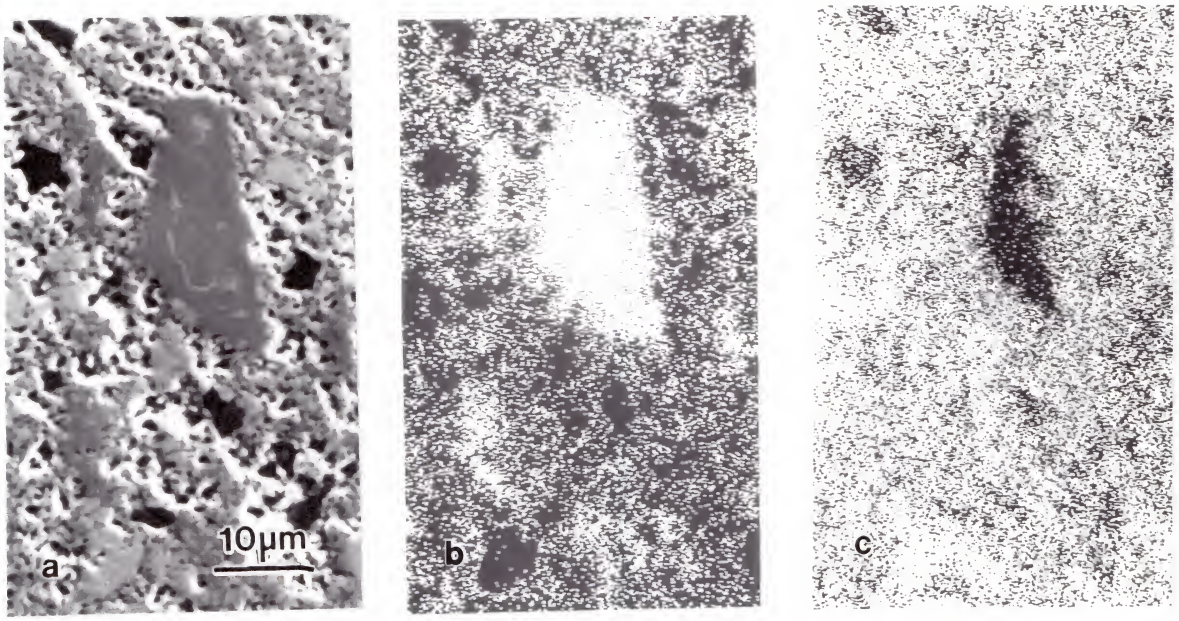


Figure 4.36 Microstructure of elemental powders hot pressed at 1150°C, showing a layer of $Ti_5Si_3$ surrounding a titanium particles. (a) SEM. (b) Ti $K_\alpha$ x-ray map of the same region. (c) Si $K_\alpha$ x-ray map of the same region.

Displacement reactions. The common feature of these microstructures is the extreme fineness of the product constituents except for the unreacted boron particles. It was possible to identify some particles of $MoSi_2$ in all samples to which this silicide was added in prereacted form and, in the 1000°C samples, some unreacted $Mo_5Si_3$ is present in particles large enough to be subjected to EMPA. The other constituents, however, are too fine for EMPA and, in the sample that could be prepared for TEM (1150°C, with $MoSi_2$ addition), too fine to obtain individual diffraction patterns. The ring patterns obtained from this sample are consistent with the presence of $MoSi_2$ and $TiB_2$. Interestingly, no noticeable difference in microstructure was observed in the TEM between the regions close to and away from the boron particles except for a somewhat higher content of titanium in the region close to the interface with the boron particle, perhaps indicating that this region could be richer in $TiB_2$. When the displacement reaction was carried out to 1150°C without any dilution with $MoSi_2$, a layer of titanium boride was present at some of the boron-matrix interface as shown in Figure 4.38.

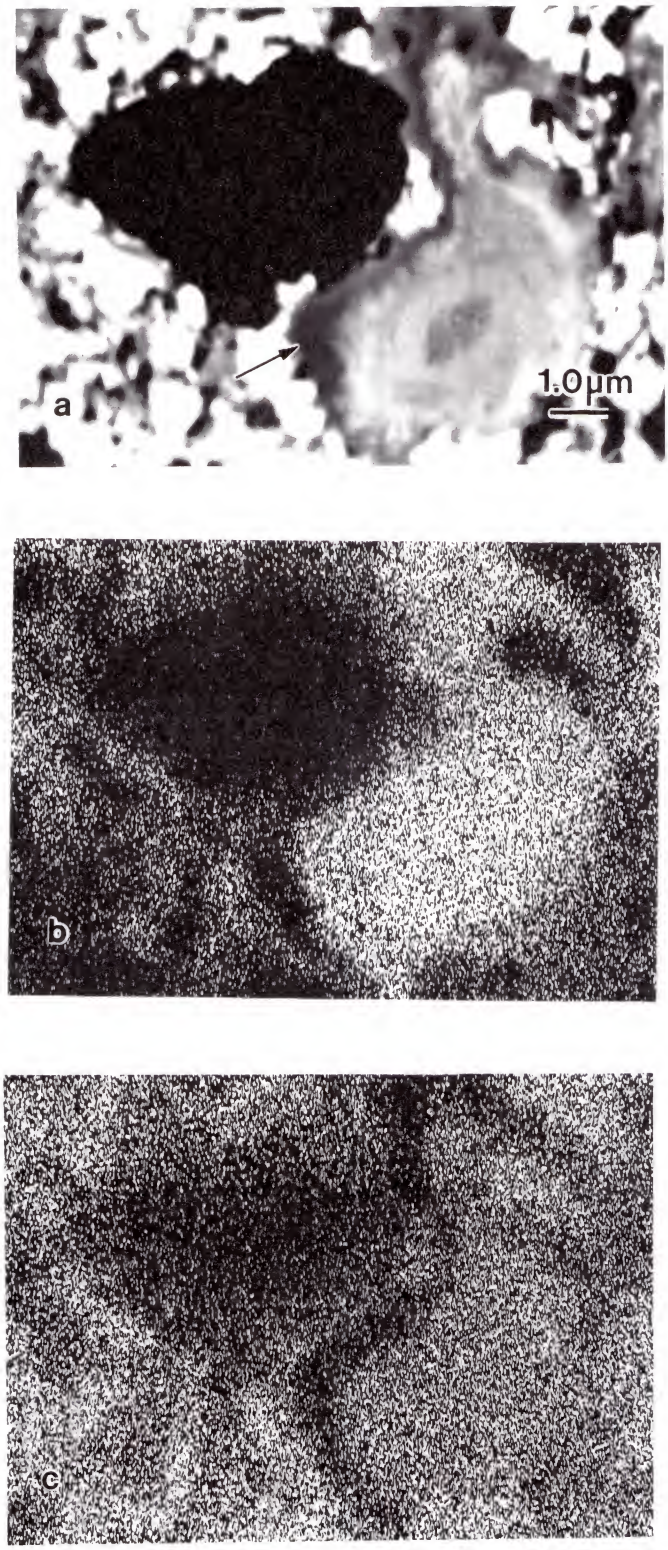


Figure 4.37 Microstructure of elemental powders hot pressed at 1150°C, showing a layer of $TiB_2$ formed between a boron particle and $Ti_5Si_3$. (a) BEI: Arrow indicates $TiB_2$, black phase is boron. (b) Ti $K_\alpha$ x-ray map of the same region. (c) Si $K_\alpha$ x-ray map of the same region.

This may be the start of the formation of the somewhat coarser areas of $TiB_2$ observed in Figure 4.28, i.e., when the exact stoichiometry for the displacement reaction is used, without diluents. Furthermore, even at 1300°C, this composition still shows some unreacted boron, albeit in a much smaller quantity.

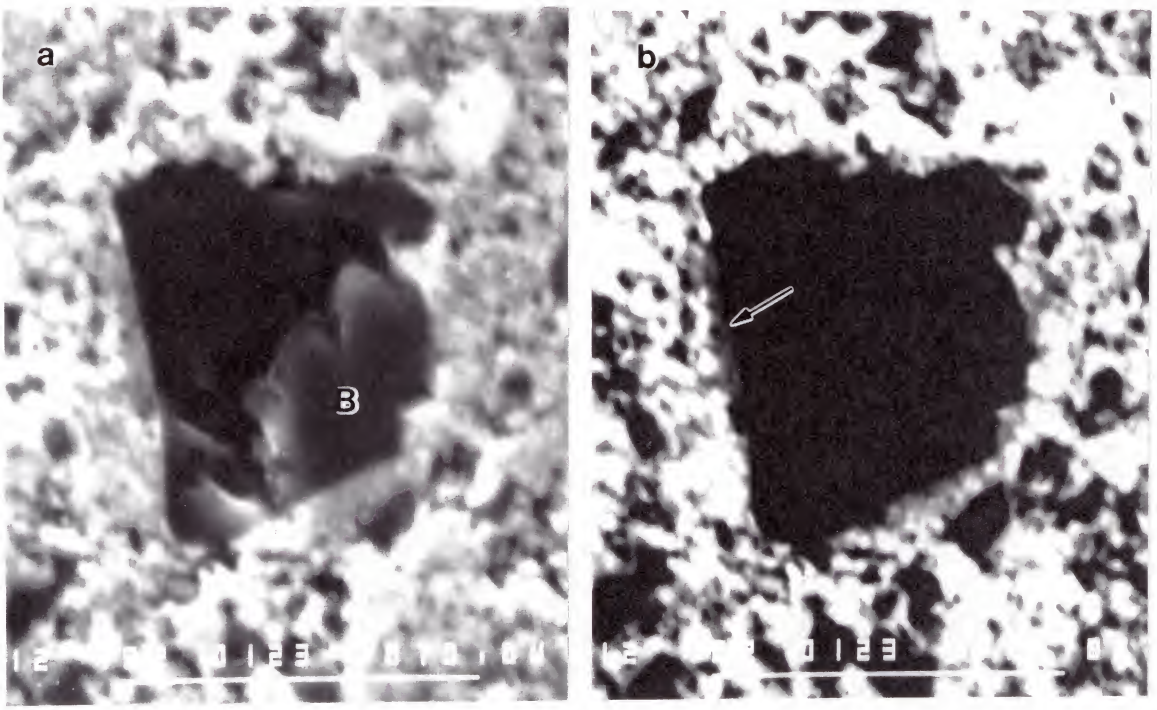


Figure 4.38 Microstructure of $Mo_5Si_3$+$Ti_5Si_3$+B hot pressed at 1150°C, showing a layer of $TiB_2$ formed between a boron particle and the matrix. (a) SEM: Large particle is boron. (b) BEI of the same region: the arrow indicates the position of the $TiB_2$ layer.

Although the mechanisms involved in the reactions described above are far from clear, some conclusions can be drawn, and some possibilities can be excluded. First, it seems evident that the coarser structure observed when elemental powders are hot pressed is the result of the early nucleation and growth of $MoSi_2$, in agreement with previous investigations. Titanium diboride is formed at a higher temperature, either between these coarse particles or in "pockets" resulting from the reaction of $Ti_5Si_3$, formed as an

intermediate product, and boron. The hypothesis that the sample reaches temperatures substantially higher than the hot pressing temperature can be ruled out based on the measurements performed. Although the overall conversion of Mo-Si-Ti-B elemental powders to $MoSi_2 + TiB_2$ is an exothermic process ($T_{ad,\ 298K} \approx 2400$ K) and one might expect that it could be carried out by SHS, this is not the case in the present experiments. It is speculated that there are three main reasons for this observation. First, the mechanical alloying process results in some dissolution of the reactants in each other (although a substantial temperature increase was observed during mechanical alloying, it is difficult to separate the effect due to reactions between the powders and that due to attrition energy dissipated as heat), as well as in the formation of intermediate compounds (e.g. C40 $MoSi_2$). Second, the formation of intermediate compounds such as $Ti_5Si_3$ occurs during heating. Finally, there is a wide temperature span over which some of the reactions (e.g., formation of $C11_b$ $MoSi_2$) occur. These reasons are consistent with the absence of noticeable peaks in the DTA.

In the case of the displacement reaction, the adiabatic temperature is substantially lowered by the fact that the two reacting silicides have considerable heats of formation. In addition, when sufficient pre-reacted $MoSi_2$ is added to achieve the desired volume fraction of $MoSi_2$, the conditions are unfavorable for SHS. Also in this case, the occurrence of SHS during hot-pressing can be excluded based on the experimental data. It is apparent that the reactions that lead to densification in this system only start at higher temperatures, consistent with the fact that $TiB_2$ formation is necessary for the progress of the displacement reaction and this is only significant at higher temperatures. It is impossible to clearly define whether the reaction proceeds through the formation of intermediate products, albeit the data available seem to indicate otherwise. None of the observations indicate the occurrence of melting at the boron-matrix interface, strongly indicating that the process is completely dominated by solid-state steps. The presence of three reactants and two products challenges the imagination of a topological scheme for

the overall reaction to occur and almost mandates the existence of some intermediate steps or phases. The fine scale of the microstructure, however, precludes the observation and characterization of these steps and/or phases.

## 4.7 Silica Modification in a MoB-$MoSi_2$ Composite

All composites produced by *in-situ* displacement reactions to generate borides (either molybdenum or titanium borides) had fine oxide inclusions in their microstructures. The TEM/EDS analyses of inclusions in the $MoSi_2$-MoB composites indicated that these are amorphous, silicon-rich and contain boron. As previously discussed, silica, and probably boro-silicate inclusions also, are not desirable in $MoSi_2$ composites. Thus, in an attempt to modify these inclusions following the approach described in section 4.1, aluminum was added to the reactants before mixing. An addition of 2.5% wt. resulted in the microstructure shown in Figure 4.31; the matrix phases are MoB and $Mo(Si,Al)_2$ as indicated by EMPA and XRD. The aluminum $K_\alpha$ dot-maps indicates that the inclusions are rich in aluminum, although their compositions could not be analyzed due to the limited spatial resolution of the microprobe. TEM analysis indicated that the particles are $\alpha$-$Al_2O_3$, as shown in Figure 4.32, and that both amorphous or silicon containing oxides are absent. The stoichiometry of the main displacement reaction taking place in these composites is:

$$^2/_3\ Mo_5Si_3 + {}^7/_3\ B = MoSi_2 + {}^7/_3\ MoB$$

such that the final mass fraction of $MoSi_2$ should be 0.59. The measured aluminum content in the C40-$Mo(Si,Al)_2$ is compatible with the aluminum addition made, albeit only a wrought mass balance estimate can be made in view of the difficulty in estimating the amount of $Al_2O_3$ present due to its size and to the fact that not only the total oxygen content in the sample is unknown but data on the solubility of oxygen in $MoSi_2$ and MoB is not available.

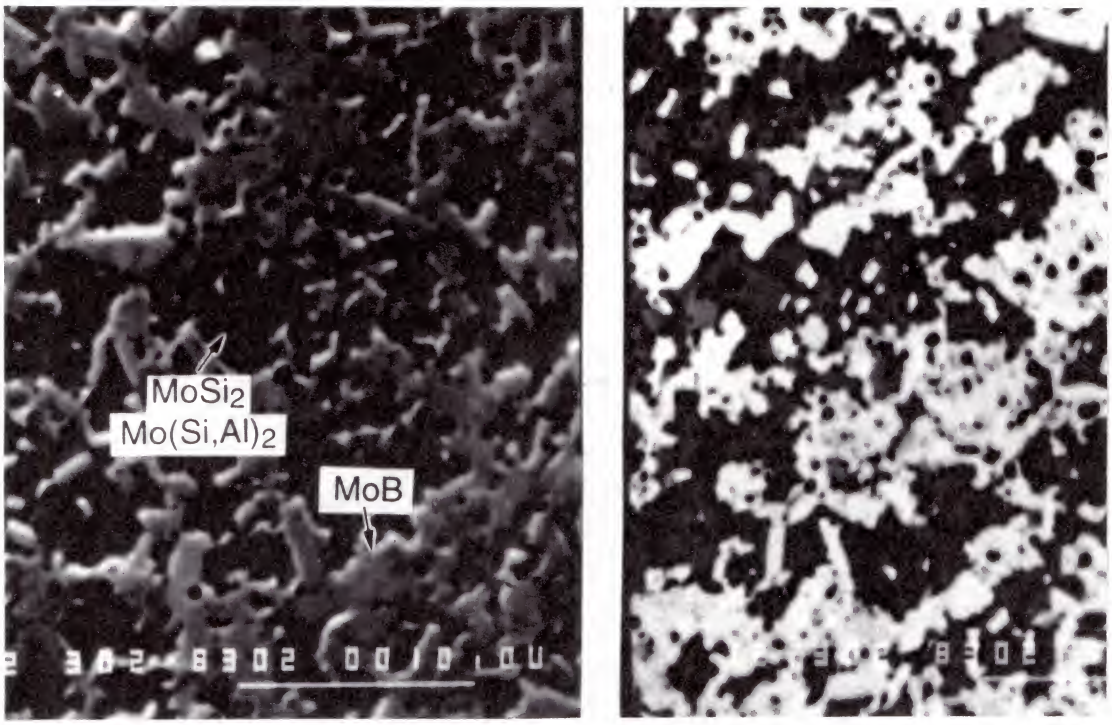


Figure 4.39 SEM and BEI image of $MoSi_2$-MoB composites with alumina produced by *in-situ* modification of oxides. (See Figure 4.40 for TEM results from black phase).

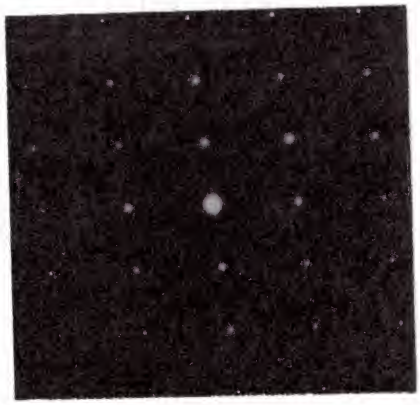

B=[$\bar{1}$20] $\alpha Al_2O_3$ (R3c)

Figure 4.40 BF-TEM analysis of typical alumina particle in $MoSi_2$-MoB composite and corresponding $\alpha$-$Al_2O_3$ diffraction pattern.

# CHAPTER 5

# GENERAL DISCUSSION

Throughout this work, several examples have been presented in which the use of thermodynamic data, together with experiments designed to clarify or obtain information on phase relations, have been instrumental in the design and understanding of processes used to produce high temperature structural materials. It has been demonstrated that this approach should significantly reduce the number of experiments required to evaluate possible matrix-reinforcement compatibility and it is suggested that it should replace, whenever data is available, the trial and error approach. Simply bringing together phases under somewhat uncontrolled conditions is a poor substitute for analysis of phase diagram and thermodynamic data gathered under controlled experimental conditions. Although the emphasis of the present study has been on *in-situ* processes using a $MoSi_2$ matrix, the techniques used can be extended to the analysis and production of other materials using these or different production processes. In fact, most of these prediction and analysis techniques are already in use, to different extents, in the design of production processes for other classes of materials such as metals and ceramics. The fact that recent experimental work in this area of $MoSi_2$-matrix composites (e.g., [174- 176]) can still be found in which information readily available from phase diagrams or previous studies of phase equilibria is not taken into consideration in its full extent is an indication that the approach described in this work, albeit somewhat obvious, has yet to find widespread acceptance, at least in the area of intermetallics. A clear challenge in the field of materials science is the fact that while so many phenomena are common to various classes of materials, the way they are described and the depth to which they have been

studied varies tremendously across these classes. Thus, it is not uncommon to find that when metallurgists study intermetallic compounds, for instance, they fail to take advantage of well established concepts from solid-state physics, chemistry and ceramics and tend to rely on concepts well established for metals, that may or may not be the most adequate to describe and thus solve the problem in question.

Evidently, the study of phase evolution and microstructure development in any material cannot be solely based on thermodynamic analysis. Some evident examples of that fact presented in this work are the formation of protective barriers on niobium fibers and the various microstructures produced in the $MoSi_2$-boride composites. In the first case, while it is possible to use thermodynamics to predict that aluminum will reduce silica and niobium oxide, as observed, it is not possible to forecast whether the conversion of niobium oxide to alumina will occur soon enough during the process to prevent further interaction between matrix and fiber; in the second example, despite the fact that the phases present after processing are well defined by the phase equilibrium and are, in principle, independent of the processing route followed (i.e. elemental powder vs. displacement reaction) the microstructure obtained depends dramatically on the actual route followed. This is a clear indication that in order to predict and explain microstructural evolution not only thermodynamic but kinetic data and modeling are required. This is presently being developed by several authors (e.g., [177]), especially in the field of metals where a wider database on nucleation, diffusion and transformation rates is established with somewhat reliable data.

# CHAPTER 6

# CONCLUSIONS

*In-situ* processing of $MoSi_2$-matrix composites is a viable route to produce materials having promising microstructures for high-temperature applications. These processes can be designed based on available and estimated thermodynamic information. To further enhance the ability to tailor the microstructures obtained through *in-situ* reactions, the ability to model the kinetics of the processes occurring should be developed.

In order to demonstrate how the use of simple methods for evaluating phase-equilibria coupled with a limited number of experiments can be used to gain information on phase-equilibria in $MoSi_2$-matrix composites, the Mo-Si-C system was investigated to establish that the third-phase in silicon-poor $MoSi_2$-SiC composites should be $Mo_5Si_3C$ and not $Mo_5Si_3$ as previously proposed by some investigators. Furthermore, phase relations for this ternary system in the range between 1200 and 1600°C have been proposed. Based on this analysis, it appears that these phase relations should extend to lower temperatures.

Silica inclusions ubiquitous in powder-processed monolithic $MoSi_2$ and its composites can be eliminated through the use of an *in-situ* process comprising aluminum additions to $MoSi_2$ powders; via this process, a smaller volume fraction of higher melting alumina inclusions is formed. Furthermore, the main phase in the material can be tailored to be tetragonal $MoSi_2$ with dissolved aluminum or hexagonal $Mo(Si,Al)_2$ or mixtures of both.

An *in-situ* process has also been implemented to produce a stable barrier to prevent the interaction between $Mo(Si,Al)_2$ and niobium reinforcement. The alumina barrier produced in this process promotes debonding; this opens interesting possibilities as far as achieving toughening in these materials while maintaining high-temperature microstructural stability.

Phase equilibria in the Mo-Si-Al ternary was determined in the region of immediate interest to $MoSi_2$-based composites. It has been shown that some of the phase boundaries as well as phase relations established in earlier works were incorrect and that the solubility of aluminum in the $Mo_5Si_3$ (T1) phase may have been overestimated. A first attempt at modeling this system using the Thermocalc software has shown that although more data are needed to achieve a better description of some of the solid phases, one can use the provisional model to estimate data for the design of *in-situ* processes.

Based on the available ternary phase diagrams and estimated quaternaries, *in-situ* processes involving relatively low temperatures were designed to generate boride reinforcements in a $MoSi_2$ matrix. These composites exhibit high hardness, reasonable fracture toughness at room temperature (when compared to monolithic $MoSi_2$) and reasonable densities, making them prospective candidates for applications where these properties are desired.

Finally, these two *in-situ* routes, oxide modification and boride formation, were combined to generate a boride-reinforced, silica-free, $MoSi_2$-matrix composite.

## REFERENCES


1. V.N. Svechnikov, Y.A. Kocherzinsky, and L.M. Yupto, Mo-Si phase diagram, *Diagrammy Sostoyaniya Metal Sistem Nauka, XVII* (1971), 116-119.

2. L. Brewer, Physico-chemical properties of molybdenum and its compounds, *Atomic Energy Review Special Issue 7, IAEA, Vienna,* (1980), 1-714.

3. A. Gokhale and G.J. Abbaschian, The Mo-Si (Molybdenum-Silicon) system, *Journal of Phase Equilibria, 12* (1991), 493-498.

4. W.J. Boettinger, J.H. Perepezko, and P.S. Frankwicz, Applications of ternary phase diagrams to the development of MoSi2-based materials, *Materials Science & Engineering A, A155* (1992), 33-44.

5. E.P. Nechiporenko, N.S. Poltavtsev, V.L. Kapustin, and Y.T. Kondratov, Homogeneity region of $MoSi_2$, *Izv.Akad.Nauk SSSR, Neorg.Mater., 9* (1973), 1829-1830.

6. E. Fitzer and F.K. Schmidt, Die Siliziumdiffusion in den $Me_5Si_3$-Phasen der Metalle Niob, Tantal, Molybdaen und Wolfram bis 1700°C, *High Temperatures-High Pressures, 3* (1971), 445.

7. J. Schlichting, Oxidation kinetics of silicon ceramic from the view point of refractory materials resistant against hot corrosion, *Revue Internationale des hautes Temperatures et des Refracr., France (Rev.int hautes Temper.Refract.), 16* (1979), 67-72.

8. S.A. Maloy, A.H. Heuer, J.J. Lewandowski, and T.E. Mitchell, On the slip systems in $MoSi_2$, *Acta metallurgica et materialia, 40* (1992), 3159-3165.

9. D.A. Hardwick, P.L. Martin, S.N. Patankar, and J.J. Lewandowski. Processing-microstructure-property relationships in polycrystalline $MoSi_2$. in *Structural Intermetallics.* 1993, Warrendale, PA: TMS-AIME. p. 665-674.

10. F.B. Pickering, *Physical Metallurgy and the Design of Steel.* 1978, London: Applied Science Publishers, Ltd.

11. S.A. Maloy, T.E. Mitchell, J.J. Lewandowski, and A.H. Heuer, {103}<331> slip in $MoSi_2$, *Philosophical Magazine Letters, 67* (1993), 313-321.

12. S.A. Maloy, T.E. Mitchell, J.J. Petrovic, A.H. Heuer, and J.J. Lewandowski, The temperature and strain rate dependence of the flow stress in $MoSi_2$ single crystals, *Mat.Res.Soc.Symp.Proc., 322* (1994), 21-26.

13. Y. Umakoshi. Yield stress and dislocation structure of MoSi2 and (MoCr)Si2 single crystals. in *High Temperature Aluminides and Intermetallics*. 1990, Warrendale, PA: TMS-AIME. p. 111-115.

14. Y. Umakoshi, T. Nakashima, T. Nakano, and E. Yanagisawa, Plastic behavior and deformation structure of silicide single crystals with transition metals at high temperatures, *Mat.Res.Soc.Symp.Proc., 322* (1994), 9-20.

15. E. Fitzer, O. Rubisch, J. Schlichting, and I. Sewdas. Das Rekristalizationsverhalten von $MoSi_2$-Sinternkoerpern ohne und mit SiC und $Al_2O_3$-Zusaetzen zwischen 1500 und 1700°C und die Auswirkung der Gefuegeanderung auf die Biegbruchfestigkeit. in *Science of Ceramics, Proc. of 6th International Conference on Science of Ceramics, Bad Honnef, DKG*. 1971. Baden-Baden: Deutsche Keramische Geselchaft. p. XVIII/1-14.

16. A.K. Vasudevan and J.J. Petrovic, A comparative overview of molybdenum silicide composites, *Materials Science & Engineering A, A155* (1992), 1-17.

17. E. Fitzer, K. Reinmuth, and H. Schnabel, Pressen und Sintern von Molybdaendisilizid, *Archiv fuer das Eisenhuettenwesen (Steel Research), 40* (1969), 895-900.

18. H. Schnabel, *Zur Pulvermetallurgie des Molybdaensilizids*. Doctoral Dissertation. 1965, Technischen Hochschule Karlsruhe.

19. D.E. Alman, K.G. Shaw, N.S. Stoloff, and K. Rajan, Fabrication, structure and properties of $MoSi_2$-base composites, *Materials Science and Engineering A, A155* (1992), 85-93.

20. A.K. Bhattacharya, Modelling of combustion synthesis of $MoSi_2$ and its composites, *Cer. Eng. Sci. Proc., 12* (1991), 1697-1722.

21. S.C. Deevi, Diffusional reactions in combustion synthesis of $MoSi_2$, *Materials Science and Engineering, A149* (1992), 241-251.

22. R. Tiwari, H. Herman, and S. Sampath, Vacuum plasma spraying of $MoSi_2$ and its composites, *Materials Science & Engineering A, A155* (1992), 95-100.

23. R.G. Castro, R.W. Smith, A.D. Rollett, and P.W. Stanek, Ductile phase toughening of molybdenum disilicide by low pressure plasma spraying, *Materials Science & Engineering A, A155* (1992), 101-107.

24. R. Madar, N. Thomas, and C. Bernard, Chemical vapour deposition precursors for metal silicides, *Materials Science and Engineering, B17* (1993), 118-125.

25. A. Basu and A. Ghosh. High temperature mechanical behavior of $MoSi_2$ based composites. in *Advanced Metal Matrix Composites for Elevated Temperatures Conf. Proc.,* 1991. Materials Park, OH: ASM International. p. 41-47.

26. L.N. Efimenko, L.F. Verkhorobin, and A.G. Shvydchenko, Oxidation of the lower silicides of tungsten and molybdenum, *Inorg.Mater. (English Transl.of Izv.Akad.Nauk SSSR Neorg.Mater.), 1* (1965), 1728-1732.

27. J. Schlichting, Molybdaensilizid als Komponente moderner Hochtemperaturverbundwerkstoffe, *High Temperatures- High Pressures, 10* (1978), 241-269.

28. P.J. Meschter, Low-temperature oxidation of molybdenum disilicide, *Metallurgical Transactions A, 23A* (1992), 1763-1772.

29. W.A. Maxwell, *Properties of Certain Intermetallics as Related to Elevated-Temperature Applications I-Molybdenum Disilicide*. 1949, Research Memorandum RM E9G01, NACA.

30. W.A. Maxwell, *Some Factors Affecting Fabrication and High-Temperature Strength of Molybdenum Disilicide*. 1952, Research Memorandum RM E52B06, NACA.

31. E. Fitzer, Klassisches Sintern, Reaktionssintern und Heisspressen von hochschmelzenden $AB_2$-Hartstoffe, *Archiv fuer das Eisenhuettenwesen (Steel Research), 44* (1973), 703-709.

32. J.D. Cotton, Y.S. Kim, and M.J. Kaufman, Intrinsic second-phase particles in powder-processed $MoSi_2$, *Materials Science & Engineering A, A144* (1991), 287-291.

33. S.A. Maloy, A.H. Heuer, J.J. Lewandowski, and J.J. Petrovic, Carbon additions to molybdenum disilicide: Improved high temperature mechanical properties, *Journal of the American Ceramic Society, 74* (1991), 2704-2706.

34. T.E. Mitchell, R.G. Castro, and J.J. Petrovic, Dislocations, twins, grain boundaries and precipitates in $MoSi_2$, *Materials Science and Engineering, A155* (1992), 241-249.

35. R.M. Aikin, Jr., On the ductile to brittle transition temperature in $MoSi_2$, *Scripta metallurgica et materialia, 26* (1992), 1025-1030.

36. A. Costa e Silva and M.J. Kaufman. Synthesis of $MoSi_2$ matrix composites using in-situ reactions. in *Processing and Fabrication of Advanced Materials for High Temperature Applications III*, 1993. Warrendale, PA: TMS-AIME. p. 585-598.

37. R.K. Wade and J.J. Petrovic, Fracture modes in $MoSi_2$, *Journal of the American Ceramic Society, 75* (1992), 1682-1684.

38. R. Gibala, A.K. Ghosh, D.C.V. Aken, D.J. Srolovitz, A. Basu, H. Chang, D.P. Mason, and W. Yang, Mechanical behavior and interface design of $MoSi_2$ alloys and composites, *Materials Science & Engineering, A155* (1992), 147-158.

39. U. Ramamurty, A.S. Kim, S. Suresh, and J.J. Petrovic, Micromechanisms of creep-fatigue crack growth in a silicide-matrix composite sith SiC particles, *Journal of the American Ceramic Society, 76* (1993), 1953-64.

40. S.R. Srinivasan, R.B. Schwartz, and J.D. Embury, Ductile to brittle transition in $MoSi_2$, *Mat. Res. Soc. Symp., 288* (1993), 1099-1104.

41. A. Costa e Silva and P.R. Mei, *Steels and Specialty Alloys (in Portuguese)*. 2 ed. 1988, Sumare, Brasil: Eletrometal.

42. S. Jayashankar and M.J. Kaufman, In-situ reinforced $MoSi_2$ composites by mechanical alloying, *Scripta metallurgica et materialia, 26* (1992), 1245-1250.

43. S. Jayashankar and M.J. Kaufman, Tailored $MoSi_2$/SiC composites by mechanical alloying, *Journal of Materials Research, 8* (1993), 1428-1441.

44. N.S. Jacobson, K.N. Lee, S.A. Maloy, and A.H. Heuer, Chemical reactions in the processing of $MoSi_2$+carbon compacts, *Journal of the American Ceramic Society, 76* (1993), 2005-2009.

45. H. Nowotny, E. Parthe, R. Kieffer, and F. Benesovsky, Das Dreistoffsystem: Molybdaen-Silizium-Kohlenstoff, *Monatshefte für Chemie, 85* (1954), 255-272.

46. J. Henager C. H., J.L. Brimhall, and J.P. Hirth, Synthesis of composites in situ using solid state displacement reactions, *Ceramic Engineering & Science Proceedings, 13* (1992), 596-604.

47. D.A. Hardwick, P.L. Martin, and R.J. Moores, Reaction synthesis of $MoSi_2$ from high purity elemental powders, *Scripta metallurgica et materialia, 27* (1992), 391-394.

48. R.B. Schwarz, S.R. Srinivasan, J.J. Petrovic, and C.J. Magiore, Synthesis of molybdenum disilicide by mechanical alloying, *Materials Science & Engineering A, A155* (1992), 75-83.

49. P.A.G. O'Hare, Thermodynamic properties of silicides. III. Specific energy of combustion in fluorine of a hyperstoichiometric molybdenum disilicide. The standard molar enthalpy of formation deltaH of $MoSi_{2.067+0.002}$ at the temperature 298.15K., *Journal of Chemical Thermodynamics, 25* (1993), 1333-1343.

50. I. Kiono, M. Sugano, R.Ryuichi, K. Hosaka, and A. Kato, Molybdenum or tungsten silicide of low oxygen content-Japanese patent, *Japan Kokai Tokkyo Koho JP 62,171,911, 62* (1987).

51. I. Sewdas, *Die Eigenschaftsaenderung von Molybdaensilizids-Sinterkoerper infolge von Hochtemperaturgluehungen*. Doctoral Dissertation. 1970, Univeristat Karlsruhe.

52. A. Costa e Silva, R. Boswell, and M.J. Kaufman, Univeristy of Florida, Pressureless sintering of $MoSi_2$ under hydrogen atmospheres- unpublished results, (1993).

53. J.J. Petrovic and J.S. Idasetima, Sintering of $MoSi_2$, *Mat. Res. Symp. Proc., 322* (1994), 107-112.

54. J.J. Petrovic, A.K. Bhattacharya, R.E. Honnell, T.E. Mitchell, and R.K. Wade, $ZrO_2$ and $ZrO_2$-SiC particle reinforced $MoSi_2$ composites, *Materials Science & Engineering A, A155* (1992), 259-266.

55. K.K. Chawla, *Composite Materials Science and Engineering*. 1987, New York: Springer-Verlag.

56. A.G. Evans, F.W. Zok, and J. Davis, The role of interfaces in fiber-reinforced brittle matrix composites, *Composites Science and Technology, 42* (1991), 3-24.

57. S.G. Fishman. Ramifications of recent micromechanical innovations on understanding in composites interfaces. in *Interfaces in Metal-Ceramic Composites.* 1989, Warrendale, PA: TMS-AIME. p 3-19.

58. S. Jayashankar, S.E. Riddle, and M.J. Kaufman, Synthesis and properties of in-situ $MoSi_2$/SiC composites, *Mat. Res. Symp. Proc., 322* (1994), 33-40.

59. J. Henager C.H., J.L. Brimhall, and J.P. Hirth, Synthesis of a $MoSi_2$-SiC composite in situ using a solid state displacement reaction, *Materials Science & Engineering A, A155* (1992), 109-114.

60. S.E. Riddle, *Microstructural Development and Characterization of Molybdenum Disilicide/ Silicon Carbide Composites formed by In-situ Displacement Reactions.* M.S. Thesis, 1994. Gainesville, FL: University of Florida.

61. B. Aronsson, T. Lundstrom, and S. Rundqvsit, *Borides, Silicides and Phosphides: A Critical Review of their Preparation, Properties and Crystal Chemistry.* 1965, London: Methuen & Co., Ltd.

62. R.A. Cutler, Ceramics and glasses, in *Engineered Materials Handbook- Ceramics and Glasses,* S.J. Schneider Jr., Editor. 1991, Materials Park, OH: ASM International.

63. J. Aikin R.M., Strenghtening of discontinuously reinforced $MoSi_2$ composites at high temperature, *Materials Science & Engineering, A155* (1992), 121-133.

64. R.A. Cutler, Engineering properties of borides, in *Engineering Materials Handbook-Ceramics and Glasses,* S.J. Schneider Jr., Editor. 1991, Materials Park, OH: ASM International. p. 787- 803.

65. J.L. Murray, P.K. Liao, and K.E. Spear, B-Ti phase-diagram, in *ASM Handbook Volume 3 Alloy Phase Diagrams,* H. Baker and H. Okamoto, Editor. 1992, Materials Park, OH: ASM International, p. 2-85.

66. C. Wagner, Oxidation of alloys involving noble metals, *Journal of the Electrochemical Society, 103* (1956), 571-580.

67. R.A. Rapp, A. Ezis, and G.J. Yurek, Displacement reactions in the solid state, *Metallurgical Transactions, 4* (1973), 1283-1292.

68. G.J. Yurek, R.A. Rapp, and J.P. Hirth, Kinetics of the displacement reaction between iron and $Cu_20$, *Metallurgical Transactions, 4* (1973), 1293-1300.

69. M. Backhaus-Ricoult and H. Schmalzried, Morphological stability in the course of solid state reactions: The system $Fe_3O_4$- $Mn_3O_4$- $Cr_2O_3$, *Ber. Bunsenges. Phys. Chem., 89* (1985), 1323-1330.

70. M. Backhaus-Ricoult, H. Schmalzried, and R.J. Tarento, Internal solid state reactions of the type A + B = AB: Diffusion controlled formation of AB from A and B dissolved in a crystalline host matrix, *Ber. Bunsenges. Phys. Chem., 95* (1991), 1593-1610.

71. P.D. Zavitsanos, J.J. Gebhardt, and A. Gatti, The use of self-propagating high-temperature synthesis of high-density titanium diboride, in *Combustion and Plasma*

*Synthesis of High-Temperature Materials,* Z.A. Munir and J.B. Holt, Editor. 1990, New York,NY: VCH Publishers. p. 170-178.

72. S.K. Roy and A. Biswas, Combustion synthesis of TiB and $TiB_2$ under vacuum, *Journal of Materials Science Letters, 133* (1994), 371-373.

73. H. Itoh, Y. Tsunekawa, S. Tago, and H. Iwahara, Synthesis and sinterability of composite powder of the $TiB_2$-$B_4C$ system, *Journal of Alloys and Compounds, 191* (1993), 191-195.

74. B. Rupp, J.B. Holt, and J. Wong, The calculation and analysis of the adiabatic temperature of solid combustion reactions, *CALPHAD, 16* (1992), 377-386.

75. J. Subrahmanyam and M.Vijayakumar, Self-propagating high-temperature synthesis, *Journal of Materials Science, 27* (1992), 6249-6273.

76. K. Monroe, S. Govindarajan, J.J. Moore, B. Mishra, D.L. Olson, and J. Disam, Combustion synthesis of $MoSi_2$ and $MoSi_2$-composites, *Mat.Res.Soc.Symp.Proc., 322* (1994), 113-118.

77. J.B. Holt, D.D. Kingman, and G.M. Bianchini, Kinetics of combustion synthesis of $TiB_2$, *Materials Science and Engineering, 71* (1985), 321-327.

78. K.V. Popov, V.A. Knyazik, and A.S. Shteinberg, Study of high-temperature reaction of Ti with B by the method of electrothermal explosion, *Combustion, explosion and shock waves (translation of Fizika Goreniya i Vzryva), 29* (1993), 77-81.

79. B.H. Rabin, A. Bose, and R.M. German, Combustion synthesis of nickel aluminides, in *Combustion and Plasma Synthesis of High-Temperature Materials,* Z.A. Munir and J.B. Holt, Editor. 1990, New York, NY: VCH Publishers. p. 114-121.

80. U. Anselmi-Tamburini and Z.A. Munir, Observations on the combustion reaction between thin foils of Ni and Al, in *Combustion and Plasma Synthesis of High-Temperature Materials,* Z.A. Munir and J.B. Holt, Editor. 1990, New York, NY: VCH Publishers. p. 100-105.

81. V.A. Neronov, M.A. Korchagin, V.V. Aleksandrov, and S.N. Gusenko, Investigation of the interaction between boron and titanium, *Journal of the Less-Common Metals, 82* (1981), 125-129.

82. Y.V. Levinskii and A.P. Petrov, Making alloyed titanium diboride powders, *Powder metallurgy and metal ceramics (Engl.Trans. of Poroshkovaya Metallurgiya), 32* (1993), 480-483.

83. D.E.R. Kehr, *Hochschmelzende, oxidationsbestaendige Metall-Silizid-Verbundkoerper mit Drahtverstaerkerung*. Doctoral Dissertation, 1975, Universitat Karlsruhe.

84. E. Fitzer and W. Remmele. Possibilities and limits of metal reinforced refractory silicides especially molybdenum silicide. in *Fifth International Conference on Composites Materials ICCM-V.* 1985. Warrendale, PA:TMS-AIME. p. 515-530.

85. D. Carter and P.L. Martin. *Ta and Nb Reinforced $MoSi_2$*. in *Intermetallic matrix composites Materials Research Society Symp. Proc.* 1990. Pittsburgh, PA: MRS. p. 131-138.

86. T.C. Lu, A.G. Evans, R.J. Hecht, and R. Mehrabian, Toughening of $MoSi_2$ with a ductile (Nb) reinforcement, *Acta metallurgica et materialia, 39* (1991), 1853-1862.

87. L. Xiao and R. Abbaschian, Interfacial modification in Nb/$MoSi_2$ composites and its effects on fracture toughness, *Materials Science & Engineering A, A155* (1992), 135-145.

88. T.C. Lu, Y.G. Deng, C.G. Levi, and R. Mehrabian. *$Y_2O_3$ coatings as diffusion barriers in $MoSi_2$-Nb composites*. in *Advanced Metal Matrix Composites for Elevated Temperatures Conf. Proc.* 1991. Materials park, OH: ASM International. p. 11-19.

89. M.J. Maloney and R.J. Hecht, Development of continuous fiber reinforced MoSi2-base composites, *Materials Science & Engineering A, A155* (1992), 19-31.

90. J.R. Rodgers and P.Villars, Trends in advanced materials data: regularities and predictions, *MRS Bulletin, XVIII* (1993), 27-29.

91. F.N. Rhines, *Phase Diagrams in Metallurgy- Their Development and Application*. 1956, New York: McGraw-Hill.

92. J. Connell R.G., A tutorial on flow diagrams: a tool for developing the structure of multicomponent phase diagrams, *Journal of Phase Equilibria, 15* (1994), 6-19.

93. O. Kubaschewski, With one auspicious and one dropping eye, *CALPHAD, 8* (1984), 355-358.

94. J.H. Norman, G.H. Reynolds, and L. Brewer, , in *MRS Symposium Proceedings*. 1990, Pittsburgh, PA: MRS. p. 369-377.

95. R.T. DeHoff, *Thermodynamics in Materials Science*. 1993, New York: McGraw-Hill, Inc.

96. O. Kubaschewski, C.B. Alcock, and P.J. Spencer, *Materials Thermochemistry*. 6 ed. 1993, Oxford: Pergamon Press.

97. F.R. de Boer, R. Boom, W.C.M. Mattens, A.R. Miedema, and A.K. Niessen, *Cohesion in Metals- Transition metal alloys*. Cohesion and Structure, F.R. de Boer and D.G. Pettifor, Editor. Vol. 1. 1988, Amsterdam: North-Holland.

98. J. Klingbeil and R. Schmidt-Fetzer, TerQuat- Approximate prediction of ternary and quaternary phase diagrams comprising stoichiometric phases, *Journal of Phase Equilibrium, 13* (1992), 522-531.

99. L. Kaufman and H. Bernstein, *Computer Calculation of Phase Diagrams*. Refractory Materials, J.L. Margrave, Editor. Vol. 4. 1970, New York: Academic Press.

100. H.L. Lukas, J. Weiss, and E.-T. Henig, Strategies for the calculation of phase diagrams, *CALPHAD, 6* (1982), 229-251.

101. S. Fries, Max Plank Forshungsinstitut für Metallkunde, Sttutgart, Unpublished research, (1994).

102. A.T. Dinsdale, SGTE data for pure elements, *CALPHAD, 15* (1991), 317-425.

103. E.A. Guggenheim, The theoretical basis of Raoult's Law, *Transactions of the Faraday Society, 33* (1937), 151-156.

104. O. Redlich and A.T. Kister, Algebraic representation of thermodynamic properties and the classification of solutions, *Ind. Eng. Chem., 40* (1948), 345-348.

105. S. McCormick, *TAPP-A database of Thermochemical and Physical Properties-Manual.* 1993, Hamilton, OH: ES Microware.

106. M. Hillert, Empirical methods of predicting and representing thermodynamic properties of ternary solution phases, *CALPHAD, 4* (1980), 1-12.

107. I. Ansara. Prediction of thermodynamic properties of mixing and phase diagrams in multi-component systems. in *Metallurgical Chemistry- Proceedigns of a symposium held at Brunel University and the NPL on 14-16 July 1971.* 1971. London: Her Majesty's Stationery Office. p. 403-430.

108. I. Ansara, C. Bernard, L. Kaufman, and P. Spencer, A comparison of calculated phase equilibria in selected ternary alloy systems using thermodynamic values derived from different models, *CALPHAD, 2* (1978), 1-15.

109. K. Chou and Y.A.Chang, A study of ternary geometrical models, *Ber.Bunsenges. Phys.Chem., 93* (1989), 735-741.

110. B. Sundman, B. Jansson, and J.O. Andersson, The Thermo-Calc databank system, *CALPHAD, 9* (1985), 153-190.

111. C. Wagner, *Thermodynamics of Alloys.* 1952, Reading, MA: Addison-Wesley, Inc.

112. M. Hillert, B. Jansson, B. Sundman, and J. Agren, A two-sublattice model for molten solutions with different tendency for ionization, *Metallurgical Transactions A, 16A* (1985), 261-266.

113. M. Hillert and L.-I. Staffansson, The regular solution model for stoichiometric phases and ionic melts, *Acta Chemica Scandinavica, 24* (1970), 3618-3626.

114. B. Sundman and J. Agren, A regular solution model for phases with several components and sublattices, suitable for computer applications, *Journal of Physical Chemistry of Solids, 42* (1981), 297-301.

115. N. Saunders, Al-Mo (Aluminium-Molybdenum), in *Binary Alloy Phase Diagrams,* T.B. Massalslki, Editor. 1990, Materials Park, OH: ASM International. p. 174-176.

116. C. Brukl, H. Nowotny, and F. Benesovsky, Untersuchungen in den Dreistoffsystemen: V-Al-Si, Nb-Al-Si, Cr-Al-Si, Mo-Al-Si bzw. Cr(Mo)-Al-Si (Research on the ternary systems:...), *Monatshefte für Chemie, 92* (1961), 967-980.

117. K. Yanigihara, T. Maruyama, and K. Nagata, Isothermal and cyclic oxidation of $Mo(Si_{1-x}Al_x)_2$ up to 2048K, *Materials Transactions JIM, 34* (1993), 1200-1206.

118. L.S. Guzei, Aluminum- Molibdenum- Silicon, in *Ternary Alloys,* G. Petzow and G. Effenberg, Editor. 1992, Basel, Switzerland: VCH. p. 225-227.

119. H. Nowotny, R. Kieffer, and H. Schachner, Strukturuntersuchungen an Disiliziden, *Monatshefte für Chemie, 83* (1952), 1243-1252.

120. H. Nowotny, H. Kudielka, and E. Parthe. Über der Aufbau von Siliziden. in *2nd Plansee Seminar "De Re Metallica".* 1955. London: Pergamon. p.166-172.

121. H. Nowotny, Alloy chemistry of transition element borides, carbides, nitrides, aluminides and silicides, in *Electronic structure and alloy chemistry of the Transition elements,* P. Beck, Editor. 1963, New York: Interscience Publishers - TMS-AIME. p. 179-220.

122. E.I. Gladyshevskii, *Crystal Chemistry of Silicides and Germanides.* 1971, Moscow: Metalurgyia.

123. D.M. Shah, D. Berczik, D.L. Anton and R. Hecht., Appraisal of other silicides as structural materials, *Materials Science & Engineering A, A155* (1992), 45-57.

124. V.U. Kodash, P.S. Kisly, and V.J. Shemet, High temperature oxidation of molybdenum aluminosilicides, *High Temperature Science, 29* (1990), 143-152.

125. M.S. Chandrasekharaiah, J.L. Margrave, and P.A.G. O'Hare, The disilicides of tungsten, molybdenum, tantalun, titanium, cobalt and nickel and platinum monosilicide: a survey of their thermodynamic properties, *Journal of Physical Chemistry Reference Data, 22* (1993), 1459-1468.

126. M. Schlesinger, Thermodynamics of solid transition-metal silicides, *Chem.Rev., 90* (1990), 607-628.

127. T.G. Chart, *A Critical Assessment of Thermochemical Data for Transition Metal-Silicon Systems.* 1972, Report NPL Chem. 18 Teddington, Middlesex, England: N.P.L. Division of Chemical Standards.

128. T.G. Chart, Termochemical data for transition metal-silicon systems, *High Temperatures-High Pressures, 5* (1973), 241-252.

129. D.A. Robbins and I. Jenkins, The heats of formation of some transition metal silicides, *Acta Metallurgica, 3* (1955), 598-604.

130. V.M. Maslov, A.S. Neganov, I.P. Borovinskaya, and A.G. Merzhanov, Self-propagating high-temperature synthesis as a method of determining heats of formation of refractory compounds, *Combustion, Explosion and Shock Waves (Eng.Transl. of Fizika Goreniya i Vzryva), 14* (1978), 73-82.

131. T.G. Chart, Thermodynamic properties of the system Molybdenum-Silicon, *Metals Science, 8* (1974), 344-348.

132. E. Arpaci and M.G. Froberg, Experimental determination of the mixing enthalpies of liquid molybdenum-silicon alloys, *Zeitschrift für Metallkunde, 76* (1985), 440-444.

133. V.S. Sudavtosva, G.I. Batalin, and V.S. Tutevich, Thermodinamic Properties of binary Si-(V,Nb,Mo) Melts, *Russ.J.Phys.Chem. (Zh.Fiz.Khim.), 59* (1985), 1282-1283.

134. G.I. Belyaeva, N.G. Ilyushchenko, and A.I. Anfinogenov, Study of the thermodynamic properties of hard alloys of the molybdenum-aluminum system (in Russian), *Akad. Nauk SSSR, Uralii Filial, Trans. Inst. of Electrochemistry (Phys. Chem. Prop. of Electrolytes), 10* (1967), 85-95.

135. A.S. Dubrovin, O.S. Gorelkin, Y.Y. Demidov, N.A. Chirkov, L.S. Kostylev, and O.D. Kolesnikova. . in *Metalloterm. Protsessy Khim. Met., Mater. Conf.* 1971. Novosibirsk: Nauka Sib. Otd. Novosibirsk, SSSR, Chem. Abs. 80 (1974),p 74903.

136. I. Shilo and H.F. Franzen, High temperature study of the molybdenum-rich regions of the Mo-Al system, *Journal of the Electrochemical Society, 129* (1982), 2613-2617.

137. S.V. Meschel and O.J. Kleppa, Standard enthalpies of formation of 4d aluminides by direct synthesis calorimetry, *Journal of Alloys and Compounds, 191* (1993), 111-116.

138. R. Hultgren, P.D. Desai, D.T. Hawkins, M. Gleiser, and K.K. Kelley, *Selected Values of the Thermodynamic Properties of Binary Alloys.* 1973, Metals Park, OH: ASM.

139. N. Chakraborti and H.L. Lukas, Thermodynamic optimization of the Mg-Al-Si phase diagram, *CALPHAD, 16* (1992), 79-86.

140. P. Dorner, E.-T. Henig, H. Krieg, H.L. Lukas, and G. Petzow, Optimization and calculation of the binary Al -Si, *CALPHAD, 4* (1980), 241-254.

141. E.M. Levin, *Phase diagrams for ceramists, vol VI.* Roth, R.S. Editor., 1987, Westerville, OH: American Ceramic Society.

142. K.E. Spear and M.S. Wang, Thermodynamic modelling of the molybdenum boron system, *CALPHAD, 5* (1981), 109-113.

143. L. Kaufman, *Kaufman Database- Larry Kaufman, Man Labs Inc., Thermocalc Program.* 1984, Pittsburgh, PA: Man Labs Inc.

144. R.W. Olesinski and G.J. Abbaschian, The B-Si system, *Bullettin of Alloy Phase Diagrams, 5* (1984), 478-484.

145. H. Nowotny, B. Lux, and H. Kudielka, Das Verhalten metallreicher, hochschemelzender Silizide gegenueber Bor, Kohlenstoff, Stickstoff und Sauerstoff, *Monatshefte für Chemie, 87* (1956), 447-470.

146. H. Nowotny, R. Kieffer, and F. Benesovsky, Silconboride der Uebergangsmetalle Vanadin, Niob, Tantal, Molybaen und Wolfram, *Planseeberichte fuer Pulvermetallurgie, 5* (1957), 86-93.

147. B. Aronsson, The crystal structure of $Mo_5SiB_2$, *Acta Chemica Scandinavica, 12* (1958), 31-37.

148. J.L. Murray, Mo-Ti phase-diagram, in *ASM Handbook Volume 3 Alloy Phase Diagrams,* H. Baker and H. Okamoto, Editor. 1992, Materials Park, OH: ASM International: p. 2-296.

149. V.N. Svechnikov and Y.A. Kocherzinsky, Molybdenum disilicide-titanium disilicide phase diagram, *Reports of the Ukranian Academy of Sciences,7* (1972), 566-570.

150. S.P. Alisova and P.B. Budberg, The Mo-Si-Ti system, in *Equilibrium Diagrams of Metallic Systems.* 1972, Moscow: PIK Viniti.

151. J.L. Murray, Si-Ti phase-diagram, in *ASM Handbook Volume 3 Alloy Phase Diagrams,* H. Baker and H. Okamoto, Editor. 1992, Materials Park, OH: ASM International. p. 2-367.

152. R.W. Olesinski and G.J. Abbaschian, The C-Si system, *Bullettin of Alloy Phase Diagrams, 5* (1984), 486-489.

153. J.-O. Andersson, Thermodynamics Properties of Mo-C, *CALPHAD, 12* (1988), 1-8.

154. E. Parthe, W. Jeitschko, and , A neutron diffraction study of the Nowotny phase Mo<5Si3C<1, *Acta Cryst., 19* (1965), 1031-1037.

155. N.W. Thibauld, Morphological and structural crystallography and optical properties of silicon carbide (SiC), *American Mineralogist, 29* (1944), 327-362.

156. L. Brewer and O. Krikorian, Reactions of refractory silicides with carbon and nitrogen, *Journal of the Electrochemical Society, 103* (1956), 38-51.

157. F.J.J. van Loo, F.M. Smet, G.D. Rieck, and G. Verspui, Phase relations and diffusion paths in the Mo-Si-C system at 1200C, *High Temperatures-High Pressures, 14* (1982), 25-31.

158. P. Steinmetz, B. Roques, and R. Pichoir, Etude de la diffusion dans des couples du systeme ternaire Mo-C-Si, *Journal of the Less-Common Metals, 48* (1976), 225-240.

159. J. Chase M.W., C.A. Davies, J. Downey J.R., D.J. Frurip, R.A. McDonald, and A.N. Syverud, JANAF Tables, 3rd. Edition, *Journal of Physical Chemistry Reference Data, 14* (1985), Supplement 1.

160. L. Lu, A.B. Gokhale, M.J. Kaufman, and R. Abbashian. in *Powder Metallurgy: Key to Advanced Materials Technology.* 1990. ASM, Materials Park, OH. p. 32-36.

161. H. Doty and R. Abbaschian. Reactive hot compaction and in-situ reinforcement coating for intermetallic matrix composites. in *Ninth International Conference on Composite Materials ICCM-IX.* 1993. Warrendale, PA: TMS-AIME.

162. G.D. Quinn, J. Salem, I. Bar-on, K. Cho, M. Foley, and H. Fang, Fracture Toughness of advanced Ceramics at Room Temperature, *Journal of Research of the National Institute of Standards and Technology, 97* (1992), 579-607.

163. M. Sakai and R.C. Bradt, Fracture toughness testing of brittle materials, *International Materials Review, 38* (1993), 53-78.

164. P. Krishnan and M.J. Kaufman, Development and characterization of interface coatings in molybdenum-reinforced NiAl matrix composites, *Metallurgical and Materials Transactions A, 25A* (1994), 2111-2116.

165. H. Nowotny and C. Brukl, Ein Beitrag zum Dreistoff: Molybdaen-Aluminium-Silizium, *Monatshefte für Chemie, 91* (1960), 312-318.

166. L. Lu, *Reactive Hot Compaction Processes for Fabrication of $NbAl_3$ Matrix Composites*. M.S. Thesis, 1991, Gainesville, FL: University of Florida.

167. E. Fitzer, K.-H. Koechling, and J. Schlichting. The Kinetics of the formation of $Me_5Si_3$ and $Me_3Si$ compounds from $MoSi_2$ and Cr or Ta. in *Metallurgical Chemistry, Proceedings of a Symposium, 14, 15, 16 July 1971*. 1971. London: Her Majesty's Stationery Office. p. 137-141.

168. E. Fitzer and K. Matthias. Siliziumdiffusion in schutzschichtbildenden Silizidphasen hochschmelzender Metalle. in *6.Plansee Seminar*. 1969, London: Pergamon. p. 741-766.

169. C. Vahlas, P.Y. Chevalier, and E. Blanquet, A thermodynamic evaluation of four Si-M (M=Mo,Ta,Ti,W) Binary systems, *CALPHAD, 13* (1989), 273-292.

170. L. Kaufman and H. Nesor, Coupled phase diagrams and thermochemical data for transition metal binary systems-V, *CALPHAD, 2* (1978), 325-348.

171. J. Rexer, Die Phasengleichgewichte im System Aluminium-Molybdaen bei Temperaturen oberhalb 1400 C, *Zeitschrift fuer Metallkunde, 62* (1971), 844-848.

172. T.B. Massalslki, *Binary Alloy Phase Diagrams*. 1990, Materials Park, OH: ASM International.

173. H. Holleck, N. Benesovsky and H. Nowotny, Ein Beitrag zu hochsmelzende Systemen, *Monatshefte fuer Chemie, 93* (1962), 1075-1079.

174. W.O. Soboyejo, K.T. Venkateswara Rao, S.M.L. Sastry, and R.O. Ritichie, Strength, fracture, and fatigue behavior of advanced high-temperature intermetallics reinforced with ductile phases, *Metallurgical Transactions A, 24A* (1993), 585-600.

175. R. Suryanarayanan, S.M.L. Sastry, and K.L. Jerina, Consolidation of molybdenum disilicide based materials by hot isostatic pressing (HIP); comparison with models, *Acta metallurgica et materialia, 42* (1994), 3741-3750.

176. R. Suryanarayanan, S.M.L. Sastry, and K.L. Jerina, Mechanical properties of molybdenum disilicide based materials consolidated by hot isostatic pressing (HIP), *Acta metallurgica et materialia, 42* (1994), 3751-3757.

177. J.-O. Andersson and J. Agren, Models for the numerical treatment of multicomponent diffusion in simple phases, *Journal of Applied Physics, 72* (1992), 1350-1355.

## BIOGRAPHICAL SKETCH

André Luiz V. da Costa e Silva was born on August 31, 1953, in Rio de Janeiro, Brazil. He graduated first in his class in metallurgical engineering and second in the graduating class of 1976 at the Instituto Militar de Engenharia (IME), Rio de Janeiro. He then joined Eletrometal Metais Especiais S.A. where he held positions in the Special Processes Department (Electroslag, Vacuum Arc Refining and Vacuum Induction Melting) and in the Melt Shop. Under the joint support of Eletrometal and the Brazilian Ministry for Industry he received his Master of Applied Science degree from the University of British Columbia, Canada, in 1979. He left Eletrometal in 1980 to collaborate with the Brazilian Institute for Nuclear Quality (IBQN) until 1987. While there he was certified as Independent Technical Inspector, Level III and was the first Brazilian to be certified Independent Technical Expert, Level III in Materials Engineering with the recognition both of the Brazilian Nuclear Regulatory Commission (CNEN) and the Independent Supervision Agency of the state of Rhine-Westphalia, RW-TÜV, Essen, Germany. He was hired by CBV Indústria Mecânica S.A. to establish and manage a Materials Engineering Department; he left CBV when he was Engineering and Quality Assurance Manager in 1990 to start graduate studies at the University of Florida.

His interests in teaching and research have lead him to accept positions as Guest Professor in the Materials Program of IME in 1980, 1982 and 1984. He joined the Universidade Federal Fluminense (UFF) as a Guest Professor in 1984 and later that year became a permanent member of the faculty. He is presently Adjunct Professor of Steelmaking. He is a consultant in Brazil in the areas of materials selection, heavy-component manufacture, inspection and quality assurance. He has several publications in

these areas, including two editions of a book on Specialty Steels and Alloys, prefaced by Prof. R.W.K. Honeycombe, as well as five papers co-authored with his Ph.D. advisor, Prof. M.J. Kaufman.

He received his Ph.D. in materials science from the University of Florida in 1994. André is married and has one daughter.

I certify that I have read this study and that in my opinion it conforms to acceptable standards of scholarly presentation and is fully adequate, in scope and quality, as a dissertation for the degree of Doctor of Philosophy.

Michael J. Kaufman, Chairman
Associate Professor of Materials Science and Engineering

I certify that I have read this study and that in my opinion it conforms to acceptable standards of scholarly presentation and is fully adequate, in scope and quality, as a dissertation for the degree of Doctor of Philosophy.

Reza Abbaschian
Professor of Materials Science and Engineering

I certify that I have read this study and that in my opinion it conforms to acceptable standards of scholarly presentation and is fully adequate, in scope and quality, as a dissertation for the degree of Doctor of Philosophy.

Timothy J. Anderson
Professor of Chemical Engineering

I certify that I have read this study and that in my opinion it conforms to acceptable standards of scholarly presentation and is fully adequate, in scope and quality, as a dissertation for the degree of Doctor of Philosophy.

Robert T. DeHoff
Professor of Materials Science and Engineering

I certify that I have read this study and that in my opinion it conforms to acceptable standards of scholarly presentation and is fully adequate, in scope and quality, as a dissertation for the degree of Doctor of Philosophy.

John J. Mecholsky, Jr.
Professor of Materials Science and Engineering

This dissertation was submitted to the Graduate Faculty of the College of Engineering and to the Graduate School and was accepted as partial fulfillment of the requirements for the degree of Doctor of Philosophy.

December, 1994

for Winfred M. Phillips
Dean, College of Engineering

Karen A. Holbrook
Dean, Graduate School